# CsA is promoting tumor-like invasion in a long-term human skin equivalent

Inaugural dissertation


for the attainment of the title of doctor
in the Faculty of Mathematics and Natural Sciences
at the Heinrich Heine University Düsseldorf

presented by

## Philipp Lukas Worst

from Mannheim, Germany


Düsseldorf, October 2019

From the IUF – Leibniz Research Institute for Environmental Medicine

At the Heinrich Heine University Düsseldorf

Published by permission of the
Faculty of Mathematics and Natural Sciences at

Heinrich Heine University Düsseldorf

Supervisor: Prof. Dr. rer. nat. Petra Boukamp

Co-supervisor: Prof. Dr. rer. nat. Jens Fischer

Date of the oral examination: November 27th, 2019

To everyone who supported me during my journey. To those who assisted me during the conduction of my observations, as well as to those who inspired me to make my own thoughts.

*"We cannot observe external things without some degree of thought; nor can we reflect upon our thoughts, without being influenced on the course of our reflection by the things which we have observed."*

William Whewell (*1794 – † 1866), British philosopher

# Zusammenfassung

Organtransplantationspatienten leiden aufgrund der Behandlung mit Immunsuppressiva häufig unter schweren Nebenwirkungen. Eines der meist verwendeten Immunsuppressiva, Cycolosporin A (CsA), erhöht zum Beispiel das Risiko für kutane Plattenepithelkarzinome (cSCC) um das 250-fache. Man nimmt an, dass, zusätzlich zu UV-Licht induzierten Schäden in den Hautzellen, die durch CsA induzierte Immunsuppression von Relevanz für das erhöhte Krebsrisiko ist. Es gibt jedoch Hinweise, dass CsA, unabhängig von der Immunsuppression, auch direkte Effekte auf die Haut hat. Ziel dieser Arbeit war es zu untersuchen, welche Veränderungen durch CsA in den Hautzellen induziert werden, und ob diese für die erhöhte Tumorrate relevant sind. Hierzu wurden *in vivo* ähnliche und immundefiziente organotypische Kulturen (OTC) verwendet. Mit Hilfe dieser OTCs, bestehend aus einem epidermalen und einem dermalen Kompartiment, konnten wir die Effekte einer Behandlung mit CsA im Gewebekontext über mehrere Wochen untersuchen. Für das epidermale Kompartiment der OTCs wurden zunächst immortalisierte aber nicht-tumorigene Keratinozyten (HaCaT) eingesetzt. Diese weisen UV-Licht spezifische p53-Mutationen sowie mehrere in cSCCs häufig aufzufindende chromosomale Veränderungen auf und repräsentieren somit präneoplastische Keratinozyten, wie sie in normaler humaner Haut zu finden sind. Die Behandlung der HaCaT-OTCs mit CsA führte zu einer deutlichen Verbesserung der epidermalen Organisation. Zusätzlich gewannen sie die Fähigkeit zum invasiven Wachstum. Dies korrelierte mit einer partiellen Degradierung von Basalmembrankomponenten, vor allem von Kollagen VII, und einer Schwächung der Kollagenstruktur der Matrix.

Die RNA-Expressionsanalyse zeigte sowohl in den epidermalen HaCaT-Zellen als auch in den dermalen Fibroblasten eine CsA-spezifische Regulation der Akt-mTOR Signalkaskade. Tatsächlich wirkte die Inhibierung von Akt1 mittels Triciribine dem durch CsA induzierten invasiven Verhalten entgegen während die Differenzierungseffekte bestehen blieben.

Um zu untersuchen, ob die beobachteten Effekte HaCaT-spezifisch sind, wurden zusätzlich OTC-Studien mit normalen epidermalen humanen Keratinozyten (NHEK) durchgeführt. Eine 10-wöchige Behandlung der NHEK-OTCs mit einer Kombination aus CsA und Sonnenlicht führte ebenfalls zu einer partiellen Degradation der Basalmembran und der dermalen Matrix, sowie zur Induktion einer Fibrose ähnlichen Differenzierung der Fibroblasten.

Zusammengefasst demonstrieren diese Ergebnisse deutliche Immunsuppression unabhängige Effekte von CsA auf die kutanen Zellen, insbesondere auf die präneoplastischen HaCaT-Zellen, welche die Fähigkeit zum invasiven Verhalten erlangen. Ein vergleichbares Phänomen könnte auch in der Haut der Transplantationspatienten auftreten, was die erhöhte Tumorrate miterklären würde.

# Summary

Organ transplant recipients submitted to immunosuppressive drug treatment often suffer from severe side effects. One of the most commonly used immunosuppressant drugs, Cyclosporin A (CsA), increases the risk for cutaneous squamous cell carcinomas (cSCC) by 250 times. It is believed that in addition to UV-induced damage in the skin cells, the CsA dependent immunosuppression is of relevance for the increased tumor risk. However, there are also indications for immunosuppression-independent off-target effects of CsA on skin cells.

The aim of this thesis was to investigate the CsA induced changes in the skin cells and to evaluate if they are of relevance for the increased tumor rates. For this purpose, we used *in vivo* like but immunodeficient organotypic cultures (OTCs). These OTCs, consisting of an epidermal and dermal equivalent, allowed us to examine the effects of CsA treatment in tissue context over several weeks. For the epidermal compartment of the OTCs we initially used immortalized but non-tumorigenic HaCaT cells. They carry UV-indicative p53 mutations as well as chromosomal aberrations characteristic for cSCCs and thus represent preneoplastic keratinocytes, as they can be found in normal human skin. The treatment of the HaCaT-OTCs with CsA clearly demonstrated an improved epidermal organization. In addition, they acquired the ability for invasive growth. This correlated with partial degradation of basement membrane components, especially Collagen type VII, and a weakening of the collagen structure in the matrix.

RNA expression analyses indicated a CsA-specific Akt/mTOR pathway regulation in both the epidermal HaCaT cells and the dermal fibroblasts. Inhibition of Akt1 by Triciribine indeed antagonized the CsA induced invasive behavior, while leaving differentiation related effects unaltered.

To investigate if the observed effects were specific to HaCaT cultures, additional OTC-studies with normal human epidermal keratinocytes (NHEK) were conducted. NHEK-OTCs submitted to a combinatorial 10-week treatment of CsA and sunlight also responded with partial basement membrane and dermal matrix degradation as well as an induction of fibrosis-like fibroblast differentiation.

Taken together, these findings clearly demonstrate immunosuppression independent effects of CsA on the skin cells, especially the preneoplastic HaCaT cells which acquired the ability for invasive growth. A similar phenomenon might also occur in the skin of transplant patients and could be a reason for the elevated tumor rates.

# List of Abbreviations

| | | | | |
|---|---|---|---|---|
| **2D** | two dimensional | | **HPV** | human papillomavirus |
| **3D** | three dimensional | | **IRA** | near infrared |
| **Amp** | Amphotericin | | **K10** | Keratin-10 |
| **APS** | ammonium persulfate | | **MeOH** | methanol |
| **BCC** | basal cell carcinoma | | **mTORC1** | mTOR complex 1 |
| **BM** | basement membrane | | **NaCl** | sodium chloride |
| **BP** | basal proliferation | | **NaN3** | sodium azid |
| **Cat. No.** | catalogue number | | **NFATc** | nuclear factor activating T-cell |
| **CDM** | cell derived matrix | | **NFATn** | nuclear NFATc binding partners |
| **Col IV** | Collagen IV | | **NHDF** | normal human dermal fibroblast |
| **Col VII** | Collagen VII | | **NHEK** | normal human epidermal keratinocyte |
| **CPD** | cyclopbutane pyrimidine dimer | | **NMSC** | non-melanomal skin cancer |
| **CsA** | Cyclosporin A | | **OTC** | organotypic culture |
| **cSCC** | cutaneous squamous cell carcinoma | | **OTR** | organ transplant recipient |
| **DMEM** | Dulbecco's Modified Eagle's Medium | | **PBS** | phosphate buffered saline |
| **EDTA** | ethylenediaminetetraacetic acid | | **Pen** | Penicillin |
| **EGF** | epidermal growth factor | | **PMSF** | phenylmethylsulfonylfluorid |
| **EMT** | epithelial-mesenchymal-transition | | **qPCR** | quantitative polymerase chain reaction |
| **ET** | epidermal thickness | | **ROS** | reactive oxygen species |
| **FBS** | fetal bovine serum | | **SDS** | sodium dodecyl sulfate |
| **FGFb** | basic fibroblast growth factor | | **Strep** | Streptomycin |
| **GOI** | gene of interest | | **SUN** | imitated solar spectrum (270 - 1,200 nm) |
| **H&E** | hematoxylin and eosin | | **TCN** | Triciribine |
| **HaCaT** | human adult low calcium high temperature | | **TEMED** | tetramethylethylendiamin |
| | | | **TEP** | total epidermal proliferation |

| | | | | |
|---|---|---|---|---|
| **TGF-β1** | transforming growth factor beta 1 | | **UVA** | ultraviolet A |
| | | | **UVB** | ultraviolet B |
| **Tris-HCl** | tris hydrochloride | | **VIS** | Visual light |

## Prefixes and Units

| | | | | |
|---|---|---|---|---|
| **°C** | degree Celsius | | **mA** | milliampere |
| **µg** | microgram | | **min** | minute |
| **cm** | centimeter | | **ml** | milliliter |
| **Ct** | threshold cycle | | **nm** | nanometer |
| **µM** | micromolar | | **sec** | second |
| **g** | gravity | | **V** | Volt |
| **Gy** | Gray | | **λ** | wavelength |
| **h** | hour | | | |

# List of Figures

# List of Tables

# Table of Content

# 1. Introduction

## 1.1. The composition of human skin

The skin is the biggest organ of the human body. Its main functions are to prevent the uncontrolled loss of water as well as to protect the internal organs to external factors such as pathogens, chemicals and irradiation. The skin also gives the human body a biomechanical property, which protects the body from extensive amounts of friction and other physical damage. To fulfill these tasks, the skin requires a strict organization in different tissue compartments and a high level of communication between them, giving it the opportunity to rapidly adjust to different external and internal changes.

The epidermis is the outermost compartment and the one that is in constant exposure with the external environment. Thus, it inhabits different forms of immune cells, microbiota and the melanocytes as pigment cells. However, most of the cells in the epidermis are keratinocytes forming layers of stratified squamous epithelium with different levels of differentiation. This causes a further subdivision of the epidermis, where the *stratum corneum* is the outermost layer consisting of corneocytes, i.e. terminally differentiated keratinocytes that have lost their nuclei and other organelles and are mainly composed of insoluble proteins. In this layer an active process of keratin filaments aggregation takes place, called keratinization. Together with the synthesis of an almost insoluble cornified envelope, the *stratum corneum* forms the first defense to the outside world (Bragulla and Homberger, 2009). It is followed by the *stratum granulosum* and the *stratum spinosum.* The lowest layer is the *stratum basale*, mostly consisting of undifferentiated keratinocytes, which follow an active cell cycle and undergo proliferation. The daughter cells then move to the surface through the different epidermal layers, while further differentiating and changing expression of distinct proteins such as keratins (Cowan, 2012; Wickett and Visscher, 2006).

The epidermis and dermis are connected via the basement membrane, a thin polymeric structure composed of fibrous matrix molecules like collagen, laminin and proteoglycans (Breitkreutz et al., 2009). The dermis consists of connective tissue, mostly formed by fibroblasts, and a high content of collagen, hyaluronic acid and other elastic fibers, which together form what is commonly termed as the dermal matrix. The dermis supplies the epidermis with nutrients by its vascular network. In addition, the dermis also harbors hair follicles with its sebaceous glands, sweat glands and sensory organelles (for touch, pressure, pain and temperature) (Thulabandu et al., 2018; Uitto et al., 1989).

The subcutis, or hypodermis, is forming the third layer and connects the skin with the muscles and the bone structure. Furthermore, it contains blood vessels and nervous fibers to supply the skin with nutrients and to connect it with the nervous system.

Disturbances in this strict organization can have major impact on the morphology and functionality of the skin leading to diseases like cancer. Especially the epidermis and the dermis play important roles in those diseases and are therefore in the major focus of the dermatological research.



© The McGraw-Hill Companies, Inc.
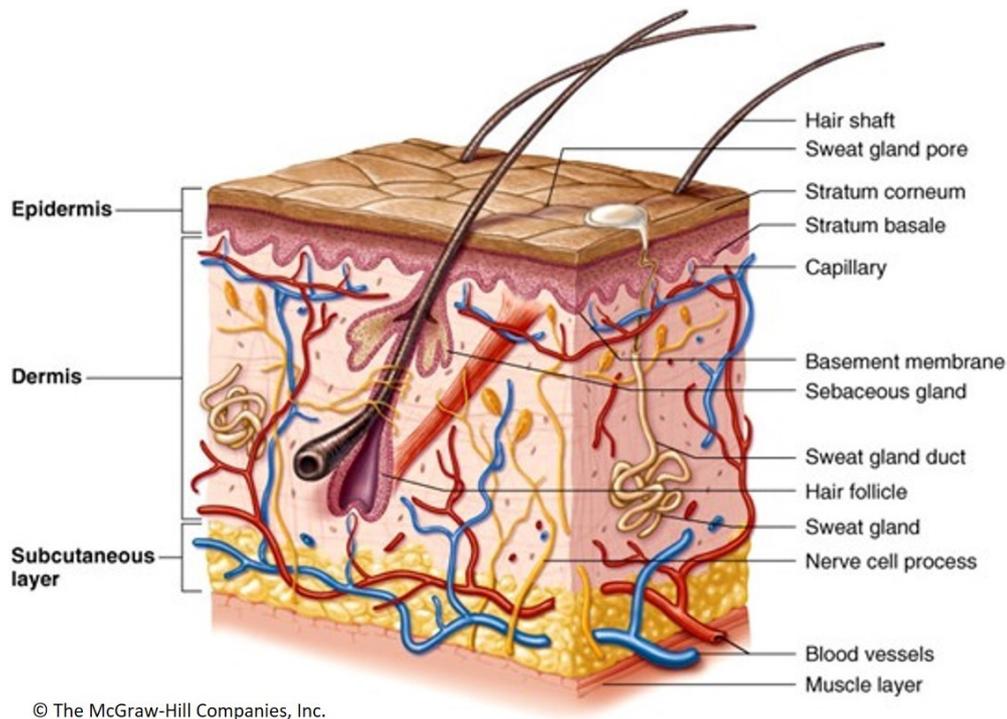
*Figure 1.1 – A cross section of the human skin and its appendages: taken from (Cowan, 2012), permission for reproduction obtained*

## 1.2. Skin cancer and cSCC development

Skin cancer is the most common type of cancer worldwide. Especially the non-melanoma forms show an occurrence of 2-3 million cases worldwide each year with increasing tendency (WHO, 2019). In the USA, for example, the non-melanoma skin cancer (NMSC) rate increased from to 2006 to 2012 by 14% (Rogers et al., 2015). About one fifth of all diagnosed NMSCs are cutaneous squamous cell carcinomas (cSCC), a cancer developing from the epidermal keratinocytes (Athas et al., 2003; Katalinic et al., 2003). Every year about 400,000 new cSCC cases are diagnosed in the

United States of which 4,000 to 8,500 cases end with a lethal outcome (Karia et al., 2013; Rogers et al., 2015). In Germany approximately 32,000 people are affected by cSCC development every year (Leiter et al., 2017). About 3.7 % of these cSCCs cases develop metastasis and 1.5 to 2.1% of the patients die from the cancer (LeBoeuf and Schmults, 2011; Schmults et al., 2013). Although the percentage of cSCC caused deaths may appear rather low, due to its high incidence rate it is causing almost as many deaths as melanoma cancer (LeBoeuf and Schmults, 2011). The latest statistics reported an increase of cSCC incidences between 1970 and 2012 by 50 to 200% (Karia et al., 2013; Staples et al., 2006; Xiang et al., 2014) and expects another doubling of the current incidence rate by 2030 (Leiter et al., 2017). However, a precise estimation of the cSCC cases is difficult to make as cases of basal cell carcinoma and cSCC cases are not required to be registered and therefore not collected by most cancer registries (Siegel et al., 2019). Especially for older skin cancer victims the death records do not often specify what type of skin cancer the patients suffered from, thus the number of annual cSCC incidences might even be higher (Garrett et al., 2016).

The mutation pattern of cSCCs is highly versatile. The average numbers of genetic aberrations in a squamous skin cell carcinoma is 3-times higher as in a cutaneous melanoma (Chalmers et al., 2017; Pickering et al., 2014). This indicates that the process of cSCC development is a multistep process and skin lesions like actinic keratosis and SCC *in situ* are considered precursor stages (Boukamp, 2005b). Two of the most common genetic aberrations found in cSCCs (about 75%) are mutations of NOTCH1 and NOTCH2, causing an inactivation of the proteins (Wang et al., 2011). Additional frequently present mutations cause defects in the genes for cyclin D1, HRAS, CDKN2A, MYC and TSP-1 (Boukamp, 2005b; Burnworth et al., 2007; Martincorena et al., 2015). One of the most discussed aberrations in skin carcinomas is the mutation of the tumor suppressor gene p53, causing its inactivation. It can be found in about 50% of all cSCC cases (Benjamin et al., 2008; Boukamp, 2005a; Brash et al., 1991) and for a long time this gene was seen as a key mutation during the development of invasive skin lesions. This is supported by observations of spontaneously occurring skin cancer in mice with an epithelial p53 knockout. Here, the mice developed skin cancer within 14 months (Page et al., 2016). However, there are also arguments speaking against such a function. For example, p53 mutations are not restricted to cSCCs, but could also be found frequently in non-lesion skin samples of patients (Khorshid et al., 1996; Stark et al., 1994). Furthermore, the global knockout of p53 in mice causes spontaneous tumor formation within only 6 months in various tissues, except for the skin (Donehower et al., 1992). This indicates that rather an accumulation of different mutations is causing the formation of skin tumors and that a loss of p53 is facilitating this process. Also, the mean age of cSCC patients is between 75 and 80 years, varying only slightly between the individual epidemiological studies, and the most frequent sites of appearance are sun exposed areas of the skin, e.g. the face and the scalp (Boukamp, 2005b; Eigentler et al., 2017; Elliott

et al., 2018; Smith et al., 2004). This speaks for the development of cSCC as a multistep process, requiring an accumulation of sunlight induced genetic aberrations.

The main treatment of cSCCs is surgical excision and for approximately 90% of all patients this method works without further complications (Bahner and Bordeaux, 2013; Potenza et al., 2018). But in cases of progressed cSCC development or for patients with a high risk for cSCC, a surgical intervention is only of limited use and effective alternative therapies as well as systemic treatments are missing (Abikhair et al., 2016; Carucci, 2004). Immunosuppressed patients, such as organ transplant recipients, comprise the biggest risk group for cSCCs, showing a speedy malignancy development, often already within the first five years after the transplantation (Ong et al., 1999). Thus, the identification of appropriate therapy targets and the conduction of clinical studies with patients carrying such a high risk for cSCCs is required (Harwood et al., 2016; Sapijaszko et al., 2015).

## 1.3. cSCC development upon immunosuppression therapy

The first successful organ transplantation in human was conducted in 1954, when a 23-year-old man decided to share his kidney with his monozygotic twin brother (Harrison et al., 1956). Five years later, the first kidney was transplanted between genetically different individuals. To avoid a rejection of the organ by the recipient, the immune response was suppressed beforehand by a whole-body x-ray exposure and the injection of cortisone (Merrill et al., 1960). However, the over-a-year survival rate of those patients was only 10%. In 1963 the first functional chemical immunosuppression approach was introduced, reporting a combined treatment with prednisone and azathioprine, which showed a 1-year survival rate of more than 70% (Starzl et al., 1963). With this technique also the first successes in the transplantation of non-renal organs like liver and heart were achieved (Barker and Markmann, 2013). In 1976 the Calcineurin inhibitor Cyclosporin A (CsA) was introduced as a new drug to achieve effective immunosuppression (Borel et al., 1976). With this new medication the 1-year survival rate for patients with a kidney graft could be reached by more than 90% (Watson and Dark, 2012). Further immunosuppressive drugs followed during the next decades, like the alternative calcineurin inhibitor Tacrolimus (Starzl et al., 1989) or the introduction of mTOR inhibitors, as well as mycophenolates (Sollinger, 1995), improving the success rate of transplantation and extending the life expectancy of the patients.

In parallel to the improved life expectancy also the number of long-term complications increased and the transplant recipients revealed to be 2-4 times more prone to the development of malignancies like skin cancer (Krynitz et al., 2013). Especially the risk for non-melanoma skin cancer
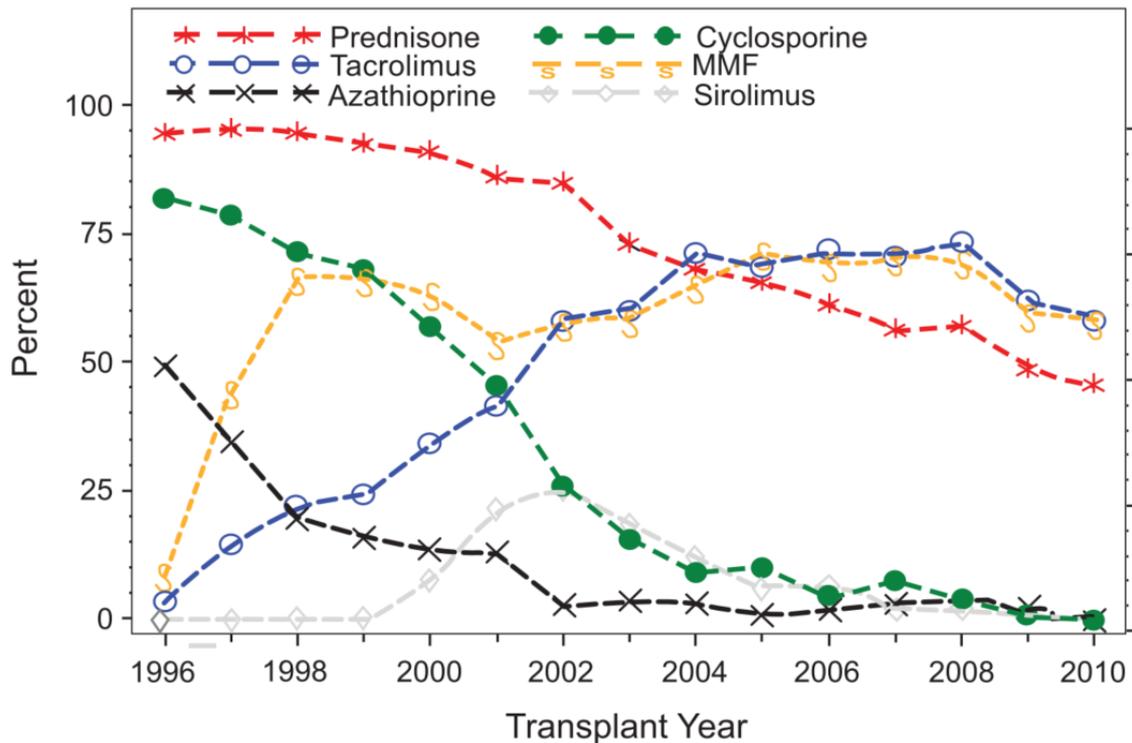
***Figure 1.2 – Use of immunosuppressive drugs in organ transplantation between 1996 and 2010:*** *taken from (Smith and Dharnidharka, 2014)*

was highly elevated. Immunosuppressed patients showed a 10-fold elevated rate of basal cell carcinomas (BCCs) and a 50-250-fold elevated rate of cSCCs (Grulich et al., 2007; Jensen et al., 1999; Lindelof et al., 2000). Particularly, the recipients of heart and lung grafts displayed a 198-fold increased chance of cSCC development. Also of high risk for such side effects are patients undergoing a kidney (120-fold) or liver (32-fold) transplantation (Krynitz et al., 2013). Furthermore, the average age of patients with a first cSCC diagnosis was about two decades younger than in the immunocompetent population (Kwa et al., 1992; Ong et al., 1999). Within 5 years after transplantation every third patient developed NMSC and in three out of four cases this cancer was a cSCC (Ong et al., 1999). It is believed, that within 20 years approximately every second organ recipient becomes affected (Berg and Otley, 2002; Bouwes Bavinck et al., 1996). In countries like Australia the numbers even rise to 73% (Bouwes Bavinck et al., 1996). Patients who already had a cSCC are also more prone to develop further skin cancer lesions. The chance of developing multiple cSCCs in such patients within 3 years after the first diagnosis is 18 to 60% (Mackenzie et al., 2010; Marcil and Stern, 2000). In some cases patients develop even several NMSC lesions within one year, sometimes even more than 100, a phenomenon often referred to as catastrophic cutaneous carcinogenesis (Berg and Otley, 2002). Additionally, the chance for metastatic cSCC increases from 5 to 8%, which is approximately 10-times higher compared to the immunocompetent population (Burnworth et al., 2007; Euvrard et al., 2003). The cSCCs are more aggressive in OTRs than in the

normal population and for these patients the cancer more often has a lethal outcome. Different studies describe a cSCC induced mortality rate in immunosuppressed patients of 12-15% (Ong et al., 1999; Tremblay et al., 2002).

To reduce the risk for such dramatic outcomes and to lower the burden for the patients, regular dermatologic follow-up examinations are a necessity. Especially OTRs who were already diagnosed with cSCC or who carry the genetic endowments for frequent skin lesions are advised to visit a dermatologist at least every 3 to 6 months (Berg and Otley, 2002; Mittal and Colegio, 2017). But statistical analysis of the registered patients revealed that there are additional risk factors for the development of multiple NMSCs in immunosuppressed patients. As already mentioned above, the risk for cSCC appearance is varying in the different transplant types (Euvrard et al., 2003; Krynitz et al., 2013). But also the type and the length of the immunosuppressive therapy seems to affect the chances for the development of NMSCs (Fortina et al., 2009; Ponticelli et al., 2014). Especially Cyclosporin A (CsA) appears to be associated with an elevated risk for accelerated skin cancer progression (Duncan et al., 2007; Herman et al., 2001; Hiesse et al., 1995). Treatments with CsA cause the appearance of cSCCs within the first 10 months in 80% of the patients (Abikhair et al., 2016). Consequently, a withdrawal from CsA and the application of a different medication leads to a reduced cSCC development (Caroti et al., 2012; Euvrard et al., 2012). Nowadays, CsA is frequently replaced by the newer Calcineurin inhibitor Tacrolimus. Although this drug leads to a more positive outcome in graft survival, it still shows cancer promoting side effects as well as increased risk for diabetes and nephrotoxicity (Bentata, 2019; Geissler, 2009; Guba et al., 2004). Inhibitors of the mTOR-pathway like Rapamycin or Sirolimus have even shown to reduce the risk for cSCC occurrence (Feldmeyer et al., 2012; Guba et al., 2002), but are barely used as they can cause adverse events like oral mucositis, impairment of wound healing or life-threatening pneumonitis (Errasti et al., 2010; Feldmeyer et al., 2012; Karam and Wali, 2015; Lacouture and Sibaud, 2018). To achieve an optimum between minimization of side effects and prevention of graft rejection, most patients today are treated with a combination of different immunosuppressants, like Tacrolimus combined with the mycophenolate mofetil (MMF) (De Simone et al., 2018; Smith and Dharnidharka, 2014). Also, the development of new medication strategies is ongoing and new drugs like Alemtuzumab are in clinical trial. In case of Alemtuzumab, humanized monoclonal antibodies are used to target CD52 on lymphocytes. This way lower doses of Calcineurin inhibitors are needed to achieve immunosuppression (Hanaway et al., 2011). Yet, at the current time we are far from a complete removal of Calcineurin inhibitors like CsA and Tacrolimus.

## 1.4. Potential roles of CsA application during cSCC induction

The ongoing necessity of immunosuppressive drugs like Tacrolimus and Cyclosporin A for a prevention of graft rejection demonstrates how important the development of an improved Calcineurin inhibitor with less negative side effects is. But to improve the efficiency and specificity of substances like CsA it is necessary to understand the mechanisms behind both their therapeutic and their adverse reactions, in particular in combination with UV exposure.

CsA is interfering with the immune response by inhibiting the calcineurin signaling in T-lymphocytes. Calcineurin is a $Ca^{2+}$-dependent phosphatase that is required for the dephosphorylation of the nuclear factor activating T-cell (NFATc). In its dephosphorylated state NFAT can transit to the nucleus and interact with multiple binding partners (NFATn). These binding partners can distinguish between different cell types and their availability is dependent on further signaling mechanisms. This way the activation of the calcineurin pathway can cause divers effects, especially in different tissues (Crabtree and Schreiber, 2009). In T-lymphocytes the induction of the Calcineurin pathway leads to the activation and proliferation of the immune cells, triggering a T-cell mediated immune response (Feske et al., 2003). CsA prevents this activation process by forming a complex with cyclophilin A. This complex attaches to Calcineurin and thus blocks its capability to bind and dephosphorylate NFATc (Liu et al., 1991; Stepkowski, 2000).
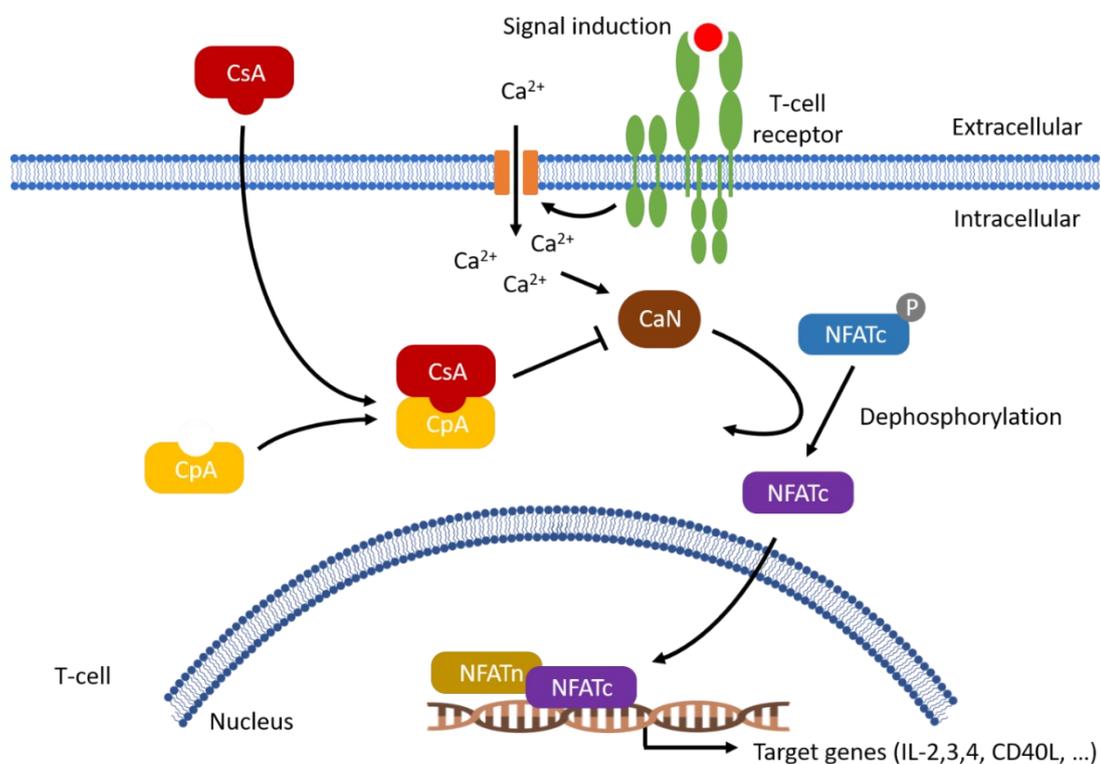


***Figure 1.3 – Calcinuerin / NFAT signaling pathway in T-cells and its inhibition by Cyclosporin A:*** *CsA – Cyclosporin A; CpA – Cyclophilin A; CaN – Calcineurin; NFATc – nuclear factor activating T-cell; NFATn - nuclear NFATc binding binding partners (based on Stepkowski, 2000)*

Although the functionality of CsA on immune cells is well investigated, it is still under debate how the drug promotes the process of sunlight induced skin cancer. Currently, there are three main theories trying to answer this question. One explanation puts forward, that the loss of the immune surveillance in transplantation patients allows an unhindered proliferation and expansion of preexisting cancer cells. The prevention of cSCCs may have a particular requirement for immune surveillance and therefore the expansion of cSCC is especially promoted in an immune suppressed environment (Dziunycz and Hofbauer, 2010; Walter et al., 2010). But this is far from the sole cause, since the cSCC promoting effect is not caused by all immunosuppressive drugs, as for instance mTOR inhibitors are proven to even reduce to reduce the risk for cSCC occurrence significantly (Feldmeyer et al., 2012).

Another theory describes an enhanced expansion of human papillomaviruses (HPV) and an increased appearance of HPV associated warts upon immunosuppression (Harwood et al., 1999; Lindelof et al., 2003; Martelli-Marzagao et al., 2016). Furthermore, there are several studies suggesting an inducing function of especially beta genus HPV during the initial stages of keratinocyte carcinogenesis, creating a potential link between HPV expansion and cSCC induction in immunosuppressed patients (Howley and Pfister, 2015; Lindelof et al., 2003; McLaughlin-Drubin, 2015). However, not all cSCC lesions in OTRs carry HPV-DNA, indicating that HPV might rather promote the development of NMSC than induce them, especially as the induction of cSCCs seems to require the exposure of the skin to sunlight.

In a third theory the induction of cSCC development in OTRs is explained by an additional immune system-independent effect of CsA, also defined as off-target effect on the skin. Evidence for such an effect came from studies on severe combined immunodeficiency (SCID) mouse models, which are unable to initiate a T-cell based immune response and are free of HPVs. A treatment of the mice carrying human adenocarcinoma cells with CsA resulted in an enhanced invasive and aggressive tumor cell growth (Hojo et al., 1999). Furthermore, in combination with UVB radiation a higher rate and tumor size was induced in SKH hairless mice (Duncan et al., 2007). Similar observations were made for UVB-irradiated and CsA-treated SCID mice. Here, CsA caused a faster tumor growth of A431 cells in the nude mice and a higher number of tumors (Han et al., 2012), supporting the theory of a cSCC promoting off-target effect of the drug.

For CsA several off-target effects have been already published. In CsA treated A-549 adenocarcinoma cells upregulation of TGFβ and enhanced anchorage-independent growth was reported (Hojo et al., 1999). Other studies described an inhibitory effect of the drug on DNA repair mechanisms, e.g. by inhibition of the xeroderma pigmentosum complementation group C (XPC) in the nucleotide excision repair mechanism or of the UVB-induced cyclobutane pyrimidine dimer

(CPD) repair (Canning et al., 2006; Han et al., 2012). Furthermore, it was published that a treatment with CsA can lead to an inhibition of UVB induced apoptosis (Han et al., 2012), a blockage of the p53 release from the mitochondria (Liu et al., 2008), and an eased epithelial-to-mesenchymal transition (McMorrow et al., 2005; Walsh et al., 2011). Primary human keratinocytes and SCC-13 cells (a SCC-derived cell line) were shown to express less p53 and more ATF3 (activating transcription factor 3), a member of the 'enlarged' AP-1 family, upon drug treatment (Rose et al., 2012; Schaper-Gerhardt et al., 2018; Wu et al., 2010).

In the work of Wu et al. from 2010 it was even described that the CsA induced changes in p53 and ATF4 expression lead to an increased SCC formation in a mouse model of chemical carcinogenesis and in biopsies of human SCCs (Wu et al., 2010).

These investigations were the basis for a first PhD thesis conducted by Lisa Schardt at the German Cancer Research Center (DKFZ) in Heidelberg with the goal to identify off-target effects of CsA in human skin keratinocytes, that would contribute or even be responsible for CsA-dependent cSCC development. Her results could not confirm a role for ATF3 during CsA promoted tumor induction. However, they revealed a number of distinct drug effects on the morphological and molecular levels in studies conducted in *in vitro* skin models. These results included an increase of chromosomal aberrations of HaCaT cells in 2D cultures, suggestive for a CsA-dependent role on genomic instability, a stimulation of their migratory potential and an improvement of the epithelial organization in 3D *in vitro* skin equivalents. Gene expression studies furthermore indicated a regulation of genes involved in cornification, cellular movement and integrin signaling. Additionally, the investigations demonstrated not only an impact of CsA treatment on the epithelium, but also on the dermal compartment, suggesting an involvement of the dermal compartment during the transformation of epithelial cells to tumor cells (Schardt, 2017).

The permanent communication between dermis and epidermis is essential for a proper development and functionality of the skin (Rognoni and Watt, 2018). Tight communication between both compartments has been reported to play a crucial role during several epithelial processes, like hair follicle development or wound healing (Babu and Wells, 2001; Sennet and Rendl, 2012), and also dermal processes can be influenced by epidermal cells. For example, the activation of Wnt signaling in basal keratinocytes can lead to an induction of dermal matrix rearrangement and proliferation among fibroblasts (Collins et al., 2011). However, in the last years several studies highlighted that the stroma can also promote the formation and the malignancy of epithelial tumors (Busch et al., 2015; Orimo et al., 2005). Also in the skin, evidence of matrix driven tumor promoting effects could be found (Ju et al., 2018; Ng et al., 2012; Otranto et al., 2012), especially during the formation of cSCCs, raising the interest for more studies on putative off-target effects of CsA on

dermal fibroblasts. First hints for such effects were already discovered in mice studies, where CsA treatment led to a reduction of matrix metalloproteases and an increase of collagen I expression (Gawronska-Kozak and Kirk-Ballard, 2013).

Nowadays it is well appreciated that the microenvironment is of similar importance for tumor progression as the actual genomic modifications in the tumor cell itself. As mentioned above, first indications for an impact of CsA on the microenvironment of cSCCs have been already reported. However, in most NMSC cases, including the catastrophic cutaneous carcinogenesis in OTRs, a frequent exposure to ultraviolet (UV) light is believed to be causal for the formation of these skin tumors. Therefore, it is important to address whether and how the combination of CsA and UV may additionally or even predominantly affect the dermal fibroblasts, leading to the formation a permissive tumor environment.

## 1.5. Challenges of sunlight studies

Sunlight is divided into three major fractions: UV-, visible-, and infrared light. Although scientific studies investigating effects of sunlight usually focused on the UV fraction, an exposure to all three fractions bears the risk of skin damage. The spectrum of UV light is divided in three parts: UVA (315-400 nm), UVB (280-315 nm) and UVC (100-280 nm). While UVC is completely absorbed by the atmosphere and thus has no effect on the skin, both UVA and UVB were shown to contribute or even induce carcinogenesis (D'Orazio et al., 2013; Strickland, 1986). During the last decades multiple articles describing the specific effects of UVA and UVB on the skin have been published. From those one can conclude that UVB mostly affects the epidermis causing DNA damages like cyclobutane pyrimidine dimers (Douki and Cadet, 2001; Douki et al., 2000; Sarasin, 1999). UVA penetrates the skin far deeper, reaching also the lower areas of the dermis, and causes the formation of reactive oxygen species (ROS), which promote cell aging and secondary DNA damages like double-strand breaks and gene deletions (Berneburg et al., 1999; Darr and Fridovich, 1994; Greinert et al., 2012). Due to technical reasons most of these investigations were made after irradiation with either UVB or UVA alone. This form of experimental setup allowed studying the effects of these parts of the UV spectrum, but it did not represent the biological conditions of sun irradiation on the human skin. Accordingly, recent studies with simultaneous exposure of both forms of UV light indicated that a combination of the two spectra does not necessarily lead to an addition of their effects but can cause new effects or may even hinder the expression of the respective damage profile. An example is the regulation of the activity of the two kinases p38 and

JNK. Neither UVB nor UVA alone had effect on them, but the sequential irradiation caused a strong activation of the kinases (Schieke et al., 2005). Furthermore, it has been shown that not only UV light, but also parts of the infrared spectrum can have skin-damaging effects. Near infrared radiation, also known as IRA, has for instance been proven to affect the transcriptome of human fibroblasts and promote photoaging (Calles et al., 2010; Grether-Beck et al., 2017). First evidences also suggest a role of visible light (VIS) during skin aging by the formation of ROS (Liebel et al., 2012; Nakashima et al., 2017). These results indicate the need for studies focusing on the effects of a light source that mimics the terrestrial spectra of the sun, in order to represent an exposure to actual sunlight. As cSCCs in CsA treated patients are thought to be induced by the exposure to sunlight, it is therefore necessary to conduct studies on the biomolecular mechanisms affected by this more biological accurate combination, representing not only the UV fraction, but also visible and infrared light.

# 2. Aim of the thesis

Medication with Calcineurin inhibitors, and in particular Cyclosporin A, is still the predominant immunosuppressive treatment for organ transplant recipients (OTRs) with the major complication being the development of cutaneous squamous cell carcinomas (cSCCs). Although alternative inhibitors such as mTOR inhibitors have already been introduced, these are in part less effective and also provide severe adverse effects (Fogel et al., 2015), which frequently necessitate the switch back to CsA treatment. Thus, understanding the mechanism of action of CsA on human skin is essential to counteract or even hinder the off-target effects of the CsA treatment regime.

To investigate this mechanism, it was necessary to experimentally simulate the physiological conditions present in the skin of OTRs. This required a model system in which the major characteristics of human skin organization are represented. As the tumor promoting effect of CsA appears to be skin specific and immune system independent, the chosen model system also required to be immune incompetent. Therefore, in this study a three-dimensional human organotypic culture (OTC) was used to investigate skin specific off-target effects of CsA. It consisted of an *in vivo* like fibroblast derived dermal matrix (CDM) which allowed a combination with different healthy or aberrant keratinocytes to simulate individual medical skin conditions and a cultivation over several months (Berning et al., 2015).

As sun exposure is believed to cooperate with CsA in promoting the increase in tumor burden in the OTRs, a novel radiation source that simultaneously emits UVB, UVA, VIS, and IRA and thereby mimics the full spectrum of sunlight, was utilized. This allowed to investigate the role of both treatment regimens on skin cancer development with a particular emphasis on their combined action.

Thereby the following questions shall be addressed:

- How does genetic predisposition cooperate with CsA-induced tumorigenic conversion?

- What is the role of CsA on the dermal fibroblasts and how does this affect the dermal-epidermal interaction?

- What is the combinatorial role of CsA and "sunlight"? Which regulatory pathways are affected in the keratinocytes and in the stroma?

# 3. Material and Methods

## 3.1. Material lists

All chemicals, substances, materials and devices used during the presented experiments are listed in the following tables. Antibodies and primers are listed in the corresponding method chapters.

**Table 3-1 – List of chemicals used, including the supplying companies and the corresponding catalogue numbers.**

| Chemical | Supplier | Catalogue number |
|---|---|---|
| 2-Phospho-L-ascorbic acid trisodium salt, 100 g | Sigma | 49752-100g |
| Acetone (2.5 l) | Carl Roth | KK40.1 |
| Adenine, 5 g | Sigma | A2786-5g |
| AKASOLV Aqua Care, 100 ml | Carl Roth | AN93.1 |
| Aprotinin, 100 mg | Carl Roth | A162.3 |
| Bovine serum albumin (BSA) (10 g) | Sigma | A7030-10G |
| Calcium acetate hydrate 100 g | Sigma | C1000-100G |
| Calcium chloride dihydrate, 100 g | Sigma | C3306 |
| Choleratoxin, 0,5 g | Sigma | C8052-.5mg |
| Color Protein Standard, Broad Range | New England Biolabs | P7712S |
| Cyclosporin A, - CAS 59865-13-3 - Calbiochem | Merck | 239835-100MG |
| DC$^{TM}$ Protein Assay Kit II | Biorad | 5000112 |
| Dimethylsulfoxid (DMSO) | Carl Roth | A994.1 |
| Dispase II | Sigma | D4693-1G |
| DNA AWAY® 250 ml | VWR | 732-2353 |
| Dulbecco's Modified Eagle Medium (DMEM) w: 4,5 g/l Glucose, w: L-Glutamine, w: Sodium pyruvate, w: 3,7 g/l NaHCO3, 500 ml | Pan Biotech | P04-03590 |

| | | |
|---|---|---|
| Dulbecco's Modified Eagle Medium (DMEM)/F12 (1:1), w: L-Glutamine, w: 15 mM, Hepes, w: 1,2 g/l NaHCO3, 500 ml | Pan Biotech | P04-41250 |
| Eosin 1 %, 250 ml | Morphisto | 10177.00250 |
| Epidermal Growth Factor (EGF) Recombinant Human Protein, 25 UG | Life Technologies | PHG0315 |
| Ethanol 99.5% (1 l) | Carl Roth | 5054.3 |
| Ethylendiamintetraacetic acid (EDTA) 1% in PBS, 100 ml | Pan Biotech | P10-026100 |
| Fetal Bovine Serum (FBS) | Merck | S0115/0522D |
| Fixing Agent for Anatomy and Histology | Morphisto | 1.200.401.000 |
| Fluorescence Mounting Medium, 15 ml | Dako | S3023 |
| Glycerol, 100 ml | Sigma | G2025-100ML |
| Hematoxylin solution, Mayer's, 250 ml | Morphisto | 10231.00250 |
| Hoechst 33258, Pentahydrate (bis-Benzimide) - 10 mg/mL Solution in Water | Life Technologies | H3569 |
| Hydrochloric Acid 1 mol/l, 1 l | Carl Roth | K025.1 |
| Hydrocortisone, 1 mg | Sigma | H0135-1mg |
| Insulin, Recombinant Human, 1 g | Sigma | 91077C-1g |
| Lysis Solution RL | Analytik Jena AG | 845-SB-0020050 |
| Magnesium chloride hexahydrate, 100 g | Sigma | M9272 |
| Methanol 99.9% (1 l) | Carl Roth | 0082.2 |
| Mounting Medium, Isomount 2000 Q Path® | VWR | 5547535 |
| Normal goat serum, 10ml | Agilent | X090710-8 |
| Normal Sheep Serum (10 ml) | Dianova | 013-000-121 |
| PBS with Ca and Mg, 500 ml | Pan Biotech | P04-35500 |
| PBS without Cag and Mg, 500 ml | Pan Biotech | P04-36500 |
| Pen/Strep/Amphotericin B Mix, 100 ml | Pan Biotech | P06-07300 |
| Penicillin/Streptomycin, 100 ml | Pan Biotech | P06-07100 |
| Phenol Red 0.5 %, 100 ml | Sigma | P0290-100ML |
| Phosphate Buffered Saline – (PBS) 10 l | Serva | 47302.02 |
| Recombinant Human Fibroblast Growth Factor (FGF) Basic, 50 UG | Life Technologies | PHG0026 |

| | | |
|---|---|---|
| Recombinant Human Tumor Growth Factor (TGF) Beta 1, 10 UG | Life Technologies | PHG9214 |
| RNase AWAY® 250 ml | VWR | 732-2270 |
| Roticlear (1l) | Carl Roth | A538.1 |
| Sodium acetate 250g | Sigma | S2889-250G |
| Tissue Tek (OCT compound) (125 ml) | Weckert Labortechnik | 4583 |
| Triciribine / Akt Inhibitor V | Absource | S1117-0050 |
| Triton X100 (0.5 l) | Carl Roth | 3051.4 |
| Trypan Blue Stain 0.4 % | Biozym | 872030 |
| Trypsin 2.5 %, 100 ml | Pan Biotech | P10-022100 |
| Vectashield Mounting Media with DAPI (10 ml) | Biozol | H-1200 |
| Vectashield Mounting Media without DAPI (10 ml) | Axxora / Biozol / Linaris | H-1000 |
| WesternBright Chemiluminescence Substrate | Biozym | 541005 |
| Xylole (1 l) | Carl Roth | 4436.1 |
| Y-27632 Dihydrochlorid, 10 mg | Abcam | ab120129 |

**Table 3-2 – List of all items used, including the supplying companies and the corresponding catalogue numbers.**

| Item | Supplier | Cat. No. |
|---|---|---|
| 10/20 µl XL Tip, graduated, Refill | Starlab | S1110-3800 |
| 10/20 µl XL Tip, graduated, Refill-Rack, 10 x 96 | Starlab | S1110-3700 |
| 1000 µl Tip, graduated, Blue, Rack | Starlab | S1111-6801 |
| 1000 µl Tip, graduated, Blue, Refill-Rack, 10 x 96 | Starlab | S1111-6701 |
| 12-Well ThinCert™ Cell Culture Insert, Pore Size 0,4 µm, Pore Density 1×10$^8$, Greiner, 48 St | Fa. Oehmen | 665640 |
| 200 µl UltraPoint Tip, graduated, Yellow, Rack | Starlab | S1113-1806 |
| 200 µl UltraPoint Tip, graduated, Yellow, Refill-Rack, 10 x 96 | Starlab | S1113-1706 |

| | | |
|---|---|---|
| 5000 µl Macro Tip, graduated, Type Gilson, sterile, 10 x 50 | Starlab | I 1050-0710 |
| Adhesive slide, HistoBond® (100 St) | VWR International | 631-0625 |
| Adhesive slide, SuperFrost® Plus (72 St) | VWR International | 631-9483 |
| Beacker, DURAN® Borosilicate, 100 ml | VWR International | 213-1105 |
| Beacker, DURAN® Borosilicate, 1000 ml | VWR International | 213-1111 |
| Beacker, DURAN® Borosilicate, 250 ml | VWR International | 213-1107 |
| Biopsie Pad, ca. 25,4x30,2 mm, 1000 St | VWR International | 720-0211 |
| Borosilicate D 263™ M, Hydrolytic Class 1, 12 mm (2000 St) | VWR International | 630-2190 |
| Borosilicate D 263™ M, Hydrolytic Class 1, 18 mm (1000 St) | VWR International | 630-2200 |
| Borosilicate D 263™ M, Hydrolytic Class 1, 18 x 18 mm (2000 St) | VWR International | 630-2185 |
| Borosilicate D 263™ M, Hydrolytic Class 1, 22 x 22 mm (2000 St) | VWR International | 630-2186 |
| Borosilicate D 263™ M, Hydrolytic Class 1, 24 x 60 mm (2000 St) | VWR International | MARI0107242 |
| Cell Counting Slides für Luna, 100 Counts | Biozym | 872010 |
| Cell Culture Insert Plates, ThinCert™, 12-Well Platte, 10 ml, Greiner, 60 St | Fa. Oehmen | 665110 |
| Cell Culture Plate, Falcon®, 10 cm, 200 St | VWR International | 734-0006 |
| Cell Culture Plate, Falcon®, 15 cm, 100 St | VWR International | 734-0013 |
| Cell Culture Plate, Falcon®, 6 cm, Easy Grip, 500 St | VWR International | 734-0007 |
| Centrifuge Tube, 15ml, PP, 500 St. | Sarstedt | 62.554.002 |
| Centrifuge Tube, 50ml, PP, 300 St. | Sarstedt | 62.559.001 |
| Ceramics Beads 1,4 mm, 325 g | VWR International | BERT03961-1-103 |
| Cell lifter, 19 mm blade, 180 mm handle, 100 St | VWR International | 734-1526 |
| Cover glass forceps | Fine Science Tools | 11073-10 |
| Cryo molds biopsy (100 St) | Weckert Labortechnik | 4565 |
| Cryo molds intermediate (100 St) | Weckert Labortechnik | 4566 |
| Cryo molds standard (100 St) | Weckert Labortechnik | 4557 |

| | | |
|---|---|---|
| Cryo Vials, CryoTubes™, Nunc™, sterile, 1,8 ml, 500 St | VWR International | 479-6853 |
| Cryostat blade, C35, disposable, Feather (20 St) | VWR International | 720-2366 |
| Dumont #7 Forceps | Fine Science Tools | 11271-30 |
| EASYstrainer 70µm, e.st., GREINER, 50 St | Oehmen | 542070 |
| Embedding Cassette, Blue, 500 St | Neolab | 7-0014 |
| Eppendorf PCR Tubes, 0.2 mL, PCR clean | Eppendorf | 30124332 |
| Eppendorf Safe-Lock Tubes, 1.5 mL, PCR clean, colorless, 1.000 St | Eppendorf | 30123328 |
| Erlenmeyer Flask, 150 ml | VWR International | 214-0337 |
| Erlenmeyer Flask, 25 ml | VWR International | 214-1102 |
| Erlenmeyer Flask, 250 ml | VWR International | 214-1110 |
| Erlenmeyer Flask, 50 ml | VWR International | 214-1104 |
| Erlenmeyer Flask, 500 ml | VWR International | 214-1114 |
| FILTER FOR P5000 AND P10ML TIPS, BAG 100 | Gilson | F161241 |
| Glass Insert 70 mm, pol. | Leica | 14047742497 |
| Hypodermic cannula Microlance™ 3, 30G, thin wall, regular bevel 13 mm 0,3 mm, 100 St | VWR | 613-3942 |
| Lysis Solution RL | Analytik Jena AG | 845-SB-0020050 |
| Measuring Cylinders, Borosilicate, 100 ml | VWR International | 612-3836 |
| Measuring Cylinders, Borosilicate, 1000 ml | VWR International | 612-3839 |
| Measuring Cylinders, Borosilicate, 500 ml | VWR International | 612-3838 |
| Microtom Blades Feather C35, 20 St | Laborversand A. Hartenstein | C35 |
| Microtom Blades, R35, 50 St | Laborversand A. Hartenstein | R35 |
| Mouthpiece Visma® ear-loop, 50 St | Carl Roth | X458.1 |
| Multi Well Cell Culture Plate, Falcon®, 6-Well, Flat Bottom, 50 St | VWR International | 734-0019 |
| Narrow Pattern Forceps, 12 cm | Fine Science Tools | 11002-12 |
| Narrow Pattern Forceps, 20 cm | Fine Science Tools | 11002-20 |
| Pasteur Pipette Glas, 150 mm, 250 St | VWR International | 612-3813 |
| Pasteur Pipette, graduiert, 3 ml (500 St) | Carl Roth | EA66.1 |
| Pipette Tips (filtered), 10 µl | Starlab | S1121-3810 |

| | | |
|---|---|---|
| Pipette Tips (filtered), 100 µl | Starlab | S1123-1840 |
| Pipette Tips (filtered), 1000 µl | Starlab | S1126-7810 |
| Pipette Tips (filtered), 20 µl | Starlab | S1120-1810 |
| Reaction Tube 500 St | Greiner | 616201 |
| Reaction Tube, 2ml, 500 St. | NeoLAB | 1-6190 |
| Reaction Tube, non-sterile, 2 ml, 500 St | VWR | 525-0584 |
| Rotilabo® Economy Magnets, 40 mm, 10 St | Carl Roth | XA19.1 |
| Sabouraud-Glucose Agar with LThTh- 30ml, 20 St. | Merck Millipore | 1460050020 |
| Safe-Lock Tubes, 0.5 mL, PCR clean | Eppendorf | 30123301 |
| SafeSeal Tips Premium 1000 µl, sterile | Biozym | 692078 |
| Scalpels, sterile, Nr. 10, 10 Stück | VWR International GmbH | 233-5363 |
| Scalpels, sterile, Nr. 10A, 10 Stück | VWR International GmbH | 233-5513 |
| Screw cap, red, 500 St. | NeoLAB | 1-6195 |
| Serological Pipette, Falcon®, 10 ml | VWR International | 734-1738 |
| Serological Pipette, Falcon®, 25 ml | VWR International | 734-1739 |
| Serological Pipette, Falcon®, 5 ml | VWR International | 734-1737 |
| Serological Pipette, Falcon®, 2 ml, 1000 St | VWR International | 734-0336 |
| Serological Pipette, Falcon®, 50 ml, 100 St | VWR International | 734-0351 |
| Soybean Casein Digest Agar (CSA) | Merck Millipore | 1460040020 |
| Spatula Collection | Carl Roth | E286.1 |
| Sputum Vial, 22/163mm, 1200 St | Fa. Oehmen | 432102 |
| Staining Chamber | Carl Roth | TP31.1 |
| Steritop-GP, 0.22 µm, Polyethersulfon, 500 ml, 33 mm, gamma-sterilized, 12 St | Merck Millipore | SCGPS05RE |
| Steritop-GP, 0.22 µm, Polyethersulfon, 500 ml, 45 mm, gamma-sterilized, 12 St | Merck Millipore | SCGPT05RE |
| Student Iris Scissors | Fine Science Tools | 91460-11 |
| Super HT Pap Pen | VWR International | 22006 |
| Super RX-N, Fuji Medical X-Ray Film | Fujifilm | 47410 19289 |
| Surgical Scissors - Sharp | Fine Science Tools | 14002-14 |
| Syringes, 0,1 ml-scaled, 100 St | VWR International | 613-3911 |
| Whatman® Prepleated Qualitative Filter Paper, Grade 1V, 100 St | Sigma | WHA1201320 |

**Table 3-3 – List of all kits used, including the supplying companies and the corresponding catalogue numbers.**

| Kit | Supplier | Cat. No. |
|---|---|---|
| Biotin Blocking Kit | Thermo Fisher Scientific | TA-015-BB |
| DC<sup>TM</sup> Protein Assay Kit II | Biorad | 5000112 |
| EnzCheck<sup>TM</sup> Gelatinase/Collagenase Assay Kit | Thermo Fisher Scientific | E12055 |
| innuPREP DNA/RNA Mini Kit - 50 reactions | Analytik Jena AG | 845-KS-2080050 |
| Mykoplasmen-Kit VENOR®GEM ONE STEP | Minerva Biolabs | 11-8050 |
| QuantiFast SYBR Green PCR Kit | Qiagen | 204054 |
| Quantikine ELISA Human MMP-9 | R&D Systems | DMP900 |
| Quantikine ELISA Human Pro-MMP-1 | R&D Systems | DMP100 |
| SensiFAST cDNA Synthesis Kit | Bioline | BIO-65053 |
| Staining kit: Picro-Sirius Red for Collagen I & III detection - 250 ml | Morphisto | 1342500250 |
| Western Bright Kit | Biozym | 541004 |

**Table 3-4 – List of all devices used, including the supplying companies and the corresponding catalogue numbers.**

| Device | Supplier | Cat. No. |
|---|---|---|
| "My Bath", digital Water Bath, 4 Liter | Biozym Scientific GmbH | 55B2000-5-E |
| Canon IXUS 170 Digital Camera | Amazon | B00RYV9R20 |
| CoolCell LX, green | Biozym Scientific GmbH | 210005 |
| CoolCell LX, orange | Biozym Scientific GmbH | 210006 |
| Cooling Unit Liebherr | Peter Oehmen GmbH | FKuv1610 |
| Cryostat | Leica Biosystems | CM3050S |
| Electrophoresis Power supply | Pharmacia Biotech | EPS 1000 |
| Freezer Liebherr | Peter Oehmen GmbH | GN4113 |
| Gas Burner, Gasprofi 1 SCS micro | Carl Roth | AN82.1 |
| Glison Pipetman L, 0,2 - 2 µl | VWR International GmbH | GILSFA10001M |
| Glison Pipetman L, 1 - 10 µl | VWR International GmbH | GILSFA10002M |
| Glison Pipetman L, 10 - 100 µl | VWR International GmbH | GILSFA10004M |
| Glison Pipetman L, 100 - 1000 µl | VWR International GmbH | GILSFA10006M |
| Glison Pipetman L, 2 - 20 µl | VWR International GmbH | GILSFA10003M |

| | | |
|---|---|---|
| Glison Pipetman L, 20 - 200 µl | VWR International GmbH | GILSFA10005M |
| Glison Pipetman L, 500 - 5.000 µl | VWR International GmbH | GILSFA10007M |
| Heracell 240 CO2-Incubator, Kupfer | VWR International GmbH | 390-4309 |
| Heraeus Megafuge 8 230 V | VWR International GmbH | 521-1765 |
| Incubator CO2, compact, MIDI-40 | VWR International GmbH | 390-0456 |
| Infinite M200 Pro Plate reader | TECAN | - |
| Luna II automated Cell Counter | Biozym Scientific GmbH | 872002 |
| Microscope Axio Imager M2 | Carl Zeiss AG | - |
| Microscope Axio Vert.A1 | Carl Zeiss AG | Axio Vert.A1 |
| Microscope Axiophot | Carl Zeiss AG | - |
| NanoDrop Lite | Thermo Fisher Scientific | ND-LITE-PR |
| O2-Regulation, 1-21 % | VWR International GmbH | HERA51900575 |
| Panasonic Ultra Refrigerator -86 °C | LMS Consult GmbH & Co. KG | MDFU-700 VX |
| Pipette Boy S1 | VWR International GmbH | 612-3985 |
| Rotiphorese® PROclamp MINI Tank Blotting System | Carl Roth | 3513.1 |
| Rotor-Gene Q | Qiagen | 9001550 |
| Sliding Microtome | Thermo Fisher Scientific | - |
| Sprout Minicentrifuge | Biozym | 552023 |
| T3000 Thermocycler | Biometra | 050-720 |
| Tissue Tek VIP Vacuum Infiltration Processor | Miles Scientific | - |
| Tissue-Tek Base Mold 15x15x5 mm | Sakura | 4162 |
| Tissue-Tek Cryo Console | Miles Scientific | 4587 |
| Tissue-Tek Dispenser | Miles Scientific | 4586 |
| Tissue-Tek Thermal Console | Miles Scientific | 4585 |
| TRIO-Thermoblock | Biometra | - |
| Vacusafe with PP Flask and Level Sensor | Integra Biosciences | 158 310 |
| Vornado Mini Vortexer | Biozym | 55BV101-E |

**Table 3-5 – List of all software programs used, including the supplying companies and the corresponding catalogue numbers.**

| Software | Supplier |
|---|---|
| Adobe InDesign 2018 CC2018 | Adobe Systems |
| EndNote X7.7.1 | Clarivate Analytics |
| GraphPad Prism 6.0 | GraphPad Software |
| ImageJ-win64 1.51h | BioVoxxel |
| TeX Live 2016 | Zahlen-kern.de |
| Microsoft Office 2013 | Microsoft |
| Photoshop Elements 13 | Adobe |
| RStudio Version 1.0.136 | RStudio |
| ZEN 2 Pro | Zeiss |

## 3.2.  2D cell system cultivation

### 3.2.1. Cell lines

Both normal human epidermal keratinocytes (NHEK) and normal human dermal fibroblasts (NHDF) were derived from the thorax or abdomen area of different individual donors. The tissue was obtained during cosmetic surgical interventions. All donors were female, healthy and between 20 and 40 years old. Isolation of cells was done by the Boukamp laboratory (DKFZ Heidelberg) in accordance with the guidelines of the Institutional Commission of Ethics at the University of Freiburg (42/2005). In short, skin samples were disinfected and cut into small pieces (2x5 mm). After incubation in 0.5 mg/ml thermolysine overnight, dermis and epidermis were separated from each other mechanically. The epidermis was floated on 0.4% trypsin (solved in EDTA 0.05%) for 10 min in 37 °C to destabilize the cell-to-cell connections. Single cell suspensions were obtained by mechanical detachment and filtration through a cell strainer. The cells were reseeded at specified concentrations (for detailed culture conditions see **Chapter 3.2.2**). The dermis was further sheared in pieces of approx. 1 mm$^2$ and distributed on a petri dish as explant cultures. The pieces were carefully covered with D20 to stimulate the fibroblasts outgrowth from the explant. At full confluency, cells were trypsinized and reseeded at specified concentrations (for detailed culture conditions see **Chapter 3.2.2**). NHEKs were used in passages 1 to 3, NHDFs in passages 5 to 9.

Additional to primary cells, the human HaCaT keratinocyte cell line (Boukamp et al., 1988) was used. These cells were isolated from the periphery of a primary malign melanoma in the back skin of a 62 years old male patient. They carry p53 mutations coupled to environmental sun damage, among others (Lehman et al., 1993). The cell line is immortalized but non-tumorigenic and shows a rather normal differentiation behavior. HaCaT cells were used in passages 28 to 34.

### 3.2.2. Cultivation of cells

NHEK – Cells were cultivated in FAD$_{complete}$ at conditions of 37 °C, 5% $CO_2$ and 95% humidity. Primary keratinocytes require a constant supply of dermal derived growth and differentiation factors. Therefore, NHEKs were seeded on feeder cells, i.e. γ-irradiated fibroblasts. Feeder cells were prepared monthly by submitting a fibroblast suspension of less than 0.5 Mio/ml to 60 Gy gamma rays and then reseeding them at a concentration of 0.5 Mio cells per 150 cm$^2$.
The keratinocytes, when reaching a confluency of 90-95%, were incubated with EDTA for 4 min followed by Trypsin for 1-2 min, both at 37 °C. The cells were mechanically suspended in serum

containing media to stop the enzymatic reaction. Subsequently, they were counted using an automated cell counter (Luna Cell Counter), pelleted (t low speed, x1000) to discard the enzymatic agent altogether, and resuspended in media. The cells were then either prepared for storage in liquid nitrogen or seeded on dermal equivalents.

NHDF – Cells were cultivated in D10 at 37 °C, 5% $CO_2$ and 95% humidity. To reach optimal growth conditions the $O_2$ concentration was lowered to 10%. The cells were split at a confluency of almost 100%. During this procedure the fibroblasts were incubated with EDTA for 3-4 min followed by a treatment with Trypsin.1 at 37 °C for 1-2 min. The cells were then suspended in serum containing media, counted and pelleted using the same automated method as mentioned above. For further passaging the fibroblasts were resuspended and seeded at a density of $1\times10^6$ cells per 15 cm dish. Otherwise, they were prepared for storage in liquid nitrogen or used for the preparation of cell derived matrices (CDMs).

HaCaT – Cells were cultivated in D10 at conditions of 37 °C, 5% $CO_2$ and 95% humidity. They were split at a confluency of 100% in a two-step event, including an 8-10 min EDTA incubation at 37 °C and an incubation with Trypsin.4 for 2 min at 37 °C. Subsequently, they were suspended, counted and pelleted using the same automated method as mentioned above. For further passage, these cells were resuspended and seeded at a concentration of $1\times10^6$ cells per 15 cm dish or seeded on matured dermal equivalents.

Cell growth and morphology of the cells were monitored on an Axio Vert.A1 Microscope (Carl Zeiss).

**Table 3-6 – Cell Culture Reagents: Recipes for media and buffer compositions used for the cultivation of 2D and 3D cell culture systems**

| Solution | Application | Ingredients |
|---|---|---|
| D10 medium | Cultivation of HaCaT and NHDF | DMEM[1], 10% (v/v) FBS[2], 1% (v/v) Pen/Strep[3] |
| D20 medium | Isolation of NHDF | DMEM, 20% (v/v) FBS, 1% (v/v) Pen/Strep |
| Freezing medium | Freezing of all cell types | DMEM, 10% (v/v) FBS, 10% (v/v) glycerol |
| rFAD medium | Cultivation of OTCs | DMEM and F12 (3:1), 10% (v/v) FBS, 1% (v/v) Pen/Strep/Amp[4], 200 µg/ml 2-phospho-L-ascorbic acid, 0.1 nM cholera toxin, 0.4 µg/ml hydrocortisone |
| FAD_complete | Cultivation of NHEK | DMEM and F12 (3:1), 5% (v/v) FBS, 1% (v/v) Pen/Strep/Amp, 0.1 nM cholera toxin, 0.4 |

| | | μg/ml hydrocortisone, 24 ng/ml adenine, 5 μg/ml insulin, 0.5 ng/ml EGF[5] |
|---|---|---|
| CDM medium | Cultivation of dermal equivalents | DMEM and F12 (3:1), 10% (v/v) FBS, 1% (v/v) Pen/Strep/Amp, 200 μg/ml 2-phospho-L-ascorbic acid, 2.5 ng/ml EGF[5], 5 ng/ml FGFb[6], 1 ng/ml TGF-β1[7], 5 μg/ml insulin |
| EDTA | Removal of calcium from the cultures | PBS -/-, 0.05% (w/v) EDTA, 0.0005% phenol red |
| Trypsin.1 | Detachment of NHDF | PBS -/-, 0.1% trypsine, 0.0005% phenol red |
| Trypsin.4 | Detachment of NHEK and HaCaT | PBS -/-, 0.4% trypsine, 0.025% (w/v) EDTA, 0.0005% phenol red |

[1] *Dulbecco's Modified Eagle's Medium;* [2] *fetal bovine serum;* [3] *Penicillin (10,000 U/ml) / Streptomycin (10 mg/ml);* [4] *Penicillin (10,000 U/ml) / Streptomycin (10 mg/ml) / Amphotericin B (25μg/ml);* [5] *epidermal growth factor;* [6] *basic fibroblast growth factor;* [7] *transforming growth factor beta 1*

## 3.2.3. Freezing and thawing

The storage of cells was made possible by suspending the cell pellet in freezing medium at a concentration of $2x10^6$ per ml. The suspension was transferred into cryo vial with 1 ml per vial and inserted into a "cryo safe" box, that gradually lowers the temperature. The vials were kept at -80 °C overnight and later moved to a liquid nitrogen storage tank.

To thaw cells, the vials were taken out of the liquid nitrogen and placed on ice for a few minutes. The cells were then warmed up in a water bath at 37 °C for 1-2 min. After thawing, the suspension was distributed on cell culture dishes containing preheated medium (for medium specificity see **Table 3-6**). In case of NHEKs the cells were seeded on feeder cell containing plates, which were prepared less than four weeks before.

## 3.3. 3D organotypic cultures (OTCs) cultivation

Most of the studies described here were performed on cell derived matrix (CDM) OTCs. These 3D cultures consist of a scaffold free dermal equivalent, where normal human dermal fibroblasts are cultured in serum dependent conditions to produce their own extra cellular matrix. This gives the opportunity to monitor treatment effects with respects to tissue morphology, proliferation, differentiation and epidermal-dermal invasion over a period of up to six months. Co-cultures were prepared with the dermal equivalent and either normal human keratinocytes (NHEK) or HaCaT cells. CDM-OTCs combined with NHEKs have strong similarities to our human *in vivo* situation, including an intact basement membrane providing a strict dermal-epidermal border, regeneration of epidermis and epidermal differentiation, and a dermal equivalent providing an authentic dermal matrix (Berning et al., 2015).

### 3.3.1. Preparation of dermal equivalents

12 well ThinCert plates were equipped with the corresponding inserts (pore size 0.4 µm). This way two reservoirs were created - a lower one between the well and the insert and an upper one inside the insert. The lower reservoir was loaded with 5 ml CDM medium. In a three-step repetitive process $0.5 \times 10^6$ fibroblasts (passage 6-9) were seeded in 1ml CDM medium in the upper well every 48 h. Meanwhile, the plates were kept at 37 °C, 5% $CO_2$ and 95% humidity. After the third and last seeding of fibroblasts, the CDM cultures were kept to mature and produce extracellular matrix for 28 days. Medium was changed every 2-3 days.
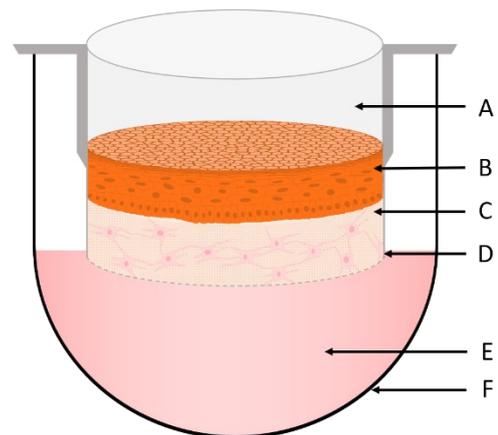


*Figure 3.1 – Illustration of a CDM-OTC loaded with normal human epidermal keratinocytes: (A) Upper Reservoir; (B) Epithelium; (C) Dermal Equivalent; (D) 0.4 µM Insert; (E) Lower Reservoir; (F) ThinCert Plate*

### 3.3.2. Loading of epidermal cells

After the *in vivo*-like matrix was established, the medium in both reservoirs was exchanged to rFAD to prime the matrix for the addition of epithelial cells and the subsequent co-culture conditions. 24 to 48 h later the reservoirs were emptied and fresh rFAD medium was applied into the lower reservoir. Onto the dermal equivalent $0.25 \times 10^6$ epithelial cells (in 1 ml rFAD) were seeded. The

cultures were kept in the incubator for 48 to 72 h to allow the cells to attach to the matrix. Then the medium from the lower reservoir was removed and fresh rFAD was applied. To initiate the process of epidermal stratification, the upper reservoir was carefully cleared from media and the cultures were "airlifted". In the following studies this refers to "day 0" in terms of further treatment. The medium in the lower reservoir was exchanged every 2-3 days. After the "airlift" the skin equivalents were cultivated over a period of 2-11 weeks. Unless further specified, the treatment started on day 7.

### 3.3.3. Irradiation procedure

The OTCs were irradiated 3 times per week, always immediately after the exchange of medium. The goal was to irradiate the cultures with a solar spectrum similar to what a person is exposed to on a sunny day in Central Europe around noon. Dr. Alexander Rapp, University of Darmstadt, and Dr. Rüdiger Greinert, Elbe Hospital Stade-Buxtehude, both members of the KAUVIR consortium, designed a lamp that not only provides such a spectrum, but also can be used to study the *in vitro* effects of different irradiation spectra in a physically controlled environment. It consists of four radiation sources: ultraviolet B (UVB, 280-315 nm), ultraviolet A (UVA, 315-400 nm), visual (VIS, 400-750 nm) and near infrared light (IRA 750-1600 nm). The lamp is equipped with beam combiner filters placed between the radiation sources and the radiation area to provide a pure and focused light source, while irradiating the specimens.

During each irradiation session, the cultures were exposed to 0.65 MED (minimal erythema dose) of the combined radiation spectrum, resulting in the following spectral intensities: UVB 0.67 kJ/m$^2$, UVA 23.9 kJ/m$^2$, VIS 53.5 kJ/m$^2$, IRA 89.5 kJ/m$^2$. For simplification, this specific irradiation spectrum is further referred to as "SUN". The exposure time required to reach 0.65 MED was 12 min 30 sec for the duration of this study. A detailed description to the calculation of the spectral intensities as well as the definition of a MED is given in the appendix section (**Chapter 8.2**).

### 3.3.4. Harvesting of OTCs

Co-cultures were always harvested 24 h after the last treatment. The OTC was removed from the mold with a scalpel and then placed on a sterile cell culture plate. The tissue was imaged with a digital camera to capture macroscopic morphological changes, caused by the treatment or the culture conditions. It was then divided with a sharp blade in two or three pieces, depending on the subsequent use of the culture. Further processing of the individual samples is described in **Chapter 3.5**. Additionally, one milliliter of conditioned media from each sample was stored at -20 °C.

## 3.4.  2D culture analysis

### 3.4.1. Protein chemistry

#### 3.4.1.1.  Protein extraction and quantification

At a confluency of 80-90% the medium from the monolayer cell cultures was removed. The cells were washed with PBS and supplemented with hot crude lysis buffer (1% SDS, 10 mM EDTA, preheated to 100 °C). The cells were mechanically separated from the dish and transferred into a reaction tube. The samples were incubated at 100 °C for 5 min and then stored on ice. Finally, the DNA was mechanically sheared with a syringe. The protein concentration was determined by performing a "DC$^{TM}$ Protein Assay" (see manufacturer's protocol for details) where the resulting absorption values ($\lambda$ = 595 nm, measured on an Infinite M200 Pro plate reader) were compared with a BSA standard curve.

#### 3.4.1.2.  SDS-PAGE and Western Blotting

Each protein sample solution (10 µg protein per sample) was mixed with loading buffer and loaded on SDS-gels (for SDS-polyacrylamide gel specifications see **Table 3-7**). The gels were then placed in running buffer and exposed to 90 V for 30 min to concentrate the proteins at the border to the resolving gel, followed by an increase of voltage to 120 V for 90 min to separate the proteins according to their size. After separation the proteins were blotted on a PVDF membrane (activated in 100% MeOH). The blotting was performed in a full wet chamber system filled with transfer buffer at 400 mA for 60 min.

**Table 3-7 – Recipes for the production of a 10% resolving gel and a 5% stacking gel**

| Ingredient | Resolving gel 10% | Stacking gel 5% |
|---|---|---|
| H$_2$O | 7.1 ml | 4.3 ml |
| 40% Acrylamid | 3.8 ml | 0.8 ml |
| 1.5 M Tris pH 8.8 | 3.9 ml | -- |
| 1.5 M Tris pH 6.8 | -- | 0.8 ml |
| 20% SDS | 0.075 ml | 0.03 ml |
| 20% APS | 0.075 ml | 0.03 ml |
| TEMED | 0.006 ml | 0.006 ml |

**Table 3-8 – Recipes for buffer compositions used during Western Blotting and subsequent antibody based protein detection.**

| Buffer | Ingredients |
|---|---|
| Lysis buffer | ddH$_2$O, 1% (w/v) SDS, 10 mM EDTA |
| 6x Loading buffer | ddH$_2$O, 240 mM Tris (pH 6.8), 6% SDS, 0.0018% Bromophenol blue, 0.3 mM DTT, 16% 2-Mercaptoethanol |
| 5x Running buffer | ddH$_2$O, 50 mM Tris, 384 mM Glycin, 0.1% SDS |
| 5x Transfer buffer | ddH$_2$O, 25 mM Tris, 192 mM Glycin, 20% (v/v) MeOH |
| 10x TBS-T (pH 7.6) | ddH$_2$O, 20 mM Tris, 137 mM NaCl, 0.5% (v/v) Tween |

After blotting the membrane was rinsed in TBS-T and blocked with TBS-T (5% BSA) for 60 min. The binding of the primary antibody (diluted in blocking solution) occurred at 4 °C overnight. The next day the membrane was rinsed in TBS-T three times for 10 min each. Incubation with the secondary antibody, diluted in TBS-T (5% BSA), occurred at room temperature for 1 h, followed by the same rinsing step as after the primary antibody. Finally, the membrane was briefly dried and transferred to an exposure cassette. The substrate mixture was applied as described in the manufacturer's protocol (Western Bright Kit, Biozym). Chemiluminescence signals, deriving from the secondary antibody coupled peroxidases, were detected by application and subsequent light stabilization of X-ray films ("Super RX-N", Fujifilm) (for antibody specifications see **Table 3-9**).

**Table 3-9 – List of all antibodies used during Western Blotting**

| Primary | | | | | |
|---|---|---|---|---|---|
| **Target** | **Origin** | **Clonality** | **Dilution** | **Supplier** | **Catalogue Number** |
| Akt total | rabbit | polyclonal | 1:5000 | Cell Signaling | 9272 |
| Akt P308Thr | rabbit | polyclonal | 1:1000 | Cell Signaling | 2965 |
| Akt P473Ser | rabbit | polyclonal | 1:1000 | Cell Signaling | 4060 |
| GAPDH | rabbit | polyclonal | 1:5000 | Cell Signaling | 2118 |

| Secondary | | | | | | |
|---|---|---|---|---|---|---|
| **Antibody** | **Origin** | **Clonality** | **Dilution** | **Link** | **Supplier** | **Catalogue Number** |
| anti-rabbit | goat | polyclonal | 1:2500 | Horseradish Peroxidase | Cell Signaling | 7074 |

## 3.5. 3D OTC analysis

### 3.5.1. Conditioned media based analysis

#### 3.5.1.1. ELISA

The Enzyme-linked Immunosorbent Assay (ELISA) is an approach to quantify the presence of a certain protein or structure. Here ELISA kits (R&D Biosystems) were used to detect protein changes in the supernatants of the OTCs. In particular, assays were used to quantify the presence of metalloproteinases (MMPs) such as Pro-MMP-1 (Cat. No. DMP100) and MMP-9 (Cat. No. DMP900). The conditioned media samples were first diluted and then processed as described in the kit manufacturer's protocols. Finally, the absorption ratios were measured on an Infinite M200 Pro ELISA reader (TECAN).

### 3.5.2. Formaldehyde fixation based analysis

#### 3.5.2.1. Embedding and section preparation

Direct formaldehyde fixation was performed for samples (either half or a quarter of an OTC), which did undergo paraffin embedding. The tissue was transferred to a vial containing a paraformaldehyde based fixing agent ("Fixing Agent for Anatomy and Histology", Morphisto) and was stored in dark for at least 24 h. Afterwards, it was enclosed in an embedding cassette and loaded into a vacuum infiltration processor. Here the samples were dehydrated by undergoing a consecutive increasing alcohol treatment finishing with a xylene bath and a subsequent transfer to 60 °C tempered paraffin. The samples were kept at an elevated temperature to prevent hardening of the wax and then placed into a preheated paraffin containing steel mold. Thereby, the cutting line of the tissue was positioned towards the bottom of the mold. The loaded molds were shifted to a cooling plate to allow quick and steady hardening of the paraffin and to provide stability for the tissue. The samples were locked on a microtome and used to prepare 7 µm thin sections. To counteract contraction of the sections they were transferred to a 40 °C water bath being mounted on a microscopy slide. The slides were placed on a 45 °C heating plate for 15 min to remove any water or air residues trapped between the slides and the section. Finally, they were stored in a closed chamber at 60 °C for 30 min to strengthen the attachment of the section to the slides by partially melting the paraffin, and to avoid a loss of material during the following staining procedures.

### 3.5.2.2. Hematoxylin and eosin (H&E) staining

The H&E staining is a standard method in histology to visualize the morphology of the tissue by labelling all basophil cellular compartments (e.g. rough endoplasmatic reticulum (ER), nuclei) in blue and all eosinophil structures (e.g. mitochondria, smooth ER, keratins) in red. A detailed description of the staining procedure is given in **Table 3-10**. For the visualization an Axio Vert.A1 light microscope (Carl Zeiss AG) was used.

**Table 3-10 – Detailed protocol for the hematoxylin and eosin staining.**

| Step | Solution | Time |
| --- | --- | --- |
| #1 – Deparaffinization | Roticlear | 10 min |
|  | Roticlear | 3 min |
| #2 – Rehydration | Ethanol 96% | 2x 2 min |
|  | Ethanol 70% | 2 min |
|  | Ethanol 50% | 2 min |
|  | Aqua dest. | Short dipping |
| #3 – Nucleus staining | Mayer's hematoxylin | 6 min |
| #4 – Blueing | Running tap water | 5 min |
| #5 – Cytoskeleton staining | Eosin 1% (aqeueous) | 6 min |
| #6 – Washing and Differentiation | Running tap water | 3 min |
|  | Ethanol 70% | 2x dipping |
| #7 – Dehydration | Ethanol 96 % | 2 min |
|  | Ethanol 99 % | 2 min |
|  | Isopropanol | 2x 2 min |
| #8 – Mounting | Isomount | Applied cover slip |

### 3.5.2.3. Picro sirius red staining

The dye sirius red binds to collagen fibers, preferably collagen I and III. When the dye is connected in longitudinal changes, an exposure to visual light causes a double refraction resulting in different color shades. Therefore, collagen I fibers, usually thick and long, appear red and collagen III fibers, usually thinner, appear green when visualized with a polarized light microscope. This allows a direct evaluation of the matrix integrity and the detection of treatment induced changes in the CDM collagen structure. A detailed description of the staining procedure is given in **Table 3-11**. Visualization of the staining was done on an Axiophot light microscope (Carl Zeiss AG).

**Table 3-11 – Detailed protocol for the picro Sirius red staining**

| Step | Solution | Time |
|---|---|---|
| #1 – Deparaffinization | Roticlear | 2x 10 min |
| #2 – Rehydration | Ethanol 96% | 2x 4 min |
| | Ethanol 70% | 4 min |
| | Ethanol 50% | 4 min |
| | Aqua dest. | 1 min |
| #3 – Collagen Staining | Pirco sirius red | 60 min |
| | Acidic Acid 30% | 2x 1 min |
| #4 – Dehydration | Ethanol 96 % | 4 min |
| | Ethanol 99 % | 4 min |
| | Isopropanol | 2x 10 min |
| #5 – Mounting | Isomount | Applied cover slip |

### 3.5.2.4. Hyaluronic acid (HA) staining

The staining procedure was performed in collaboration with Dr. Daniel Gorski from the research group of Prof. Dr. Jens Fischer at the Institute for Pharmacology at the Heinrich Heine University in Düsseldorf. This staining was used to detect treatment induced changes in the HA distribution. The visualization of hyaluronic acid was achieved using a two-step streptavidin biotin based protocol. Initially, the structure of the molecule was recognized and marked by a biotinylated HA-binding protein. This was followed by the addition of a fluorophore linked streptavidin molecule which bonded with the biotin, allowing the detection of HA with a fluorescence microscope. Staining procedures were performed by Dr. Daniel Gorski. A detailed description of the staining procedure is given in **Table 3-12**. For the visualization an Imager M2 fluorescence microscope (Carl Zeiss AG) was used.

**Table 3-12 – Detailed protocol for the hyaluronic acid staining**

| Step | Solution | Time |
|---|---|---|
| #1 – Deparaffinization | Roticlear | 3x 15 min |
| #2 – Rehydration | Ethanol 100% | 2 min |
| | Ethanol 95% | 2 min |

| | Ethanol 70% | 2 min |
| | PBS +/+[1] | 2x 5 min |
| #3 – Hyaluronidase treatment | Strep Hyase 1*25 in PBS+/+ at 37 °C, humid environment | 60 min |
| | PBS+/+ | 2x 5 min |
| #4 – Blocking | Avidin (Thermo Fisher Scientific, Cat. No. TA-015-BB) | 10 min |
| | Biotin | 10 min |
| | PBS+/+ | 2x 5 min |
| | TBS[2] (10% FBS, 1% BSA) in dark wet chamber | 60 min |
| #5 – HA labelling | HABP (Millipore, Cat. No. 385911) 1:200 in PBS+/+ (1% BSA) at 4 °C in dark wet chamber | Over night |
| | PBS+/+ | 2x 5 min |
| #6 – Biotin detection | Streptavidin (Invitrogen, Cat. No. SA1010) 1:200 in PBS+/+ (1% BSA) at RT in dark wet chamber | 60 min |
| | PBS+/+ | 2x 5 min |
| #7 – Mounting | Fluorocare DAPI mounting media | Applied cover slip |

[1] PBS (0.9 mM $CaCl_2*2H_2O$, 0.5 mM $MgCl_2*6H_2O$); [2] $ddH_2O$ (2 mM Tris, 13.7 mM NaCl)

## 3.5.3. Cryoconservation based analysis

### 3.5.3.1. Embedding and section preparation

To store OTC tissues for sectioning without prior paraformaldehyde fixation the samples were transferred into plastic cryo molds and embedded with embedding media ("Tissue Tek", Weckert Labortechnik). The molds were placed in the liquid-gaseous interphase of a liquid nitrogen container and kept there until the entire embedding media and tissue were frozen. The samples were then transferred into the liquid nitrogen phase for several minutes and finally stored at -80 °C. Normally, the half of the organotypic culture was dedicated to cryoconservation.

For sectioning, the blocks were acclimatized to a temperature of -23 °C. The material was sectioned at -20 °C to a thickness of 7 µm, collected on microscopy slides ("Super Frost Plus", VWR) and shifted to room temperature for several minutes to strengthen the attachment of the section to the glass

by drying the samples. This way a loss of material during the following staining procedures was prevented. Finally, the samples were placed at -20 °C for short-term storage (for up to four weeks).

### 3.5.3.2. Indirect immunofluorescence (IIF) staining

IIF describes the binding of a protein or structure in the tissue with a first antibody and a fluorescent labelling of this antibody with a second antibody, carrying a fluorophore, to allow its visualization on a fluorescence microscope. Here, IIF was performed on sections from frozen OTCs. The sections were acclimatized to room temperature (RT) before submitting them to a two-step fixation process of 80% Methanol at 4 °C for 10 min and acetone at -20 °C for 2 min. Afterwards they were kept at RT until all the solvent was evaporated. An antigen blocking step with 3% BSA in PBS (0.9 mM $CaCl_2*2H_2O$, 0.5 mM $MgCl_2*6H_2O$, further called PBS+/+) was also performed at RT for 30 min. Right after removing the blocking solution, the diluted primary antibody (in blocking solution) was applied and the samples were incubated in dark wet chambers at 4 °C overnight. Next morning the slides were rinsed with PBS+/+ (with additional 0.1% Triton X-100) for 5 min and three times with PBS+/+ for 10 min each. The slides were partially dried with a tissue and the secondary antibody, also diluted in the blocking solution, was applied. Asecondary antibody incubation occurred at RT in a dark wet chamber for 60 min. This was followed by the same rinsing procedure as described above. Finally, the slides were dried entirely, mounted with "Vectashield+DAPI" (Biozol) mounting medium and covered with cover slips. Imaging was performed on an Imager M2 fluorescence microscope (Carl Zeiss AG). For detailed information on the antibodies see **Table 3-13**.

**Table 3-13 – List of all antibodies used during indirect immunofluorescence staining**

| Primary | | | | | | |
|---|---|---|---|---|---|---|
| **Target** | **Origin** | **Clonality** | **Dilution** | **Fixation** | **Supplier** | **Cat. No.** |
| Keratin 15 | guinea pig | monoclonal | 1:250 | MeOH/ Aceton | Progen | GP-CK15 |
| Ki67 | rabbit | polyclonal | 1:200 | MeOH/ Aceton | Abcam | ab15580 |
| Keratin-10 | guinea pig | serum | 1:500 | MeOH/ Aceton | progen | GP-K10 |
| Collagen VII (clone LH7.2) | mouse | monoclonal | 1:250 | MeOH/ Aceton | Sigma Aldrich | C 6805 |

| | | | | | | |
|---|---|---|---|---|---|---|
| Pan-keratin (GP14) | guinea pig | serum | 1:100 | MeOH/ Aceton | Progen | GP14 |
| Collagen IV | rabbit | polyclonal | 1:1000 | MeOH/ Aceton | Progen | 10760 |
| Vimentin | mouse | monoclonal | 1:200 | MeOH/ Aceton | Progen | 61013 |
| α-smooth muscle actin | mouse | monoclonal | 1:1000 | MeOH/ Aceton | Sigma Aldrich | A2547 |
| Pan-keratin (GP14) | guinea pig | serum | 1:100 | MeOH/ Aceton | Progen | GP14 |
| Laminin-5 (γ2 chain) | mouse | monoclonal | 1:200 | MeOH/ Aceton | Merck Millipore | MAB19562 |
| Thrombospondin (A6.1) | mouse | monoclonal | 1:50 | MeOH/ Aceton | Thermo Fisher Scientific | MA5-13398 |
| Histone H3 (phospho S10) [E173] | rabbit | monoclonal | 1:500 | MeOH/ Aceton | Abcam | Ab32107 |

**Secondary**

| Antibody | Origin | Clonality | Dilution | Link | Supplier | Cat. No. |
|---|---|---|---|---|---|---|
| anti-rabbit | goat | polyclonal | 1:400 | Cy3 | Dianova | 111-165-144 |
| anti-mouse | donkey | polyclonal | 1:400 | Cy3 | Dianova | 715-166-151 |
| anti-guinea pig | donkey | polyclonal | 1:400 | Cy3 | Dianova | 706-165-148 |
| anti-guinea pig | donkey | polyclonal | 1:400 | Alexa-488 | Dianova | 706-546-148 |
| anti-mouse | sheep | polyclonal | 1:400 | Alexa-488 | Dianova | 515-545-003 |
| anti-rabbit | goat | polyclonal | 1:400 | Alexa-488 | Dianova | 111-545-003 |

### 3.5.3.3. Quantitative IIF based measures

Certain staining panels were used to measure the epidermal thickness and the proliferation rate within the epidermal compartment. For the determination of the epidermal thickness (ET) at least two sections per OTC were stained for Keratin-10 and Collagen VII. The ET was defined as the distance from the basement membrane, as a border between dermal and epidermal compartment (indicated by the signal of Collagen VII in the basement membrane), to the last differentiated but still viable (indicated by the presence of a nucleus) epidermal layer. As OTCs carrying HaCaT cells usually do not form a *stratum corneum*, the entire area giving a signal for Keratin-10 was considered viable. Of each section three independent sectors were imaged. Each image represented a section sector of at least 900 µm width. The average epidermal thickness of each section was determined by in total three individual measurements - two at both edges and one in the middle of the sector. The ET of one OTC was estimated by calculating the mean value of all six sectors. For each treatment condition and time point the ET of at least six individual OTCs was determined.

To measure proliferation the sections were stained for Ki67 and Pan-keratin. Pan-keratin antibody highlights all keratinocytes and thus allows to clearly distinguish between epidermal and dermal cells in a section. Image recording was done as described above for the ET determination. The quantification was performed automatically by using a "Fiji" based macro that first counted all epidermal cell nuclei, followed by all those that were positive for Ki67. The macro was designed by Dr. Damir Krunic of the German Cancer Research Centre in Heidelberg. The detailed macro-code can be found in a table located in **Chapter 8.1**.

Dr. Anke Hüls, Emory University in Alabama USA, assisted with the statistical calculations of all quantitative measurements. The data was loaded into the open source "R" software and a linear mixed model was fitted with the number of experiments as a random intercept. P-values were gained by applying the Wald test as implemented in the R function Anova.

### 3.5.3.4. Collagenase Assay

This approach is used to evaluate changes in the activity of enzymes with gelatin or collagen degradation activity in unfixed tissue. Cryosections from frozen OTCs were covered with a collagenase buffer ("EnzCheck, Gelatinase/Collagenase Assay Kit", Life Technologies) and kept in a dark chamber at RT for 60 min. Then the sections were covered with a cover slip (no washing!) and immediately examined on an Imager M2 fluorescence microscope (Carl Zeiss AG).

### 3.5.4. Gene expression analysis

### 3.5.4.1. Dispase treatment

As dermal and epidermal compartments had to be investigated individually, a separation of both via a dispase treatment was required. For this purpose, one quarter of an OTC culture was transferred to a cell culture plate filled with its own conditioned culture medium. Dispase II was added to a final concentration of 1 mg/ml and the plate was placed into an incubator at 37 °C for 60 min. Then the outer edges were removed with a scalpel. Dermal and epidermal compartments were gently separated using forceps and transferred to individual RNase free reaction tubes. The samples were directly snap frozen in liquid nitrogen. For long-term storage they were kept at -80 °C.

### 3.5.4.2. Tissue homogenization and RNA isolation

The frozen tissue was mixed with ~20 Zirconium oxide 1.4 mm beads and 450 μl lysis buffer in a 2 ml micro packaging vial. The lysis buffer was part of the innuPREP DNA/RNA Mini Kit used for the RNA purification (Analytik Jena AG, Cat. No. 845-KS-2080050). The samples were then lysed in a Precellys 24 (Peqlab) by shaking with 5000 rpm for two rounds of 15 s each and then centrifuged at 10,000 g for 2 min. RNA purification was performed from the supernatant as described in the manufacturer's protocol. RNA concentrations were determined on a NanoDrop Lite absorbance reader (Thermo Fisher Scientific). The purified RNA was then used for either Microarray gene expression analysis or reverse transcription and subsequent quantitative RT-PCR.
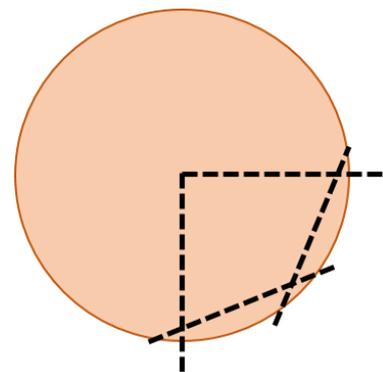


*Figure 3.2 – OTC cutting pattern for RNA isolation: One quarter of an OTC was cut out and the edges were removed. The black lines indicate the cutting edges.*

### 3.5.4.3. Whole genome RNA expression profiles

Microarray gene expression experiments allow to get a quick overview on the changes in the regulation of gene expression in a tissue after a certain treatment. For this project the epidermal and dermal samples were analyzed in cooperation with Iris Martin and Dr. Hans-Jürgen Stark at the laboratory of Prof. Dr. Magnus von Knebel Doeberitz and the Genomics and Proteomics Core Facility at the DKFZ Heidelberg. The arrays were performed on Illumina HumanHT-12 v 4.0 Expression Bead Chips.

Subsequent analysis of the raw gene expression data was done with the open source software oposSOM v2.0.0 (https://bioconductor.org/). This software allows for the organization and grouping of genes according to their regulation pattern in a self-organizing map (SOM). With this approach genes with a similar regulation pattern are grouped together as a so-called "metagene". One SOM usually consists of 400 metagenes. To identify the metagenes of highest interest, different methods can be applied. Here. a Distance Map Cluster Analysis was performed to identify the most regulated and therefore the most relevant gene groups. During this procedure the average distance of the metagenes in the data frame was used as sorting criteria. Metagenes situated in proximity in the data frame, meaning they shared a similar regulation pattern with their neighbors, were indicated in red. Metagenes being located at a larger distance from each other, meaning they differed in their regulation pattern from their neighbors, were indicated in blue. This resulted in the formation of red clusters, the so called spots, on a blue landscape. The gene groups in those red spots were blasted against an oposSOM internal gene function databank resulting in overlaps between the regulated genes and certain cellular functions and mechanisms. This workflow is further referred to as "SOM-analysis". SOM-analysis was done separately for RNA samples from the dermal and the epidermal compartment. The bioinformatics aspects of that work, including raw data processing and SOM calculation, were conducted by Dr. Maria Herberg at the laboratory of Dr. Jörg Galle at the Interdisciplinary Centre for Bioinformatics in Leipzig.
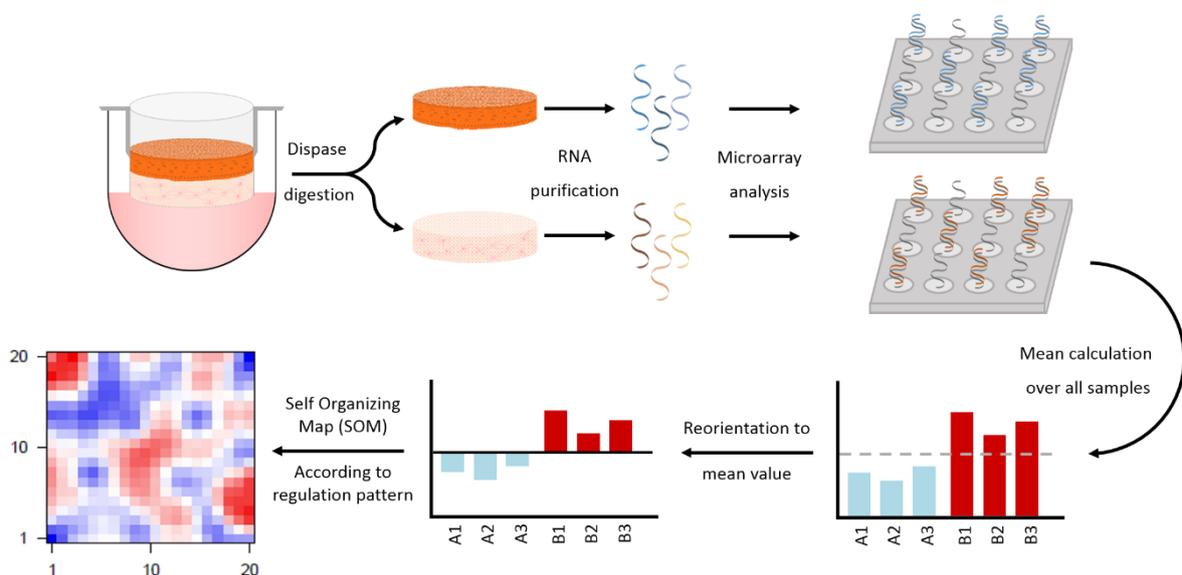


***Figure 3.3 – Microarray workflow:*** *Epidermal and dermal compartments were separated by Dipase digestion. Of both compartments the RNA was isolated and used for a gene expression microarray on Illumina HumanHT-12 v 4.0 Expression BeadChips. The results were analyzed by sorting the genes in a self-organizing map (SOM) according to their relative regulation pattern over all samples. This way the most regulated gene groups could be identified.*

### 3.5.4.4. Reverse transcription

To evaluate some of the genes from the array, the RNA extracted from the dermal samples underwent reverse transcription and subsequent quantitative polyermase chain reaction analysis. During reverse transcription, an RNA template is translated into a double stranded DNA strand. This cDNA served as a template for polymerase chain reaction (PCR) based analysis methods. The reverse transcription was performed using the SensiFAST cDNA Synthesis Kit (Bioline, Cat. No. BIO-65053) in accordance with the manufacturer's protocol.

### 3.5.4.5. Quantitative polymerase chain reaction (qPCR)

During the qPCR a certain DNA template was amplified and the copies were labelled with a fluorescence marker. Therefore, the monitoring of the increase of fluorescent signals over the PCR cycling process allowed for relative quantification of the initial template amount in a sample. The qPCR was done by using the QuantiFast SYBR Green PCR Kit (Qiagen). Sample preparation, in PCR 0.1 ml 4-Tube Strips, followed the manufacturer's protocol. Negative control samples (without DNA templates) were included for each primer set. The PCR cycling was performed in a Rotor-Gene Q (Qiagen) using the following settings for the amplification: 95 °C for 7 min, followed by 47 cycles with first 95 °C for 10 sec and ending with 60 °C for 35 sec. A list of primers is given in **Table 3-14**.

**Table 3-14 – List of all primers used during qPCR analysis**

| Gene Name | Forward primer | Reverse primer |
|---|---|---|
| Integrin αv | TGTGCAGCCAATACCCATCTCAAT | CGTTCAAACCAGCCAACCAACA |
| Collagen XIII | GGAGACGGCTATTTTGGGACG- | TCCTTGAGTGGAGCTTCCATT |
| Periostin | TGCCCAGCAGTTTTGCCCAT | CGTTGCTCTCCAAACCTCTA |
| Lumican | CTTCAATCAGATAGCCAGACTGC | AGCCAGTTCGTTGTGAGATAAAC |
| HPRT1 | CTCATGGACTGATTATGGACAGGAC | GCAGGTCAGCAAAGAACTTATAGCC |
| β-Actin | CCCCAGGCACCAGGGCGTGAT | GGTCATCTTCTCGCGGTTGGCCTTGGGGT |

The resulting cycle threshold (Ct) values were used to determine the gene expression values relative to the control. In this approach we used two reference genes, HPRT1 (Hypoxanthin-Guanin-Phosphoribosyl-transferase) and β-Actin, to create a stable normalization coefficient. First, for both, the gene of interest (GOI) and the reference genes an average Ct of the control (DMSO treated)

samples was calculated (ØCt$_{DMSO}$). From this value the Ct values of all samples were subtracted resulting in ΔCt.

$$\Delta Ct_{HPRT1} = Ct_{HPRT1} - \varnothing Ct_{HPRT1.DMSO}$$
$$\Delta Ct_{\beta Act} = Ct_{\beta Act} - \varnothing Ct_{\beta Act.DMSO}$$
$$\Delta Ct_{GOI} = Ct_{GOI} - \varnothing Ct_{GOI.DMSO}$$

Second, the ΔCt values were used for an exponential amplification ($2^{\Delta Ct}$), resulting in the relative quantities (RQ) of the target sequences.

$$RQ_{HPRT1} = 2^{\Delta Ct_{HPRT1}}$$
$$RQ_{\beta Act} = 2^{\Delta Ct_{\beta Act}}$$
$$RQ_{GOI} = 2^{\Delta Ct_{GOI}}$$

Finally, for each sample the RQ of the GOI was divided by the geometric mean of both reference genes RQs resulting in the relative gene expression of the GOI (rel.GE$_{GOI}$).

$$rel.GE_{GOI} = \frac{RQ_{GOI}}{\sqrt[2]{RQ_{HPRT1} x RQ_{\beta Act}}}$$

Statistics was done with the help of Katharina Rolfes at the IUF Düsseldorf, Germany. The data was loaded into the GraphPad Prism Software and P-values were gained by applying Turkey's multiple comparisons test as implemented in the GraphPad Prism function One-way Anova.

## 3.5.5. Protein expression analysis

### 3.5.5.1. Tissue homogenization and protein analysis

One quarter of an OTC culture was transferred into a reaction tube and immediately snap frozen in liquid nitrogen and kept at -80 °C. The frozen tissue was mixed with ~20 Zirconium oxide 1.4 mm beads and 400 µl cold PIRA buffer (25 mM Tris-HCl (pH 7.4), 150 mM NaCl, 0.1 mM EDTA (pH 8.0), 1% (w/v) Nonidet p-40, 1% (w/v) deoxycholic acid, 0.1% (w/v) SDS, 0.025% (w/v) NaN3, 2 µl/ml Protease Inhibitor Cocktail, 5 µl/ml PMSF) in a 2 ml micro vial. The samples were lysed using a Precellys 24 (Peqlab) by shaking with 5000 rpm for two rounds of 15 s each and then centrifuged at 10,000 g for 2 min. The supernatant was kept and protein purification as well as Western Blotting was performed, as described in **Chapter 3.4.1**.

# 4. Results

## 4.1. The role of genetic aberrations in a CsA-dependent phenotype

The requirement of an exposure to both sunlight and CsA, over a long period for cSCC induction in organ transplant recipients (OTRs) indicates that a combination of UV induced genetic predispositions and CsA specific regulations are needed for a tumorigenic conversion of the epidermal keratinocytes. Thus, the question emerged how keratinocytes with a different genetic make-up would respond to prolonged CsA treatment.

To address this question and to unravel potential mechanisms involved in the CsA induced tumorigenic conversion, we first studied the behavior of normal human epidermal keratinocytes (NHEK), HaCaT cells carrying mutated p53, and other cell lines incorporating genetic changes, that are all known to play a role in tumorigenic conversion of skin SCC cells (including HaCaT cells overexpressing the cell cycle regulator cyclin D1 , as well as HaCaT cells exhibiting a altered TGFß pathway overexpressing Smad-7), on the cell derived matrix (CDM) cultures. One week after the seeding of the epidermal cells, all cultures were treated with 1 µg/ml CsA for a period of 21 days. We analyzed for phenotypical changes of the cultures after CsA treatment by performing routine hematoxylin and eosin (H&E) staining. In addition, we stained for the expression of Keratin-15 and Ki67, as markers for basal cells and proliferation, by indirect immunofluorescence (IIF) (see **Figure 4.1**). These initial studies were performed in collaboration with L. Schardt at the DKFZ in Heidelberg who cultivated the organotypic cultures (OTCs) while the analysis was performed by me at the IUF.

The CsA treatment did not cause any visual morphological changes in the NHEK-based OTCs. For both treatment conditions a hyperplastic, well stratified and differentiated epithelium is visible in the H&E staining. The proliferation rate seemed only slightly increased and Keratin-15 expression stayed restricted to the basal layer.

In HaCaT OTCs the 3-week CsA treatment caused an improved tissue organization, including a more regular differentiation and in addition the cells gained the ability for growing invasively into the dermal equivalent. Interestingly K15 was absent in the untreated control cultures and was also not induced upon CsA treatment. However, proliferation was increased and was particularly prominent in invasive areas.
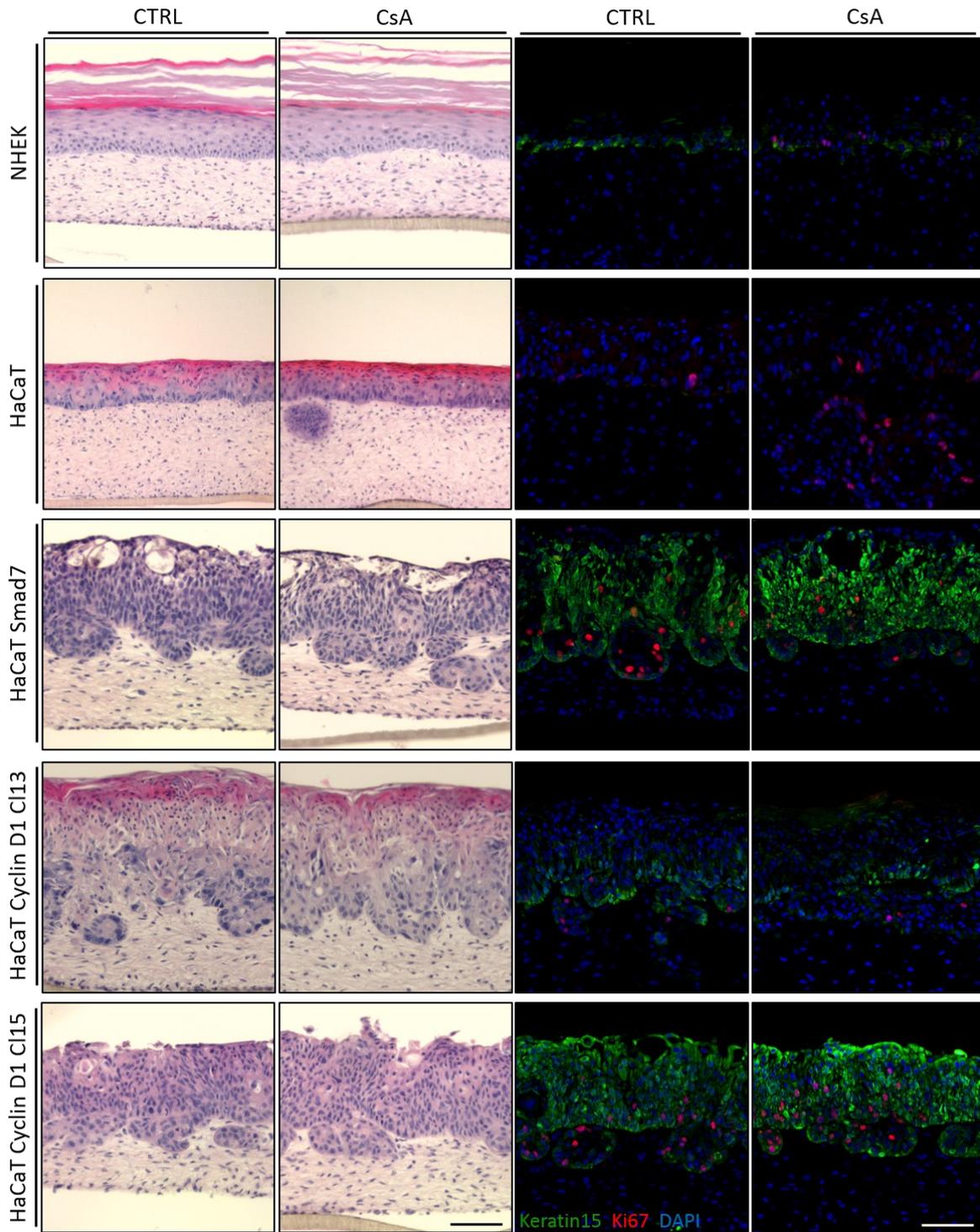
**Figure 4.1 – Different genetic predispositions and their effect during CsA treatment**: *The OTCs were composed of either NHEKs or different aberrant keratinocyte cell lines. Samples were treated with DMSO (CTRL) or 1 µg/ml CsA over a period of 21 days (CsA). H&E stainings (left side) were conducted on paraffin sections, IIF stainings for Keratin-15 and Ki67 (right side) were conducted on frozen OTC-sections. Displayed are representative images of the control versus the treated samples. The scale bars represent 100 µm.*

Impaired TGFß-signaling caused tumorigenic conversion of the HaCaT cells, allowing them to grow invasively already under control conditions. An additional application of CsA did not alter this phenotype. K15 was expressed throughout the epithelia and proliferation occurred throughout the epithelium, as well as in the invasive buds under both conditions.

Additional overexpression of Cyclin D1 alone or in cooperation with up-regulated CdK4 also promoted invasion of the HaCaT cells. Also here, additional CsA treatment did not seem to have any effect, neither on tissue morphology, K15 expression, nor proliferation, suggesting that overexpression of cyclin D1 rendered the cells insensitive to CsA.

From this initial work we concluded that the HaCaT-OTCs exhibited the most pronounced phenotype in response to CsA treatment and were therefore used, in addition to NHEK, as the model of choice for all further studies.

## 4.2. The CsA effects on HaCaT-OTCs

As an important step in understanding the effects of CsA we needed to investigate if the CsA concentration used in our previous studies was comparable to the physiological conditions in the patients undergoing organ transplantation. The literature states that the CsA concentration in the blood of organ transplant recipients varies between 25 ng/ml and 1.25 µg/ml (Saigal et al., 2002; Sommerer et al., 2011). It has also been reported that CsA can accumulate in the tissue reaching concentrations of even 2.8 µg/ml in the skin (Fisher et al., 1988). Studies conducted by L. Schardt, at our DKFZ laboratory, indicated that a concentration of at least 10 µg/ml in the medium was required to reach levels in the epithelium comparable to the patients' *in vivo* condition (Schardt, 2017). Her studies further suggested, that the outcome of the drug treatment can be affected by the source of serum (fetal bovine serum, FBS) used to supplement for the culture medium.

With all this in consideration, we decided to use a CsA concentration to 10 µg/ml and two different FBS for the following studies. Serum A was the serum used during the experiments at the DKFZ and serum B as the standard serum for our experiments at the IUF. Furthermore, the CsA treatment period was extended to 49 days in total. Starting from treatment day 7, samples were harvested in a 14 days interval. Histochemical H&E staining was performed to monitor CsA and serum effects on the morphology of the OTCs during the treatment period (**Figure 4.2**).

While the untreated HaCaT cells formed a stratified and differentiated surface epithelium, the CsA treated HaCaT cells in addition gained the ability for invasive growth. This was seen already after three weeks of treatment and was maintained up to the latest time point, making the first three weeks a critical time frame for the initiation of tumor like behavior of HaCaT cells in the OTCs. Using two different sera for the OTCs seemed to affect the invasion phenotype. With serum A the epidermal cells remained bulk, with clear borders when invading into the dermal compartment, remaining close to the basement membrane for the entire treatment. In contrast, supplementing with serum B made the invading cells appear more singularized. Small groups of cells were spread all over the dermal matrix.
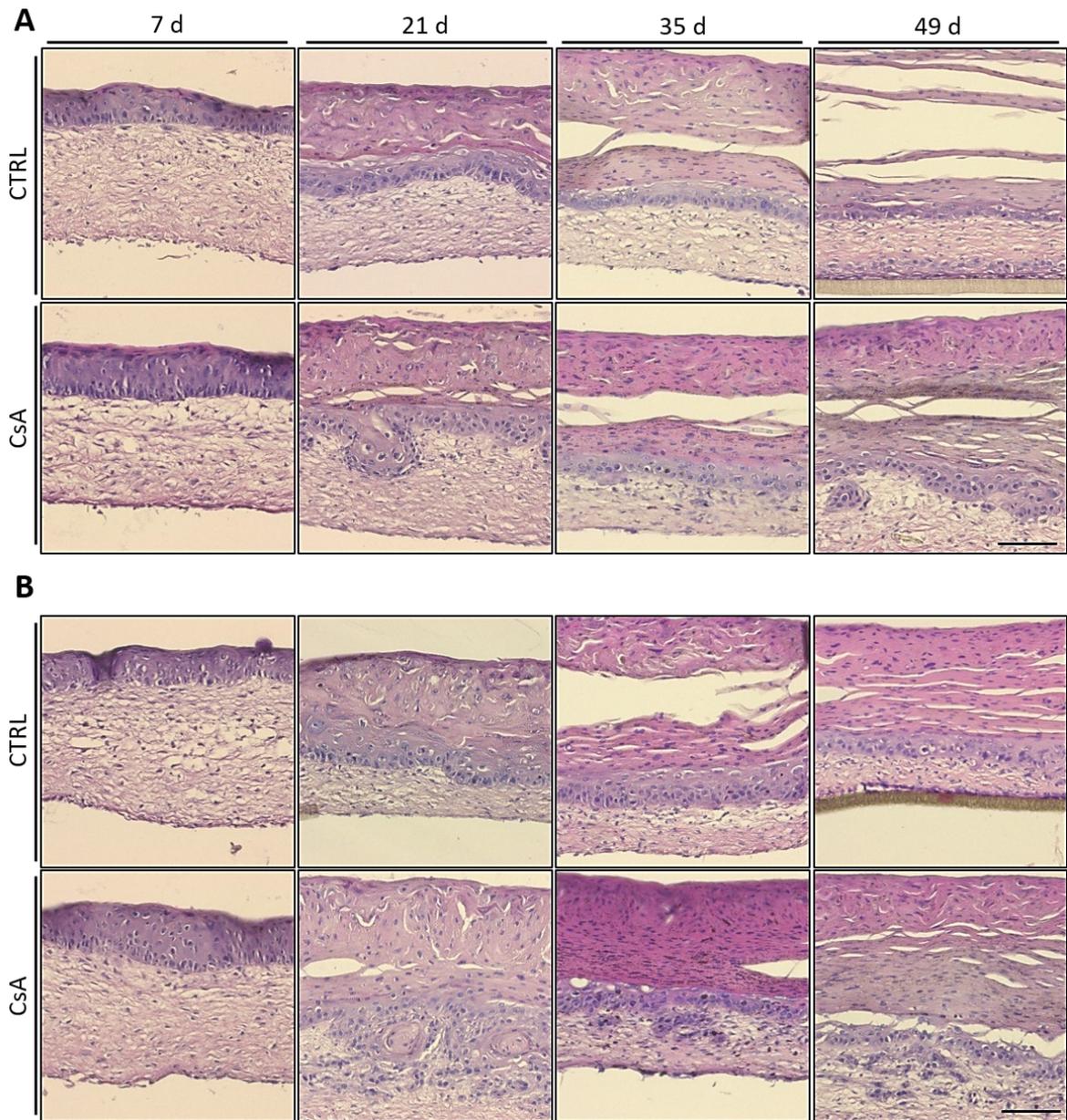
***Figure 4.2 – Morphological changes upon CsA treatment in HaCaT-OTCs:*** *Samples were treated with DMSO (CTRL) or 10 µg/ml CsA over a period of up to 49 days. H&E staining was performed on paraffin-sections of HaCaT-OTCs. Displayed are representative images of the control versus the treated samples. The OTC media was either supplemented with the bovine serum used in our laboratory at the DKFZ (A) or with the regular FBS of our laboratory at the IUF (B). In both setups first signs of invasion could be seen after 21 days. The invasion phenotype was affected by the choice of serum. With serum A the cells remained bulk, while serum B caused a singularization of the HaCaT cells in the dermis. The scale bars represent 100 µm.*

To determine wether and how CsA would affect differentiation or induce changes on the basement membrane (BM) integrity, we used Keratin-10 (K10), an early epidermal differentiation marker, in combination with an antibody directed against the BM component Collagen VII (Col VII) (**Figure 4.3**).
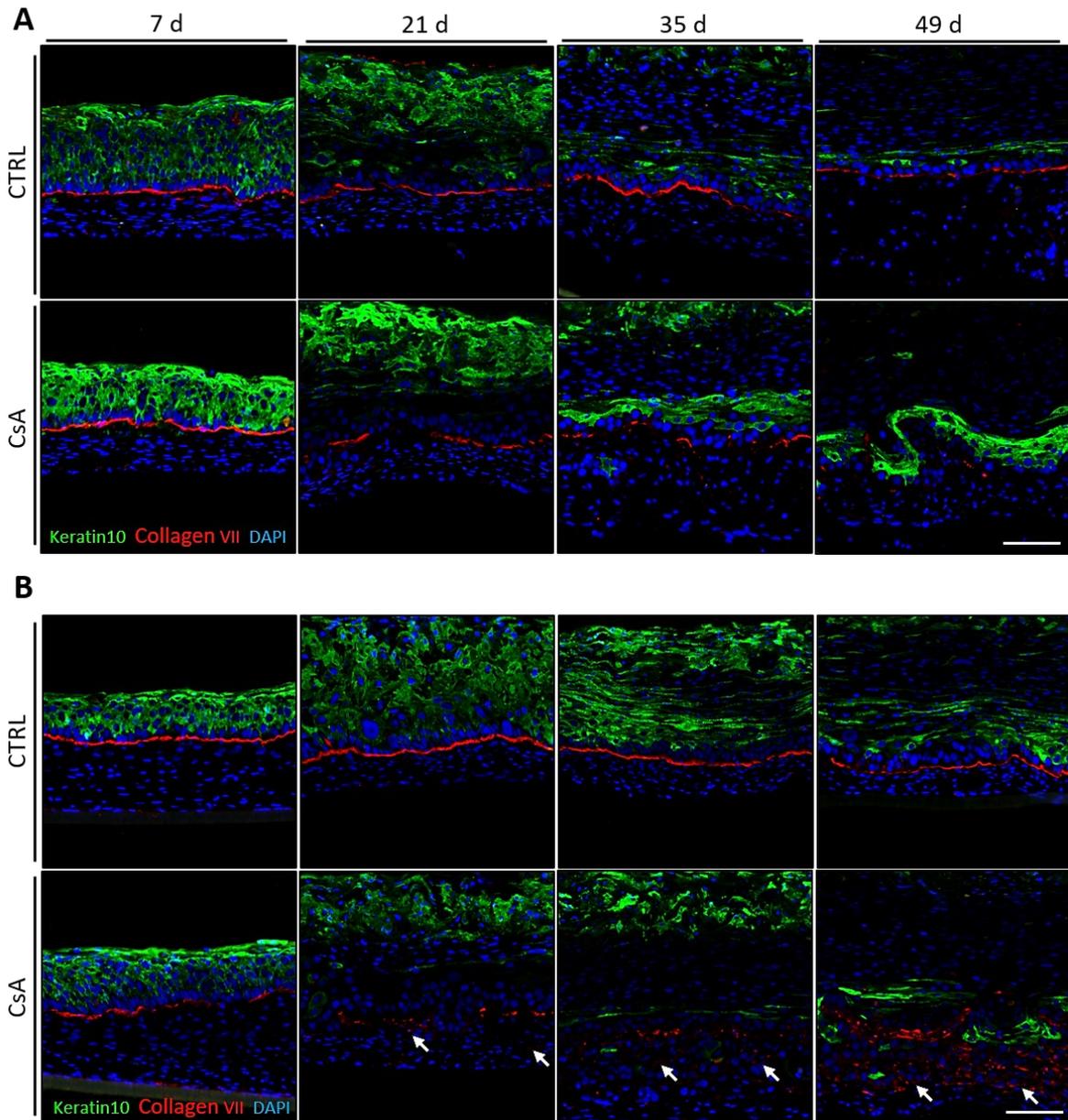
***Figure 4.3 – Modulation of differentiation and BM integrity upon CsA treatment in HaCaT-OTCs:*** *Samples were treated with DMSO (CTRL) or 10 µg/ml CsA over a period of 49 days. IIF staining was performed on frozen sections of HaCaT-OTCs to detect the expression levels of Keratin-10 as differentiation and Collagen VII as BM marker. Displayed are representative images of the control versus the treated samples. White arrows indicate signals for Collagen VII within the matrix. The OTC media was either supplemented with serum A (A) or serum B (B). In both setups, CsA led to an improved epithelial organization, but only in the serum B setup K10 got permanently restricted from the basal layer upon CsA application. Also, only here Collagen VII could be detected within the matrix. The scale bars represent 100 µm.*

In the control cultures Keratin-10 (K10) was expressed all over the suprabasal epidermal compartment and during the first weeks of culture, even in some cells of the basal layer. Furthermore, it was difficult to clearly define the different strata typically found in the epithelium

of normal human skin keratinocytes. Upon CsA treatment in the serum A setup a similar distribution of K10 and epithelial organization as in the control samples could be observed (**Figure 4.3A**). However, in the serum B setup CsA caused a clear shift of K10 expression towards the upper and differentiated layers and at all four time points the basal layer was free of K10 (**Figure 4.3B**). Another observation made in both setups was an increase in epidermal thickness (see also **Figure 4.4A**) and a change in epidermal organization, causing an improved presentation of distinct strata. At the epidermal-dermal junction, i.e. the basement membrane (BM), the Col VII structure was disrupted already after seven days of CsA treatment. The decrease in Col VII protein expression persisted and Col VII almost disappeared after five to seven weeks of treatment indicating that CsA has a major impact on this protein. Also, upon supplementation with serum B, a treatment with CsA did not lead to a total disappear of Collagen VII, but appeared to cause a dermal redistribution of this protein (**Figure 4.3B**).
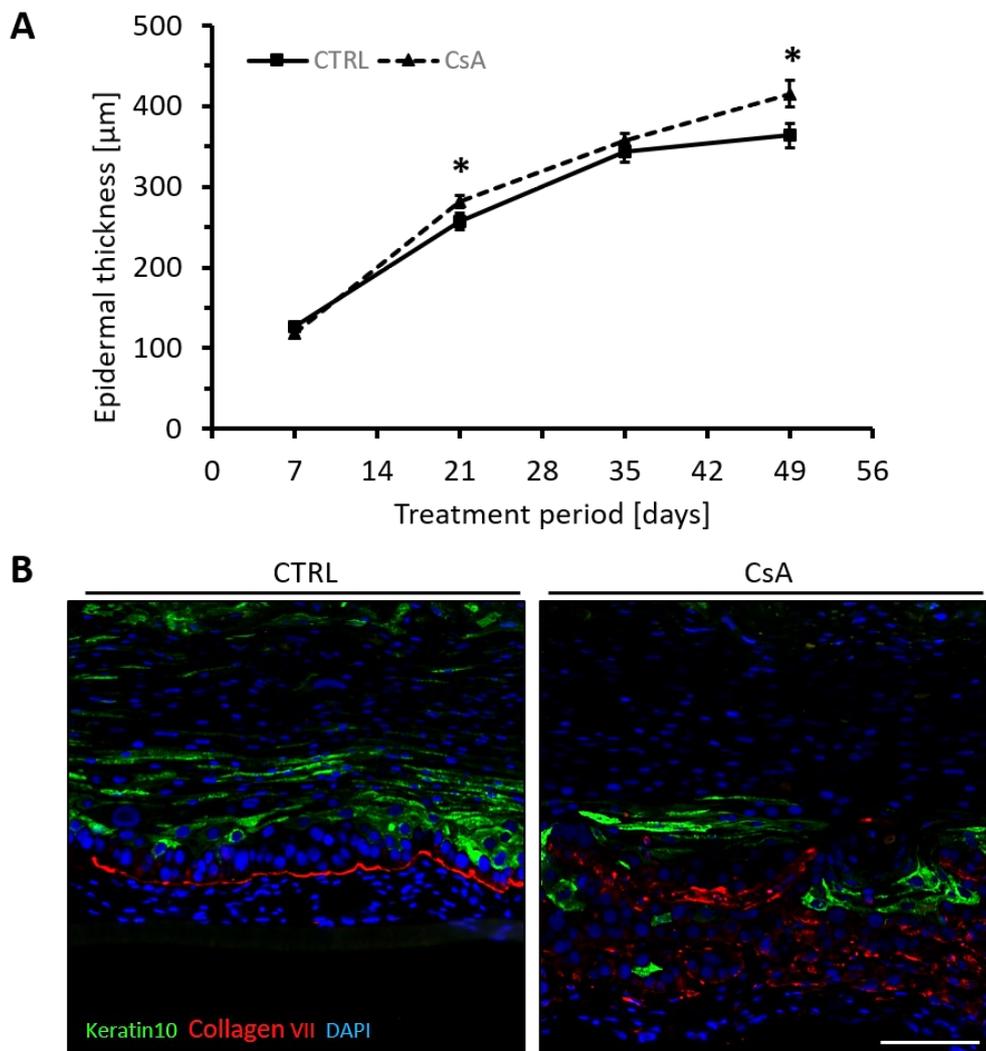


***Figure 4.4 – Detailed overview on selected CsA effects on HaCaT-OTCs:*** *The epidermal thickness of HaCaT-OTCs was monitored over a CsA treatment period of 49 days (A). Cryosections of HaCaT-OTCs treated with CsA for 49 days were stained for Keratin-10 and Collagen VII (B). The error bars represent the standard error mean; * = p-value < 0.05; n=3; The scale bar represents 100 μm.*

Especially after 49 days, an enhanced presence of Coll VII could be detected within the dermal compartment. Those signals, if evaluated visually, most likely represent invading epidermal cells in the matrix which are still partially surrounded by Col VII, supporting the invasion pattern behavior observed in the histology pictures of this particular serum setup (see magnification in **Figure 4.4B**). However, only few K10 positive cells could be detected in the matrix. So, to confirm the presence of HaCaT cells in the dermal compartment, a different and more general way of labelling keratinocytes had to be chosen.
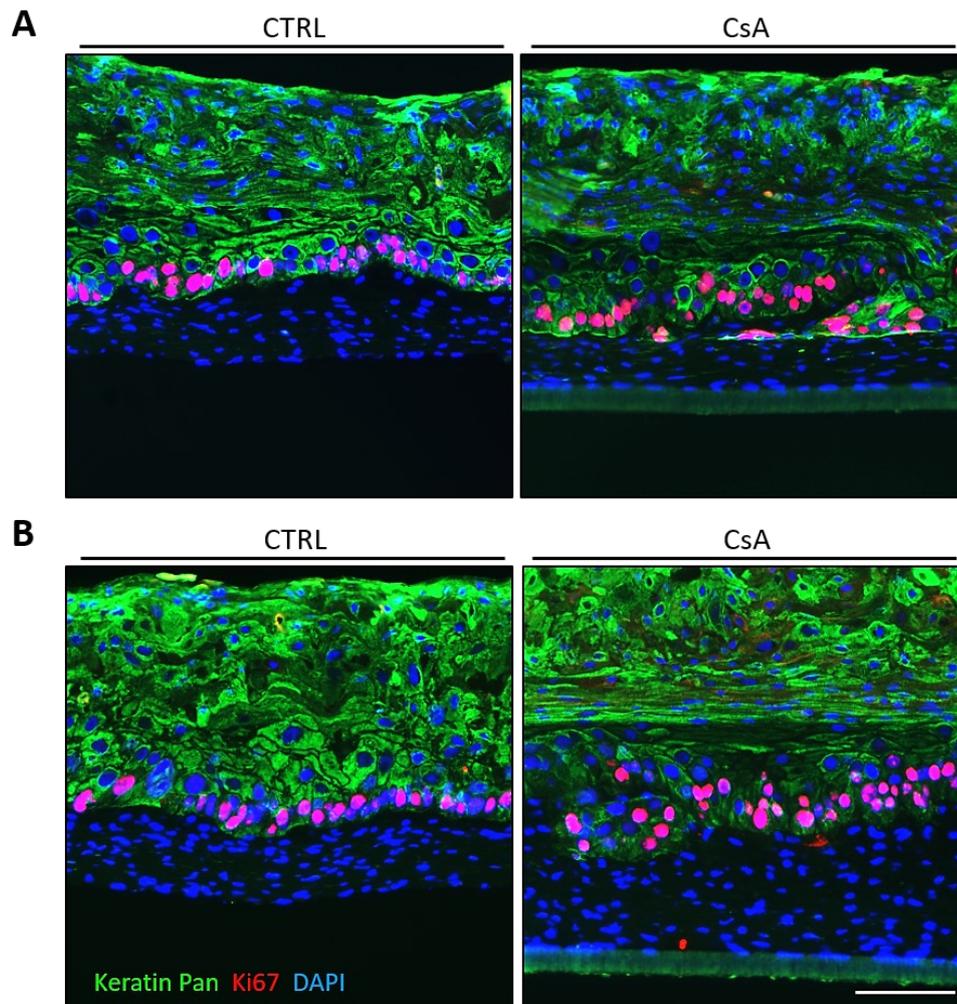


***Figure 4.5 – Modulation of epidermal structure and proliferation upon CsA treatment in HaCaT-OTCs:*** *Samples were treated with DMSO (CTRL) or 10 μg/ml CsA over a period of 21 days. IIF staining was performed on frozen sections of HaCaT-OTCs to detect the expression levels of pan-keratin as marker for epithelial cells and Ki67 as proliferation marker. Displayed are representative images of the control versus the treated samples. The OTC media was either supplemented with FBS A (A) or FBS B (B). The scale bar represents 100 μm.*

Therefore, the second staining panel included an antibody, directed against a spectrum of different keratin forms (pan-keratin). It was combined with the Ki67 specific antibody to identify effects of CsA on the proliferative behavior of the cells. As invasion was already seen after 21 days of CsA

treatment, this time point was chosen for further general analysis (**Figure 4.5**). The staining for pan-keratin confirmed the localization of HaCaT cells within the matrix. It also supported the observed changes on epithelial organization as described above. Ki67 expression was most prominent in the basal layer of both the control and the treatment group samples, but was also found within the dermal compartment of CsA treated OTCs. These cells were also positive for pan-keratin, demonstrating that the proliferative cells in the dermis are in fact invasive HaCaT cells.
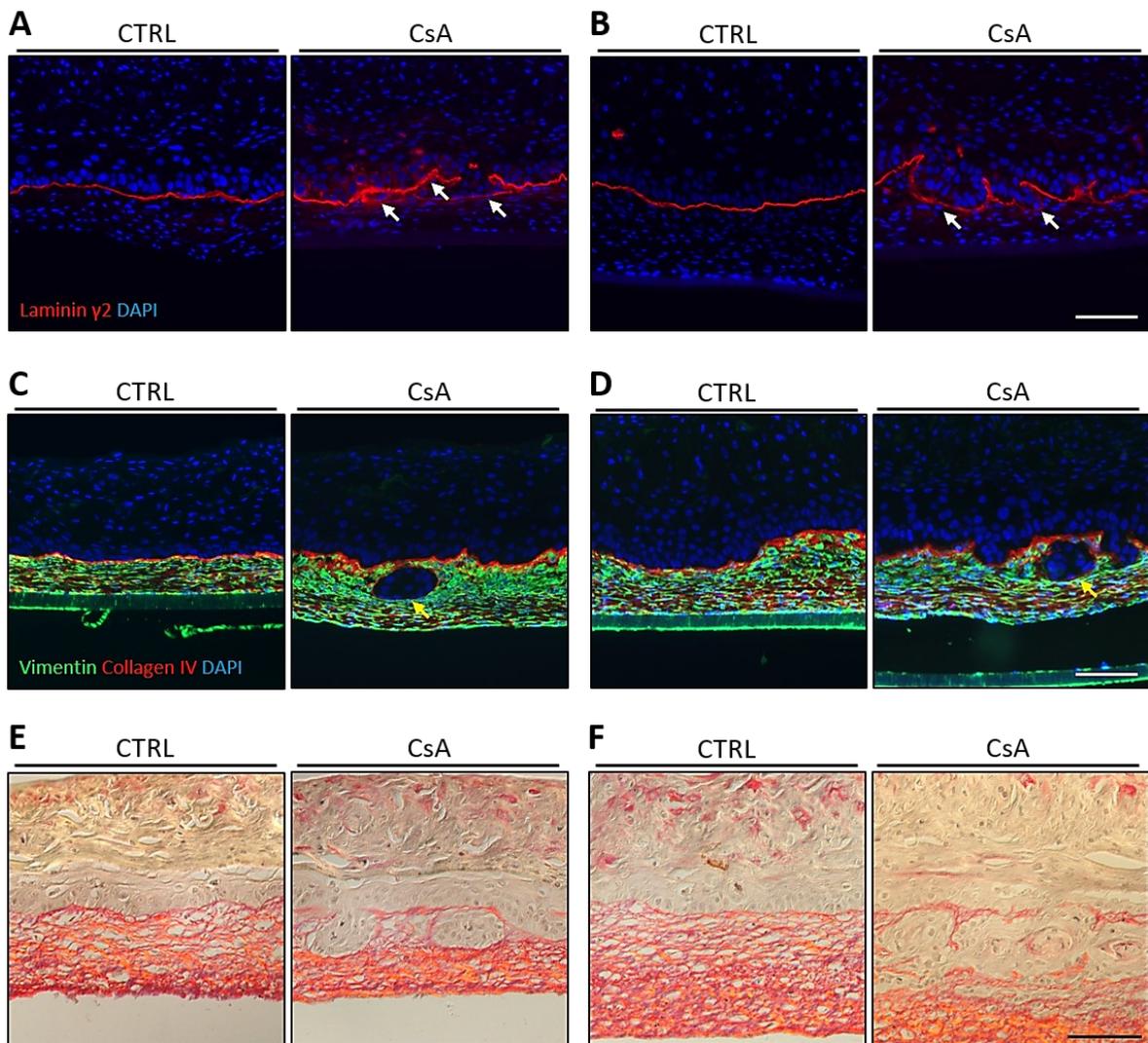


***Figure 4.6 – Effects of CsA on further BM components and the matrix in HaCaT-OTCs:** Samples were treated with DMSO (CTRL) or 10 µg/ml CsA over a period of 21 days. IIF staining was performed on frozen sections of HaCaT-OTCs to detect the expression levels of Laminin-5 (y2 chain) (A+B) and Collagen IV (C+D) as further components of the basement membrane. Further IIF staining was done to identify Vimentin as fibroblast marker(C+D). Paraffin sections were treated with picro sirius red to visualize Collagen I and III within the dermal compartment. Displayed are representative images of the control versus treated culture samples. White arrows indicate sites of Collagen VII redistribution. Yellow arrows indicate epidermal invasion "bulges". The OTC media was either supplemented with FBS A (A, C, E) or FBS B (B, D, F). The scale bars represent 100 µm.*

As CsA caused a loss of the basement membrane (BM) component Col VII, it was important to see if this effect was specific for Col VII or if also further components of the BM were affected. Therefore, sections were stained for Laminin-5 (**Figure 4.6A+B**) and Collagen IV (**Figure 4.6C+D**). A counterstaining with Vimentin as a fibroblast marker allowed distinguishing the epidermal and dermal tissues (**Figure 4.6C+D**).

In our model system, Laminin-5 forms a clear line between the dermis and the epidermis, visible here in the control samples (**Figure 4.6A+B**). Upon CsA treatment this structure got disrupted, especially at sites of ongoing invasion. But, unlike the CsA effect on Col VII, the protein amount was barely reduced. Instead Laminin-5 was forming local "cloud"-like signals (indicated by white arrows), surrounding the invading cells.

Another BM component, Collagen IV (Col IV), was only partially affected by CsA (**Figure 4.6C+D**). It showed a highly abundant expression in both BM and the matrix of the control samples and was only absent at the front of invasive buds upon CsA treatment (indicated by yellow arrows). Its high abundance in the matrix is a known artifact in the specific *in vitro* model caused due to its scaffold-free fabrication.

Within the epidermal invasion buds, no vimentin could be detected, indicating the absence of fibroblasts. However, the treatment seemed to cause a morphological change among the fibroblasts surrounding these buds. In the control samples the dermal fibroblasts showed an elongated cell shape and were spread regularly throughout the matrix. Upon treatment with CsA the fibroblasts started to round up and appeared particularly dense in the upper part of the dermal equivalent and around the invasive buds.

An additional histochemical staining with picro sirius red supported the observation of a change in dermal organization (**Figure 4.6E+F**). This staining provides an overview of collagen fibers and illustrates their position as well as thickness. While collagens were well distributed over the entire matrix in the control samples, CsA caused a restriction and accumulation of mainly the thick collagen crosslinks (highlighted in the staining in orange) to the lower part of the dermal compartment. This effect was most prominent in the serum B setup. Here only thin red fibers remained between the invading epidermal cells, indicating a significant degradation and thus weakening of the matrix meshwork.

In summary, CsA caused an improved epithelial organization of the HaCaT-OTCs. In addition, CsA promoted the invasion of HaCaT cells into the dermal compartment by causing degradation of the basement membrane and weakening of the dermal matrix. Although the principal outcome of CsA treatment was similar in both sera, the effects were most prominent in cultures supplemented with serum B. Therefore, this serum was used for all following studies.

## 4.3. Combinatorial CsA and sunlight effects on HaCaT-OTCs

As CsA-promoted cutaneous cancer formation is mostly arising at sun exposed sites of the human skin, sunlight appears to be a necessity for those lesions (Bavinck et al., 1993; Espana et al., 2000). Although the circumstances of sunlight exposure could be partially represented with a model system carrying already UV induced predisposed damage, we wanted to see if studies including an additional irradiation of the OTCs lead to a similar or different outcome. To allow an optimal modeling of the physiological and environmental conditions we decided to conduct the irradiation sequences with a radiation source, representing the combined sunlight spectrum in range from 270 nm to 1,200 nm. This selection, further referred to as "SUN", represents those parts of the sunlight spectrum (UVB, UVA, VIS, and IRA) that are crossing the atmosphere and penetrating the skin barrier of the human body. Detailed information on radiation source as well as the irradiation routine is given in **Chapter 3.3.3**.
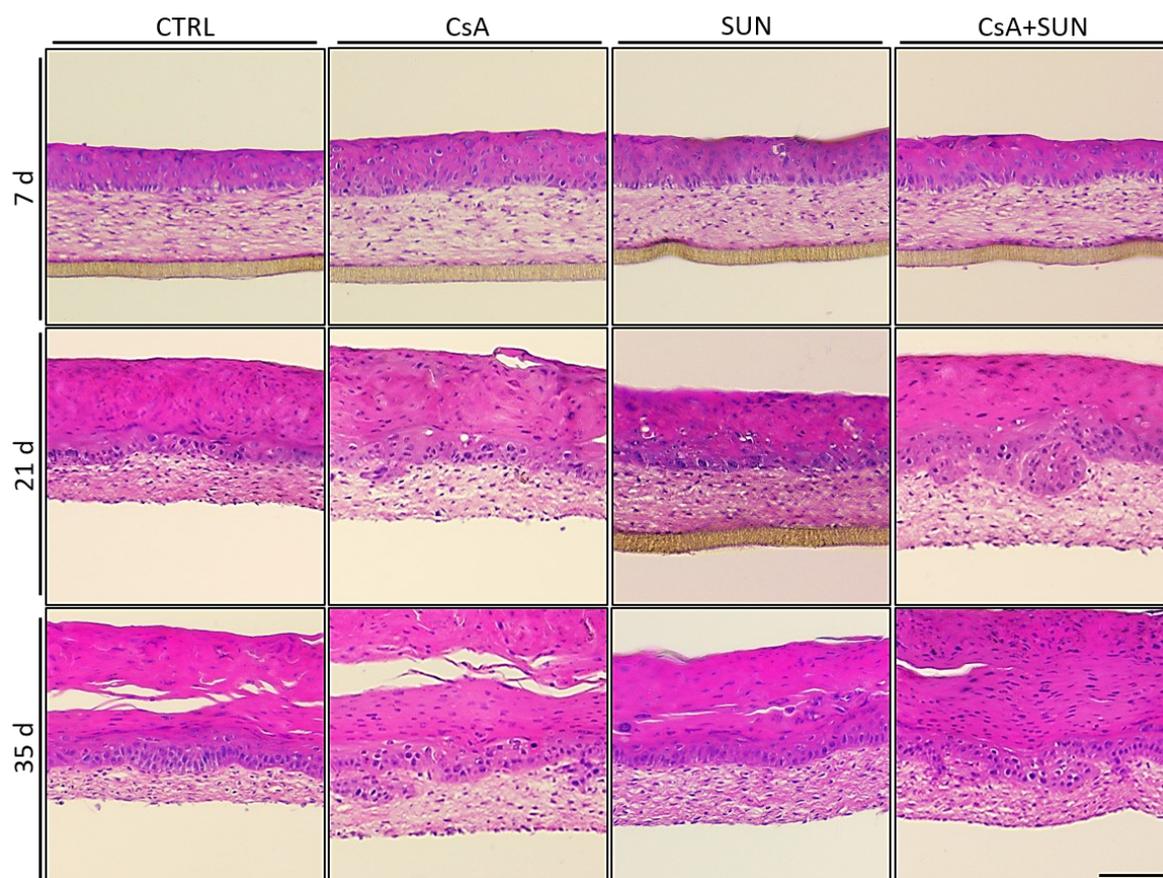


***Figure 4.7 – Morphological changes upon CsA and SUN treatment in HaCaT-OTCs:*** *Samples were treated with DMSO (CTRL) 10 µg/ml CsA or 0.65 MED SUN or a combination of both (CsA+SUN) over a period of 35 days. H&E staining was performed on paraffin-sections of the HaCaT-OTCs. Displayed are representative images of the control versus treated cultures. The scale bar represents 100 µm.*

Having already established a CsA responsive model with the HaCaT-OTCs, we next performed a combination treatment of the HaCaT-OTCs with CsA plus SUN. Therefore, co-cultures were treated with 10 µg/ml CsA and/or 0.65 MED SUN over a period of 35 days. Histological analysis (H&E staining on paraffin-sections) revealed that, as with the previous studies, CsA alone caused an invasive behavior after 21 days of treatment (**Figure 4.7**). Irradiation on its own did not cause obvious phenotypic changes, i.e. no signs of invasion could be detected compared to control. Combinational treatment with CsA and SUN caused a similar phenotype as CsA only, with multiple invasion sites visible after 21 and 35 days. Thus, chronic SUN exposure did not seem to interfere with the CsA response, neither by inhibiting, nor accelerating the invasion of the HaCaT cells.

In accordance with the invasive phenotype, staining for Col VII demonstrated a marked degradation of this BM component in cultures treated with CsA alone or in combination with SUN. The Collagen VII structure was entirely degraded under both treatment conditions, while present all along the BM zone in the control and the solely SUN-exposed cultures (**Figure 4.8A**).
Collagen IV expression, on the other hand, and as shown above, was only partially affected by CsA and a combination with SUN did not change the outcome (**Figure 4.8B**). The BM-like structure got deformed around the epidermal invasion buds and at their tips Col IV presence was either reduced or entirely absent.
The fibroblasts around those bulges had the same rounded shape as observed before. Samples which underwent only irradiation showed neither a change in BM, nor in dermal fibroblast organization, compared to the control samples.

As described above, a staining for K10 revealed an expression of the protein over the entire epidermis for the controls (**Figure 4.8A**). An exposure to SUN alone did not change this pattern. However, a treatment with CsA alone or in combination with SUN caused a restriction of the keratin to the suprabasal layers, indicating a reorganization and normalization of K10 expression.

In the picro sirius red stainings the previous observations for the CsA treatment were also confirmed and similar results were seen with the combination of CsA and SUN, which led to a change in the matrix structure (**Figure 4.8C**). Especially around the invasion sites the meshwork became wider and thinner crosslinks and fibers were visible. The radiation alone also caused a looser structure, although this effect was much weaker, compared to the one seen in the CsA treated samples.
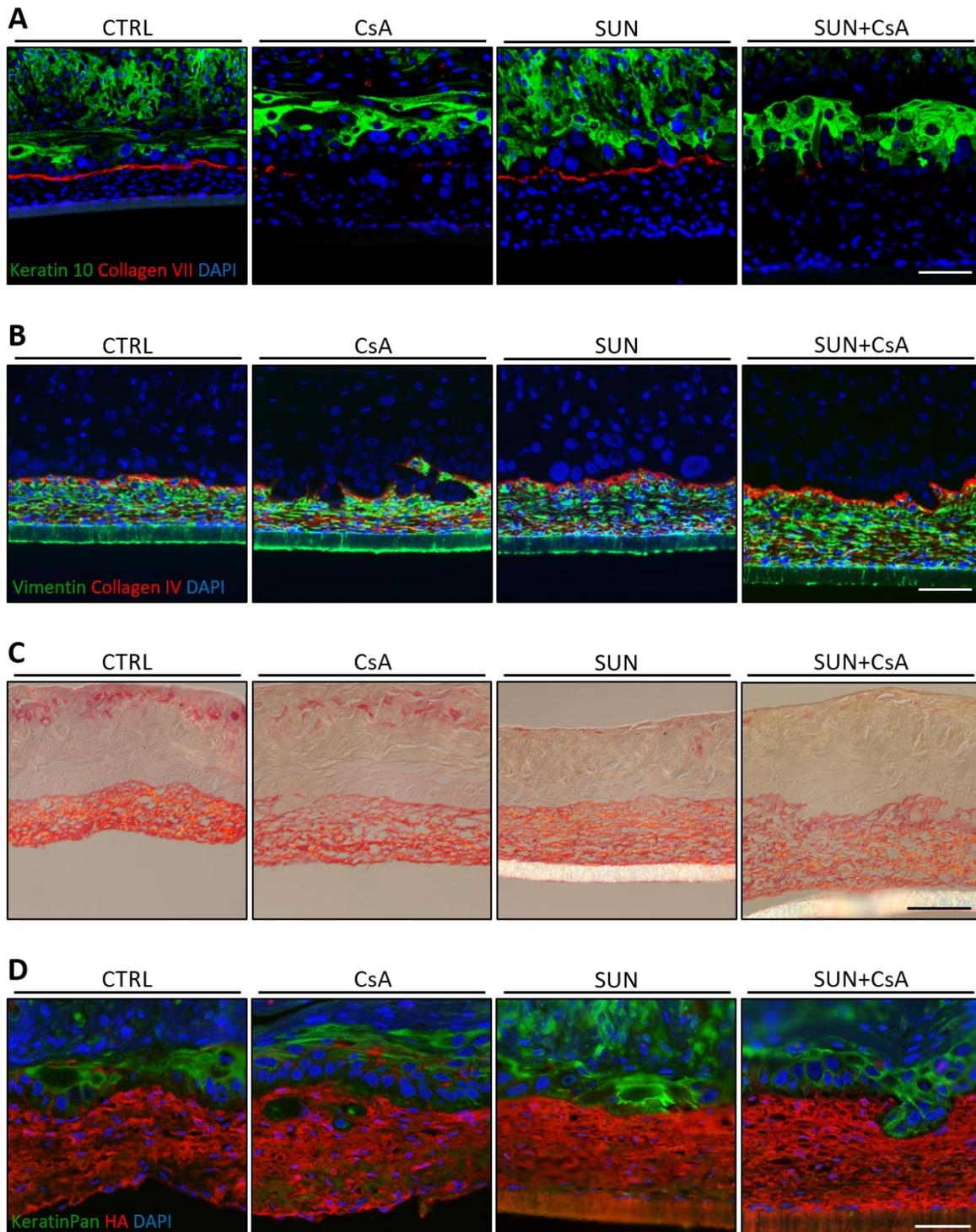
***Figure 4.8 – Effects of CsA and SUN on the epidermal and dermal structure in HaCaT-OTCs:***
*Samples were treated with DMSO (CTRL) 10 µg/ml CsA or 0.65 MED SUN or a combination of both (CsA+SUN) over a period of 21 days. IIF staining was performed on frozen sections of HaCaT-OTCs to detect the expression levels of K10 and Collagen VII (A), Vimentin and Collagen IV (B). Paraffin sections were treated with picro sirius red to visualize Collagen I and III (C) or stained for hyaluronic acid (HA) and Pan-keratin (D). Displayed are representative images of the control versus treated cultures. The scale bars represent 100 µm (A-C) or 50 µm (D).*

Due to the clear changes seen in the collagen meshwork, we next looked into whether CsA or the combination of CsA and SUN would also influence the presence of hyaluronic acid (HA), a glycosaminoglycan present in the inter-collagen spaces and responsible for skin hydration. (**Figure 4.8D**). The staining was done in cooperation with Dr. Daniel Gorski from the research group of Prof. Dr. Jens Fischer at the Institute for Pharmacology at the Heinrich Heine University, Düsseldorf. However, HA was present in abundance over the entire dermal compartment under all different treatment conditions and neither CsA nor the irradiation with SUN caused obvious changes or local rearrangements. Even in direct proximity to the invasion sites, HA stayed equally distributed.

Finally, we examined the proliferative behavior, especially among the epidermal cells, during the individual treatment procedures. For this, frozen sections were stained with antibodies directed against pan-keratin and Ki67 to detect all HaCaT cells and investigate their proliferative behavior (**Figure 4.9A**). Ki67-positive cells were frequently detected in the basal layer of the epithelia of all samples. In the CsA and CsA+SUN treated samples Ki67-positive cells were also seen in the invasive buds. Conspicuous was the increased number of ki67-positive cells in the basal layer directly above the invasion sites in the CsA and CsA+SUN samples. However, the quantification of these signals revealed a highly significant increase in proliferative cells only with the combined treatment of CsA and SUN (**Figure 4.9B**).

In summary, many of the effects seen upon treatment with CsA alone were also detected after a combination with SUN. The combination was also causing a normalization of K10 expression, a rearrangement of the matrix components and a similar level of invasion as seen with CsA alone. In addition, the combined treatment also caused a boost in proliferation by approximately 50%. This suggests that solar irradiation indeed plays an additional role in increasing proliferation and by that may contribute to tumorigenicity.
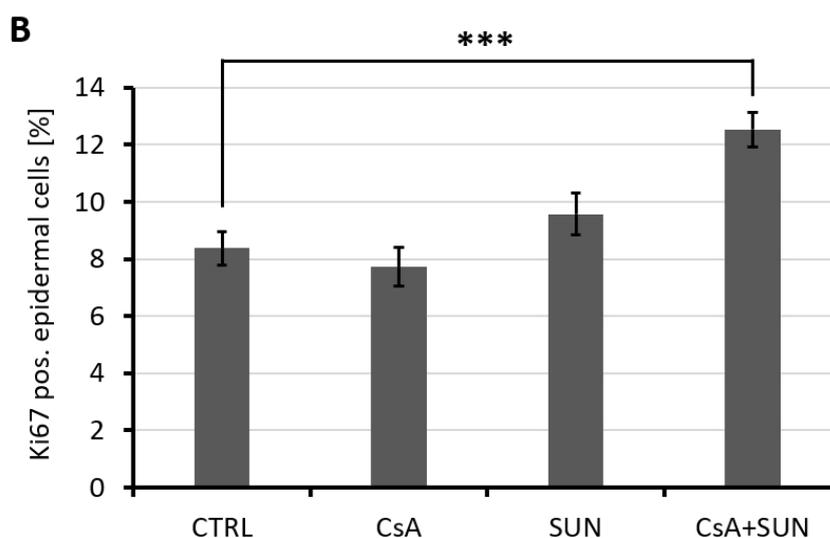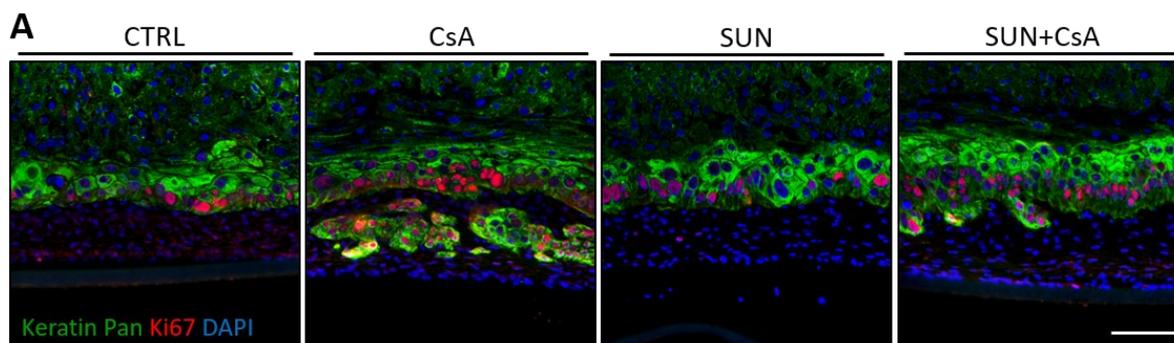
***Figure 4.9 – Modulation of proliferation upon CsA and SUN treatment in HaCaT-OTCs:*** *Samples were treated with DMSO (CTRL), 10 µg/ml CsA or 0.65 MED SUN or a combination of both (CsA+SUN) over a period of 21 days. IIF staining was performed on frozen sections of HaCaT-OTCs to detect the expression levels of Pan-keratin as keratinocyte marker and Ki67 as proliferation marker. Displayed are representative images of the control versus treated cultures (A). The scale bar represents 100 µm. The images were also used to determine the relative amount of Ki67 positive cells among all epidermal cells (B). The error bars represent the standard error mean; \*\*\* = p-value < 0.0005; n=3*

## 4.4. The combinatorial CsA and sunlight effects on NHEK-OTCs

Although HaCaT is a well-established model system for epidermal studies, its genetic predispositions limits its comparability to the actual physical situation in the human body. To determine whether the same effects of CsA on epidermal and dermal organization can also be detected in OTC systems without significant genetic predispositions, cell derived matrices (CDMs) were combined with normal human epidermal keratinocytes (NHEK), i.e. primary keratinocytes, and the same treatment conditions as described above were applied. Also, in contrast to HaCaT-OTCs, cocultures carrying NHEK can be cultivated for up to six months and thus also allow to assay for long-term effects. Therefore, the treatment period was extended to 70 days. After this period, histological examination was performed in order to identify putative morphological effects of the treatments (**Figure 4.10**).
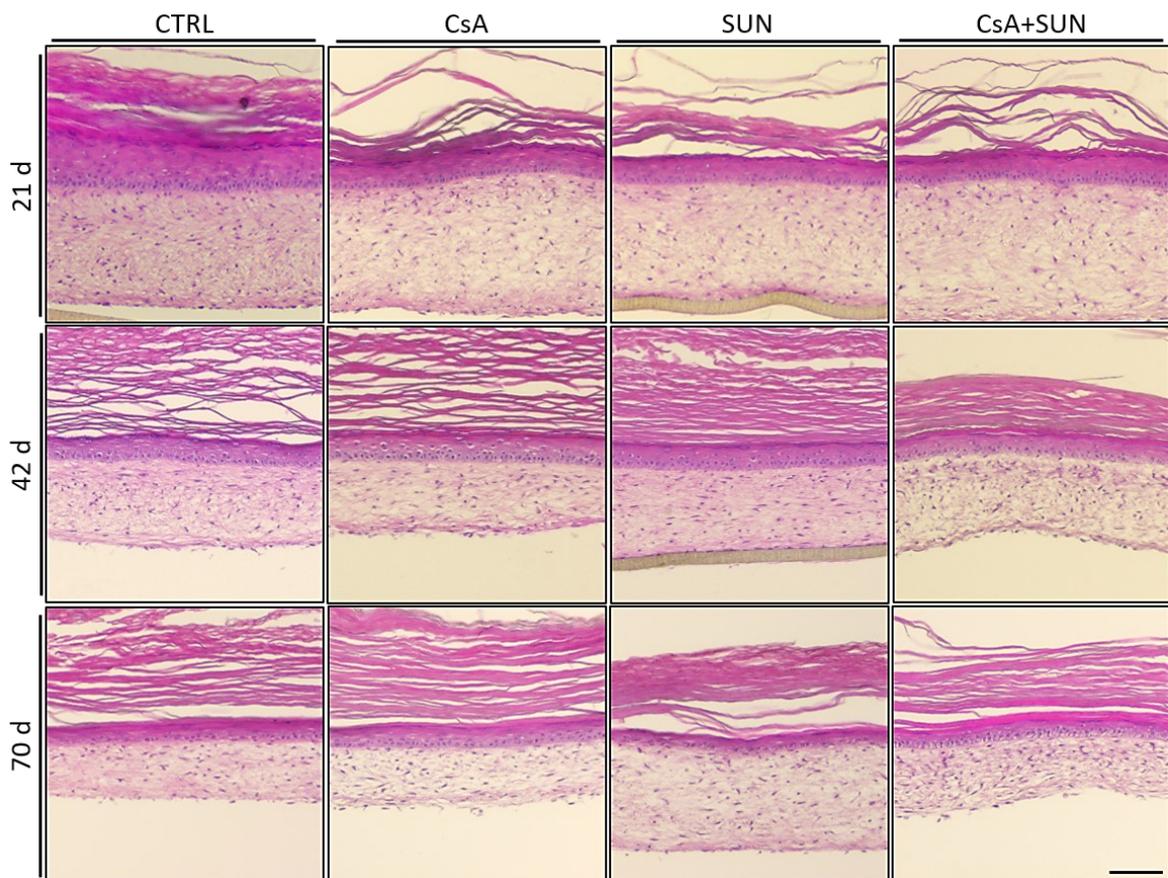


***Figure 4.10 – Morphological changes upon CsA and SUN treatment in NHEK-OTCs:*** *Samples were treated with DMSO (CTRL), 10 µg/ml CsA or 0.65 MED SUN or a combination of both (CSA+SUN) over a period of 70 days. H&E staining was performed on paraffin-sections of the NHEK-OTCs. Displayed are representative images of control samples versus treated cultures. The scale bar represents 100 µm.*

In the epithelium, no significant differences could be seen between the individual treatment conditions and the control cultures. All the samples showed an ongoing process of epidermal differentiation. However, after 42 days, a treatment with CsA alone and in combination with SUN caused changes in the dermal structure. The control and the solely SUN irradiated samples showed a smooth and even pink staining all over the matrix. In contrast, for CsA and CsA+SUN the signals got concentrated to bundle structures resulting in a higher contrast between the bundles and the background.
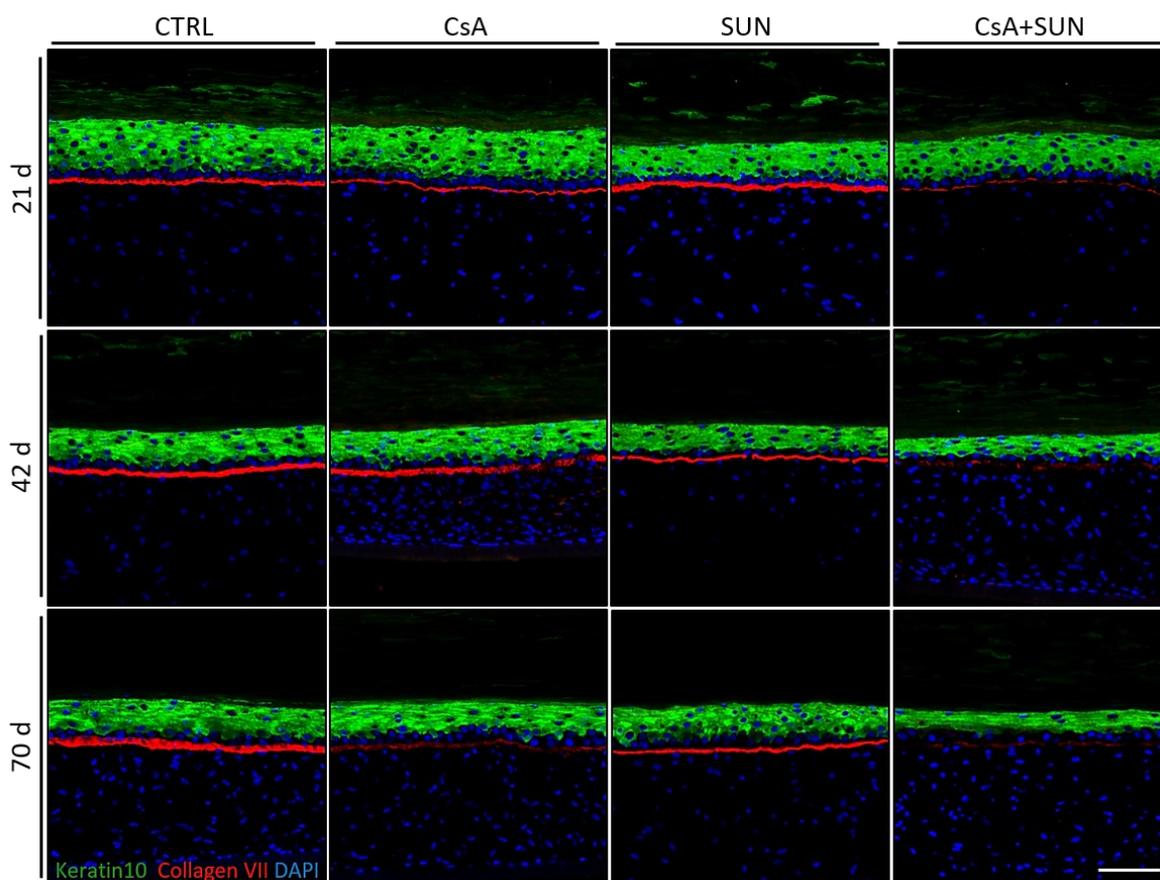


*Figure 4.11 – Effects of CsA and SUN on the epidermal and basement membrane structure in HaCaT-OTCs: Samples were treated with DMSO (CTRL), 10 µg/ml CsA or 0.65 MED SUN or a combination of both (CsA+SUN) over a period of 21 days. IIF staining was performed on frozen sections of HaCaT-OTCs to detect the expression levels of K10 and Collagen VII. Displayed are representative images of the control versus treated cultures. The scale bar represents 100 µm.*

To allow a better visualization of the epidermal and dermal characteristics of the NHEK-OTCs, different staining panels were applied. First, frozen sections were stained for K10. This antibody, together with one directed against Collagen VII, allowed an evaluation of the epidermal organization and a first impression of the basement membrane (BM) integrity (**Figure 4.11**).

The expression pattern of K10 was comparable for all treatment conditions, meaning that all suprabasal cells were K10-positiv. However, the combinational treatment caused a thinning of the epidermis and flattening of the individual cell layers after 70 days.

Like in the HaCaT-OTCs, CsA supplementation caused a continuous time-dependent decrease in Col VII. But even after 70 days of treatment some protein was present, decorating the BM zone suggesting for a still intact BM. In combination with SUN, however, the expression of Col VII was already significantly reduced after 3 weeks and hardly visible later on. This may suggest for an additive effect of CsA and SUN on the regulation of Col VII.

A second staining panel directed against Collagen IV as additional BM marker did not reveal a reduction of the protein upon CsA or SUN treatment. On the contrary, Col IV presence appeared increased at the BM zone after 42 and 70 days in both the CsA and CsA+SUN treated cultures (**Figure 4.12A**).

Similar as in the HaCaT-OTCs, supplementation with CsA caused a morphological change in the vimentin expressing fibroblasts. The cells became bigger and adapted a more circular shape. In approximately half of the samples a condensation of the matrix was observed. The irradiation with SUN caused no morphological change of the fibroblasts and also a shrinking of the matrix was never observed. Instead, the number of cells in the dermal compartment appeared to be reduced after long-term irradiation (70 days). The combinational treatment was leading to a similar outcome as with CsA alone. The fibroblasts became bigger and adapted a more rounded shape. But the matrix kept its size and the number of cells remained constant (**Figure 4.12A**).

The pikro sirius red staining gave similar information about the dermal matrix. Treatment with CsA led to a shrinking of the matrix and a loss of collagen fibers in several cultures. A combination with SUN irradiation resulted in a similar phenotype as with CsA alone but also the space between the fibers did increase, causing the formation of big gaps in the collagen meshwork, suggesting that the additional sunlight was leading to a distension of the matrix. SUN irradiation alone had no effect on the collagen structure indicating the importance of a combination of CsA and SUN for the induction of the matrix rearrangement (**Figure 4.12B**).

The distribution of hyaluronic acid (HA) was affected under all three treatment conditions. While control samples showed a strong and even HA expression, small HA free gaps could be seen in the CsA treated as well as SUN irradiated samples compared to the control. With the combination treatment this effect increased, leaving a matrix with numerous small but also large HA-free gaps. (**Figure 4.12C**). Although quantification has yet to be performed (by investigating more experiments), the above data suggests a role for CsA and SUN, and in particular for their combination, in modulating the HA matrix.
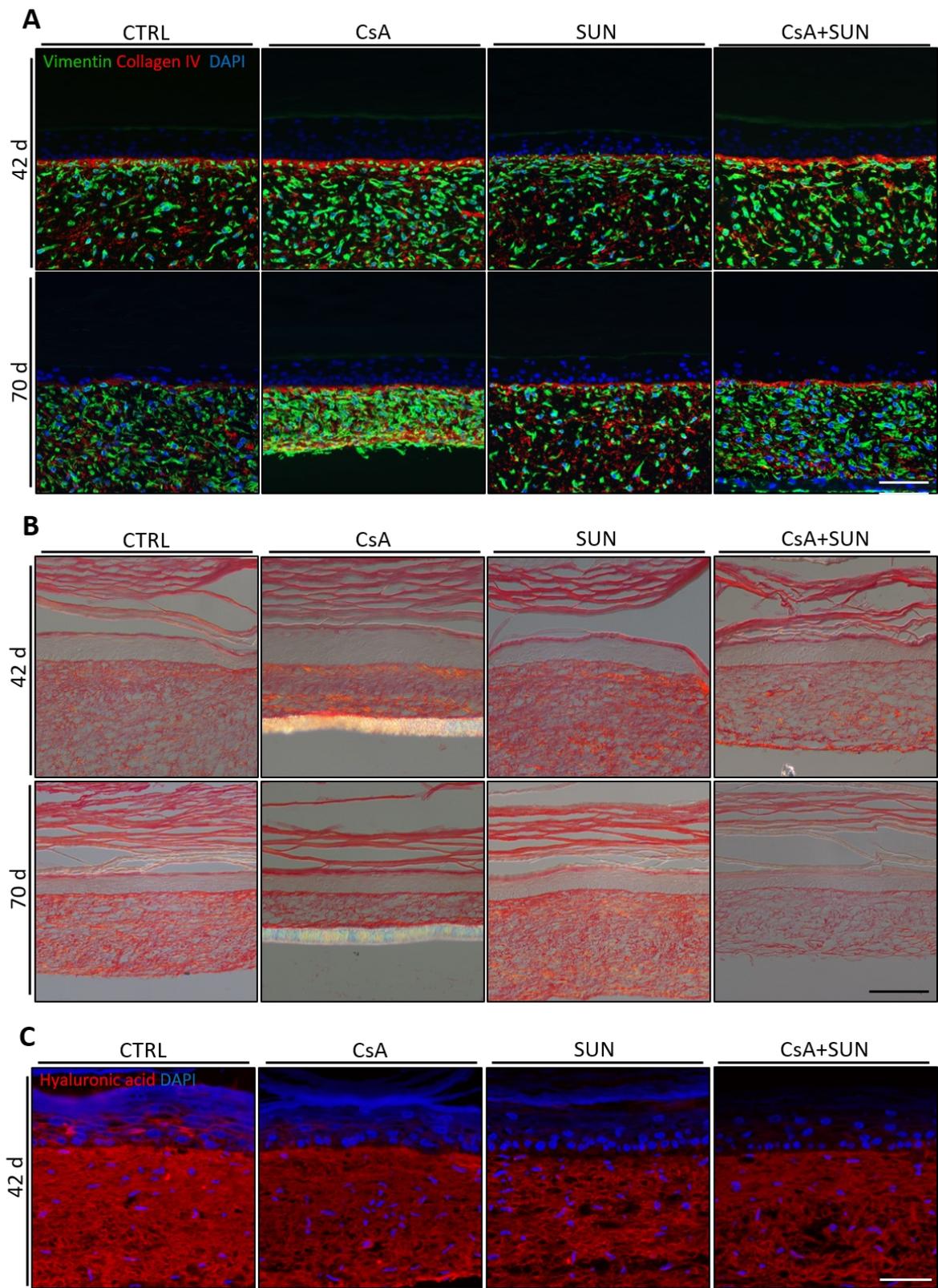
***Figure 4.12 – Effects of CsA and SUN on the dermal structure in NHEK-OTCs:*** *Samples were treated with DMSO (CTRL), 10 µg/ml CsA or 0.65 MED SUN or a combination of both (CsA+SUN) over a period of 42-70 days. IIF staining was performed on frozen sections of the OTCs to detect the expression levels of Vimentin and Collagen IV (A). Paraffin sections were treated with picro sirius red to visualize Collagen I and III (B) or stained for hyaluronic acid (HA) (C). Displayed are representative images of control samples versus treated culture. The scale bar represents 100 µm (A-B) or 50 µm (C).*

In summary, CsA as well as CsA plus SUN had little effect on epidermal morphology. But the CsA treatment caused reduced expression of Col VII and the combination with SUN led to an almost complete loss of this BM component. In contrast, the expression of Col IV appeared to be boosted by both treatment conditions. Both CsA and SUN treatment had a strong effect on the dermal compartment. CsA caused a change of fibroblast morphology and a reduction of collagen fibers as well as matrix condensation, while the combination with SUN led to a destruction of the matrix meshwork. HA production seemed to be reduced by all treatment conditions, although this effect was strongest with the combinatorial treatment, suggesting for their synergistic action on HA expression.

## 4.5. Donor response differences to CsA

To explore interpersonal differences in the response to CsA and irradiation treatment, we repeated the OTC experiment but this time included NHEK from an additional adult donor. "NHEK 1" is the same keratinocyte source used in the experiments above and "NHEK 2" is the new one. Initial experimental plans also included a third donor, but for this NHEK source the keratinocytes failed to create a stable attachment between dermal matrix and thus to develop a viable epithelium (data not shown). Therefore, these cultures were excluded from the later analysis and focus was set on the NHEK1 and NHEK2 based OTC systems.

The co-cultures were treated for 42 days as most of the described effects could be seen already at this time point. Histology confirmed, that for both OTC systems none of the treatments had any effect on the epidermal organization. Under all conditions the epidermis remained stratified and well differentiated with a massive stratum corneum. Similar changes in stuctures as described above were also observed in the matrix (**Figure 4.13A**).

Next we applied a staining panel directed against Keratin 10 and Collagen VII (**Figure 4.13B**). The analysis of Col VII confirmed the role of CsA in regulating its expression. Treating the cultures with CsA caused a significant reduction of the protein in both the NHEK 1 und NHEK 2 OTCs. Similarly, co-treatment with CsA and SUN resulted in a severe reduction of Col VII.

For both OTC systems an even K10 expression in all suprabasal cells and a similar epidermal structure under all treatment conditions was detectable. This confirms the observation from above that CsA and SUN seem to have only little effect on the epidermal morphology of the NHEK-OTCs.
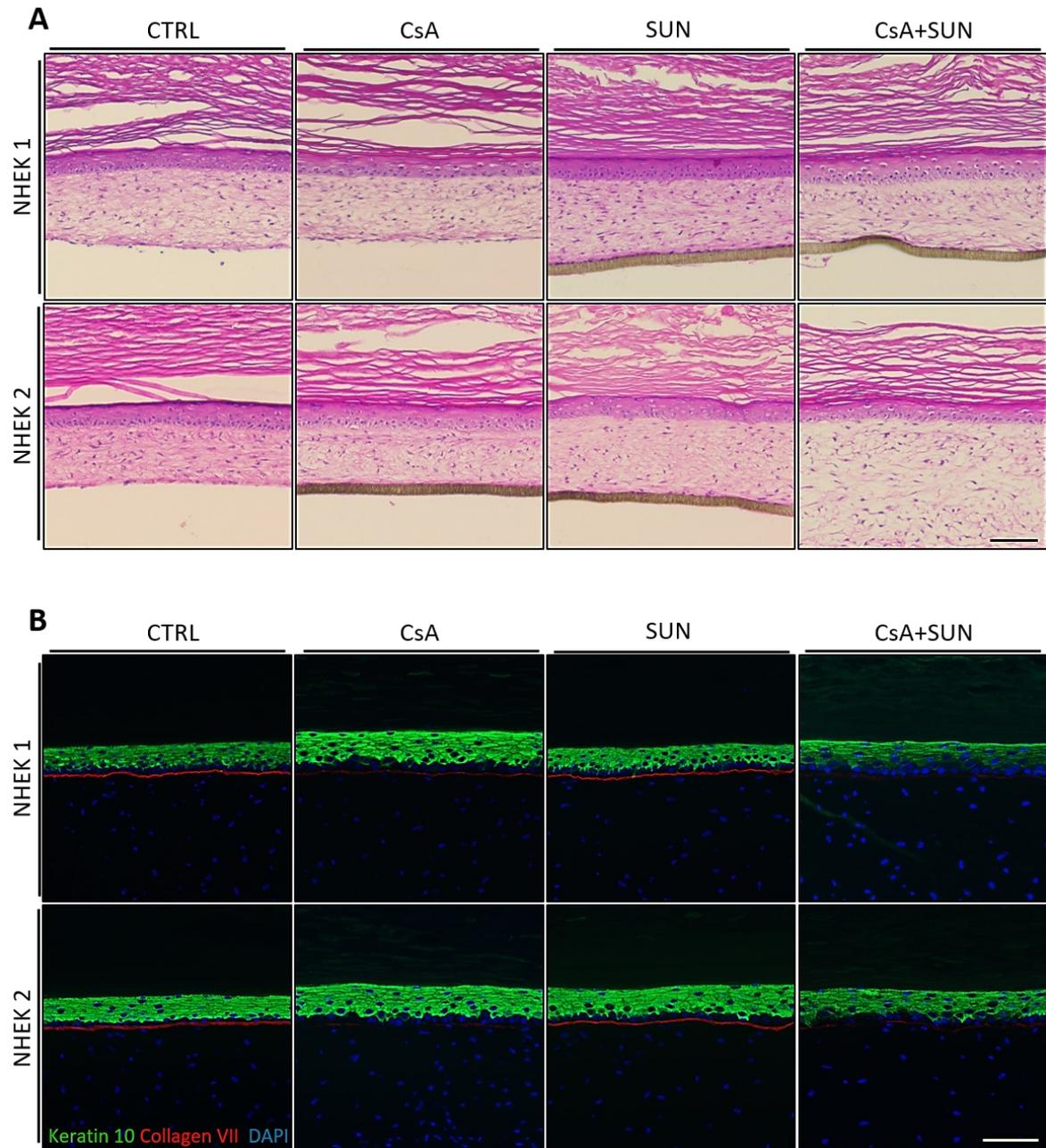
***Figure 4.13 – Comparison of CsA and SUN effects for NHEK-OTCs of different donors:*** *Individual CDMs were loaded with keratinocyte of two different donors (NHEK1 and 2). The OTCs treated with DMSO (CTRL), 10 µg/ml CsA or 0.65 MED SUN or a combination of both (CsA+SUN) over a period of 42 days. H&E staining was performed on paraffin sections to investigate for morphological changes (A). IIF staining were performed on frozen sections of the OTCs to detect the expression levels of K10 and Collagen VII (B). Displayed are representative images of treated cultures versus the control samples. The scale bar represents 100 µm.*

## 4.6.  Microarray analysis on gene expression

Additional to the morphological and protein based long-term responses of CsA we were interested in understanding the mechanistical effects caused by this immune suppressant on the HaCaT-OTCs. Thus, we conducted two sets of gene expression microarrays. One was aiming for the investigation of changes in gene expression levels in the epidermal compartment and the other on changes in the dermal compartment. The samples used for this analysis were described in **Chapter 4.2**. To also allow for a better evaluation of serum effects, both experimental setups (supplementation with serum A and B) were included. The arrays were conducted by the Genomics and Proteomics Core Facility of the German Cancer Research Center. Dr. Maria Herberg and Dr. Jörg Galle at the Interdisciplinary Centre for Bioinformatics in Leipzig assisted with the subsequent analysis of the array results.

### 4.6.1. Epidermal gene expression pattern

The array results were initially used for a sample similarity analysis. This allowed for an evaluation of the comparability of the treatment replicates and a first assessment of the serum effects. During this procedure all samples were compared to each other based on their gene regulation pattern and then positioned in a "correlation spanning tree" within a two-dimensional frame (**Figure 4.14A**). All samples from the control group were sorted in the upper right corner in direct proximity to each other, indicating many similarities in their gene regulation patterns. Correspondingly, all CsA treated samples could be found in the lower left corner. However, here the distance between the marks was bigger compared to the control group, demonstrating a higher deviation between the CsA treated samples. This clustering indicated a clear change in gene expression upon CsA application. An additional serum dependent organization of the samples within the frame was not observed, indicating that the choice of serum only had a minor impact on the gene regulation.

Following this first part of scrutiny, the samples were further analyzed using the OposSOM based Distance map cluster (D-Cluster) approach to obtain a collection of all functional gene sets, regulated upon CsA application. This analysis resulted in a self-organizing map (SOM) which indicated three gene clusters (spots) as the most relevant ones (**Figure 4.14B**). Each spot represented a different gene regulation pattern and two of them had a pattern which showed a dependency on the CsA treatment. Spot #1 represented genes that appear to be upregulated upon CsA application (**Figure 4.14C**), Spot #3 enclosed genes which were downregulated in all treated samples (**Figure 4.14D**).
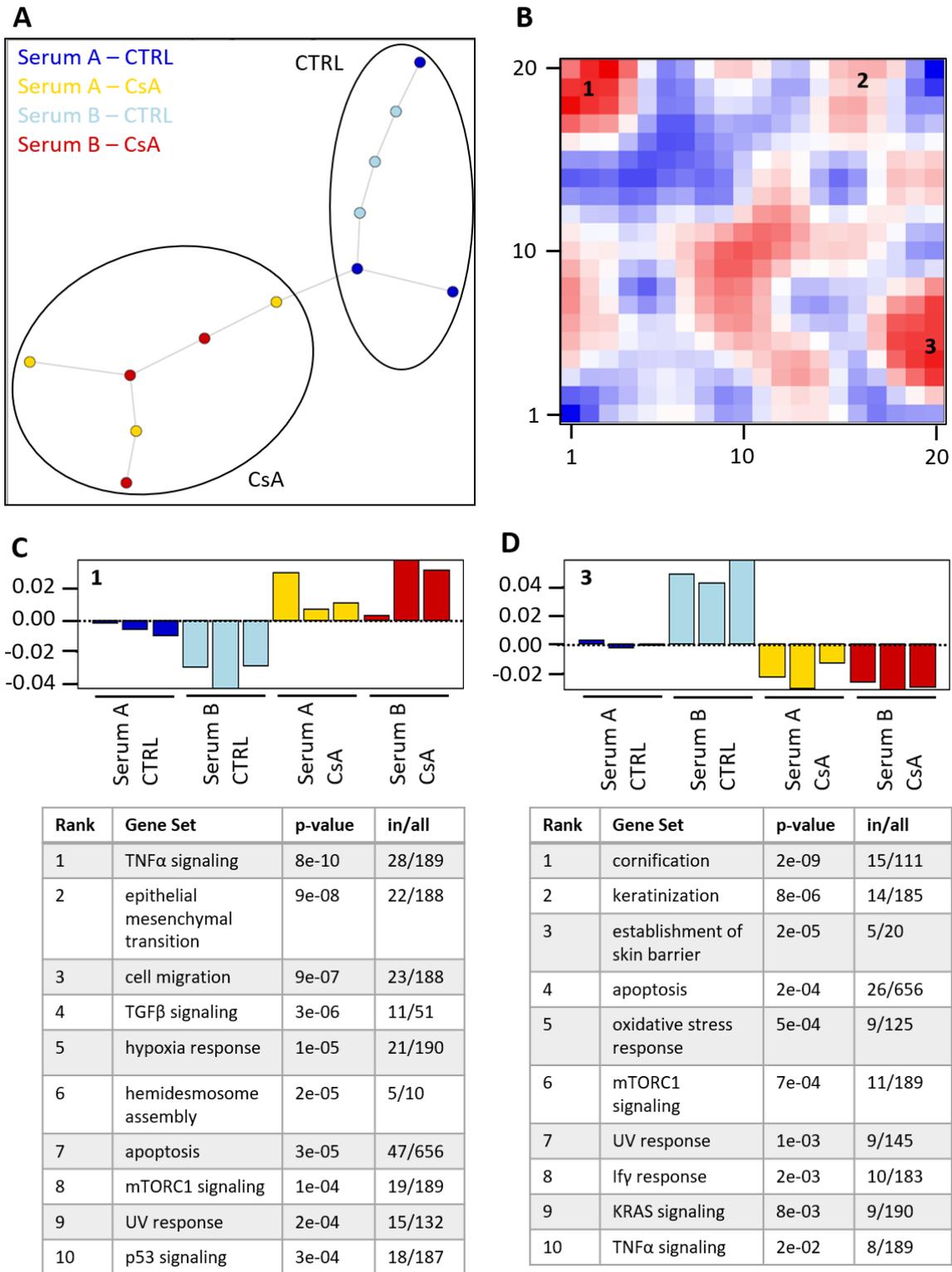
**Figure 4.14 – Epidermal gene expression microarray:** *(A) To demonstrate the comparability between the treatment replicates, the array results were included in a correlation spanning tree. Each mark represents one sample. Close marks had similar and distant marks had different array results. (B) Potentially relevant gene sets were identified by applying a D-Cluster analysis over all samples. In the resulting SOM each pixel represents a group of genes sharing the same regulation pattern (metagene). In red areas metagenes with a similar regulation pattern clustered, blue areas illustrate metagenes with different regulation patterns. The numbers represent those metagene clusters (spots) with the highest relevance. (C) The regulation patterns of spot #1 (C) and of spot #3 (D) and a list of the most significant gene sets found in these spots are demonstrated underneath.*

The results indicated a downregulation of several genes related to the establishment of skin barrier, cornification and keratinization. Among these was also the gene coding for K10. The IIF staining directed against this keratin did not show a reduced K10 presence upon CsA treatment, indicating that the changes in gene regulation did not necessarily lead to a change in the expression of these differentiation related proteins. However, the morphological analysis displayed a clear change in epidermal organization and a normalization in differentiation, suggesting a mechanistical regulation of these processes by CsA.

Many genes known to be involved during epithelial mesenchymal transition (EMT) and cell migration appeared to be upregulated. These results go hand in hand with the morphological observations described above, demonstrating an invasive behavior after CsA treatment.

When focusing on the EMT gene set, many different BM components like Laminin subunits appeared affected. This included an upregulation of the subunits α3, β3, γ2. Together they form Laminin-332, also known as Laminin-5. The results from the IIF staining illustrated a degradation of the Laminin-5 structure at the invasion sites. But the signal intensities at the BM zone did not get reduced. Also, the staining revealed the formation of local strong signals for the protein close to lose BM zone and in the proximity of the invasion sites. Thus, it appeared that parallel to the CsA induced BM degradation, Laminin-5 became upregulated, allowing for a "relining" of laminin around the invading epithelial buds.

Interestingly, a regulation of the expression of Collagen IV and in particular Collagen VII was not seen in the microarray. This indicated that the loss of Col VII, as one of the molecular characteristics of CsA treatment, was not a direct regulatory consequence of CsA but is likely to be regulated post-transcriptionally in a yet unknown fashion. Of the known BM destabilizing proteases only MMP-1 appeared upregulated.

Further affected function pathway clusters were hypoxia response, oxidative stress response and UV response. Also, the process of hemidesmosomes to assembly was upregulated, indicating a stronger connection between keratinocytes and BM. A closer look on this particular gene set demonstrated an upregulation of the previously described Laminin subunits as well as of the tetraspanin CD151 and Integrin α6.

Other genes of those spots were associated with signal transduction pathways like TNFα, TGFβ, mTORC1, Ifγ, KRAS or the p53 pathway. Genes related to TNFα signaling or the mTOR pathway were even found in both investigated metagene clusters. All these pathways are known to be involved in tumor formation and therefore could be involved in the invasive phenotype induced by CsA in the HaCaT cells.

## 4.6.2. Dermal gene expression pattern

Like for the epidermal samples, also the dermal samples were first evaluated for comparability between the treatment replicates by applying the sample similarity analysis. Similarly, this led to an arrangement in a "correlation spanning tree" within a two-dimensional frame, according to their similarities in their gene regulation pattern (**Figure 4.15A**). All samples from the control group were sorted in the upper half of the frame and CsA treated samples in the lower, indicating principal differences in their gene expression patterns (see dashed line). However, the sample replicates did not group as well as previously seen in the epidermal data set. For the CTRL treatment, four samples grouped as a cluster in the upper right corner (blue marks highlighted with a circle) while the other two gathered on the left side of the data frame (blue marks highlighted with stars). For the CsA treatment, three samples grouped as a cluster in the lower left corner (red and yellow marks highlighted with a circle) while the other two got located in the lower middle of the data frame (red marks highlighted with stars). This means that the gene regulation pattern of the "outliers" (samples marked with stars) distinguished from the pattern of their treatment replicates. Especially the big distance between the CTRL samples (in the upper half of the data frame) highlights the presence of an additional external influence on the fibroblasts which affected the RNA levels in these samples. This heterogeneity among the sample replicates did complicate the analysis and interpretation of the dermal array results.

Nevertheless, the samples were further analyzed using the OposSOM based Distance map cluster (D-Cluster) approach. This analysis resulted in a SOM which indicated four spots as being most relevant (**Figure 4.15B**). Each spot represented a different gene regulation pattern and two of them had a pattern which showed a certain dependency on the CsA treatment. Spot #2 represented genes that appeared to be downregulated upon CsA application (**Figure 4.15C**), Spot #4 included genes which were upregulated in all CsA treated samples (**Figure 4.15D**).

The gene sets represented in spots #2 and #4 indicated, like in the epidermal gene expression array, an effect of CsA treatment on cellular processes like cell migration, EMT, hemidesmosome assembly, UV response and apoptosis.

As seen before, several different signal transduction pathways appeared in the list of regulated gene sets, including p53, KRAS, mTORC1 and TNFα signaling. Especially the p53 and the mTORC1 signaling cascade appeared in both the dermal and the epidermal setup. An evaluation of their potential influence is presented later in the thesis.

Furthermore, the cell-to-cell adhesion and the ECM organization appeared to be affected, confirming the observation of a change in the matrix structure.

**A**

Serum A – CTRL
Serum A – CsA
Serum B – CTRL
Serum B – CsA

CTRL

*
*
*
*

CsA

**B**

| Rank | Gene Set | p-value | in/all |
|------|----------|---------|--------|
| 1 | p53 signaling | 4e-12 | 30/187 |
| 2 | cell migration | 9e-07 | 22/188 |
| 3 | apoptosis | 2e-06 | 48/656 |
| 4 | cell-cell adhesion | 4e-06 | 16/119 |
| 5 | proliferation | 8e-06 | 33/406 |
| 6 | hemidesmosome assembly | 1e-05 | 5/10 |
| 7 | cell adhesion | 3e-05 | 41/591 |
| 8 | UV response | 2e-04 | 15/145 |
| 9 | KRAS signaling | 4e-04 | 17/190 |
| 10 | mTORC1 signaling | 7e-03 | 14/189 |

| Rank | Gene Set | p-value | in/all |
|------|----------|---------|--------|
| 1 | epithelial mesenchymal transition | 9e-08 | 19/192 |
| 2 | mTORC1 signaling | 2e-06 | 17/189 |
| 3 | TNFα signaling | 7e-06 | 16/189 |
| 4 | Hypoxia response | 3e-05 | 15/190 |
| 5 | ECM organization | 4e-05 | 15/193 |
| 6 | cell adhesion | 5e-04 | 27/591 |
| 7 | angiogenesis | 8e-04 | 5/33 |
| 8 | p53 signaling | 4e-03 | 11/187 |
| 9 | apoptosis | 2e-02 | 8/152 |
| 10 | PI3K Akt mTOR signaling | 2e-02 | 6/98 |

***Figure 4.15 – Dermal gene expression microarray:*** *(A) To demonstrate the comparability between the treatment replicates the array results were included in a correlation spanning tree. Each mark represents one sample. Close marks had similar and distant marks different array results. (B) Potentially relevant gene sets were identified by applying a D-Cluster analysis over all samples. In the resulting SOM each pixel represents a group of genes sharing the same regulation pattern (metagene). In red areas metagenes with a similar regulation pattern clustered, blue areas illustrate metagenes with different regulation patterns. The numbers represent those metagene clusters (spots) with the highest relevance. (C) The regulation patterns of spot #2 (C) and of spot #4 (D) and a list of the most significant gene sets found in those spots are demonstrated below. (\*) samples which showed high variation from their treatment replicates during the sample similarity analysis.*

## 4.6.3. Induction of myofibroblast differentiation and fibrosis

A more detailed analysis of the cell-to-cell adhesion and the ECM organization gene sets demonstrated a regulation of different ECM and BM associated genes, like those coding for fibronectins and integrins, including: FLRT3 ($\downarrow$), FSD1L ($\downarrow$), Syndecan 1 ($\downarrow$), Integrin α1 ($\uparrow$), Integrin α6 ($\downarrow$), Integrin αv ($\uparrow$), Integrin β1 ($\uparrow$), and Integrin β4 ($\downarrow$).

The regulation of so many different integrin subunits indicated an induction of fibroblast differentiation. The microarray also revealed an induction of alpha smooth muscle actin (αSMA) expression. The induction of this protein, along with the differential expression of the integrins, argued for a CsA-induced fibroblast differentiation, i.e. transition into myofibroblasts. Support for this interpretation also came from the histological analysis, demonstrating a change in fibroblast morphology upon CsA treatment in both, HaCaT- and NHEK-OTCs.

To further validate the expression array data, we analyzed HaCaT- and NHEK-OTCs for the expression of αSMA. Frozen sections of both culture types were used for an IIF staining directed against αSMA (**Figure 4.16**). Although the positive control demonstrated a functionality of the antibody, we hardly detected αSMA in the OTCs. While NHEK OTCs were completely free of the protein, HaCaT OTCs showed a few αSMA-positive fibroblasts at the lower border of the dermal equivalent in both the control and CsA treated cultures. Thus, the CsA-dependent increase in αSMA protein could not be confirmed.
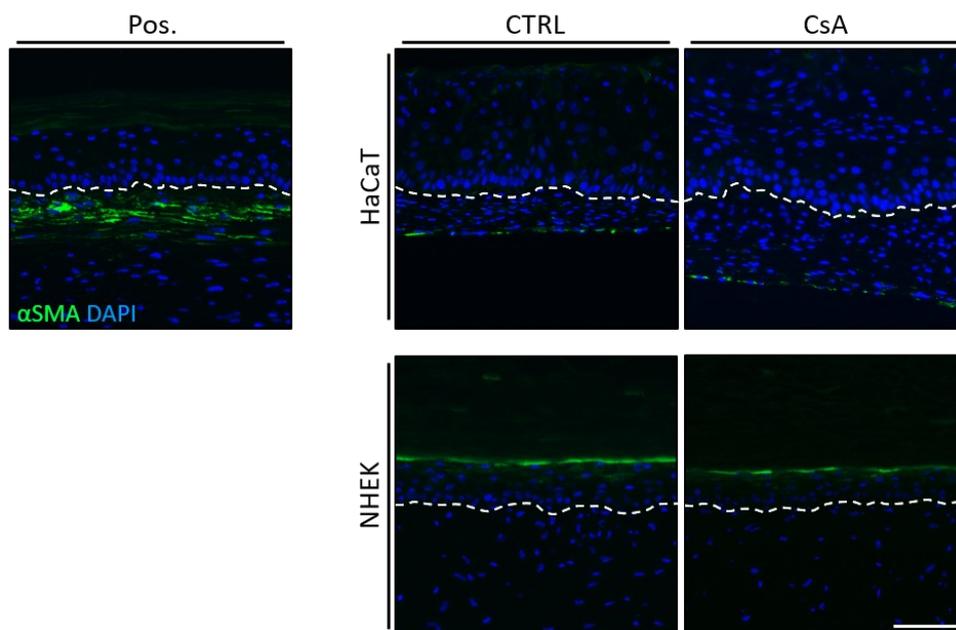


*Figure 4.16 – Detection of αSMA in HaCaT- and NHEK-OTCs:* CDMs carrying either HaCaT or NHEK cells were treated with DMSO (CTRL) or 10 µg/ml CsA over a period of 21 days (HaCaT) or 42 days (NHEK). IIF staining was performed on frozen sections of the OTCs to detect the expression levels of αSMA. As a positive control an untreated NHEK-OTC with primary fibroblasts from a 74-year-old donor was used (Pos.). Displayed are representative images of control versus treated cultures. The dashed line indicates the position of the basement membrane. The scale bar represents 100 µm.

The further analysis of the dermal microarray data gave indication for an induction of fibrosis. Several fibrosis associated genes like Periostin, Lumican and Collagen XIII appeared to be upregulated upon CsA. The appearance of myofibroblasts is often accompanied with the induction of fibrosis (Bansal et al., 2017). Thus, we decided to determine the relative mRNA levels of these three genes as well as of Integrin αv, as it serves as key player during myofibroblast induction (Lygoe et al., 2004) and also showed an upregulation upon CsA in the microarray. For this purpose, the dermal RNA of CsA and SUN treated HaCaT-OTCs was used for a quantitative polymerase chain reaction (qPCR) analysis (**Figure 4.17**).
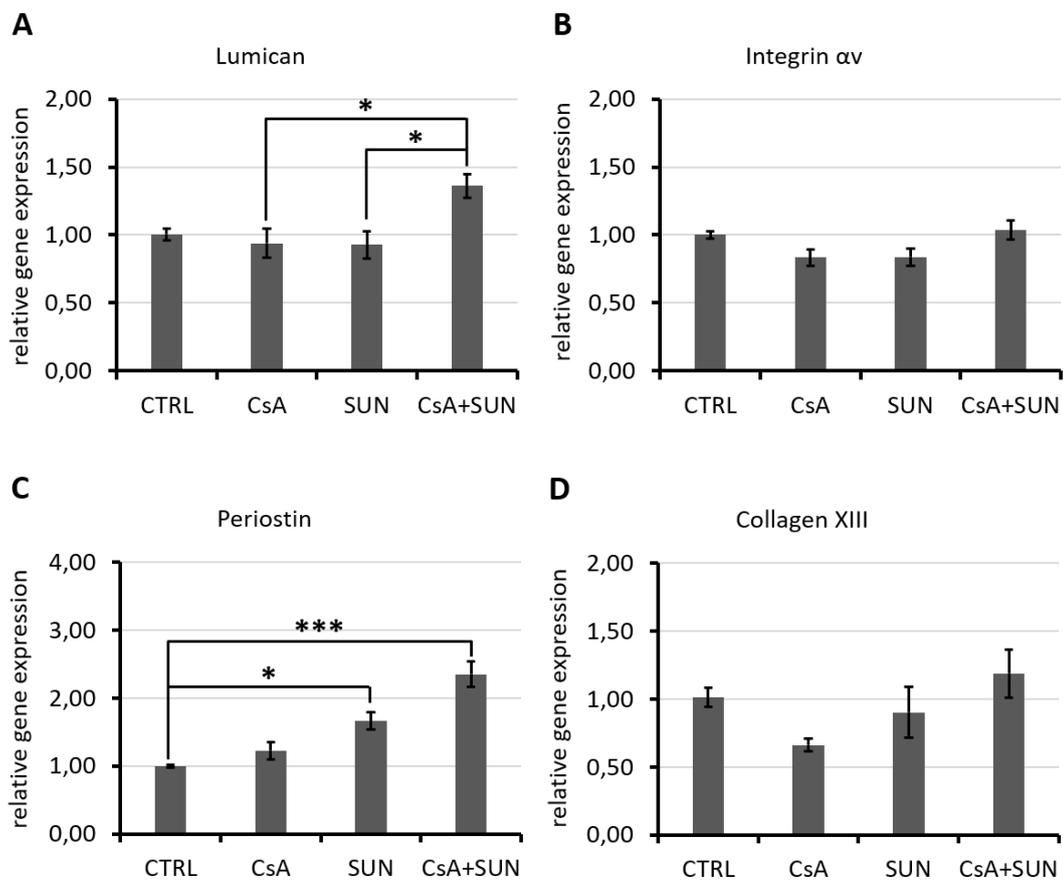


*Figure 4.17 – relative gene expression of fibrosis associated genes upon CsA treatment:* *HaCaT-OTCs were treated with DMSO (CTRL), 10 µg/ml CsA or 0.65 MED SUN or a combination of both (CsA+SUN) over 21 days. Subsequently the RNA of the dermal cells was purified and used qPCR analysis. During the analysis the relative gene expression levels of Lumican (A), Integrin αv (B), Periostin (C) and Collagen XIII (D) were determined. The error bars represent the standard error mean; * = p-value < 0.05; *** = p-value < 0.0005; n=3.*

The data shows that CsA only induced the expression of Periostin. The expression of αv integrin and Col XIII was rather inhibited upon CsA treatment. Similarly, irradiation with SUN only induced expression of Periostin, while the combination of both treatments (CsA plus SUN) seemed to affect regulation of all 4 genes with a slight increase in αv integrin and Col XIII and a significant increase

in Lumican, and particularly Periostin. For Lumican the effects where not significant compared to the control, but it was significantly induced when comparing between single and combination treatment.

In summary, the results of the microarray analysis, and in particular of the myofibroblast differentiation gene set, were only partially confirmed. CsA treatment, especially in combination with SUN irradiation, did lead to the upregulation of the fibrosis associated gene Periostin. However, a myofibroblast differentiation inducing effect of CsA could not be validated. Furthermore, we could show that CsA und SUN have similar effects on the investigated genes but, as with Integrin αv and Collagen XIII, a combination of both does not necessarily lead to an addition of the effects. For a further investigation of the combinational effects of the drug and SUN on fibrosis, Periostin and Lumican are worth to be taken into consideration.

## 4.6.4. Increase of collagenase activity

As described above, the microarray analysis did indicate a regulation of BM components in the epithelium and of genes associated with ECM organization in the dermal compartment. Furthermore, the histological analysis showed a loss of matrix stability and degradation of BM components like Col VII. These findings suggested for an enhanced activity of matrix metalloproteases (MMPs), which are known for their collagenolytic activity (Jablonska-Trypuc et al., 2016).

The epidermal RNA expression array analysis showed an upregulation of MMP1, and in the fibroblast array we found indication for a downregulation of MMP9 upon CsA application. To validate these findings and quantify the protein levels of these MMPs in our cultures, conditioned media samples of CsA and SUN treated HaCaT-OTCs were collected and used for enzyme linked immunosorbent assays (ELISA). One assay targeted the inactive form of MMP1 called "pro-MMP1", as the active MMP form cannot be detected with an ELISA assay (**Figure 4.18A**), and the other MMP9 (**Figure 4.18B**).

The results of the ELISA revealed that CsA caused a significant reduction of the pro-MMP1 level but had no effect on MMP9. SUN irradiation was leading to a non-significant increase in pro-MMP1 and decrease in MMP9 concentration. A combination of both the drug and SUN lead to a non-significant induction of MM9 activity but had no effect on pro-MMP1.

In the next step, we wanted to see if a treatment with CsA or SUN leads to a general induction of collagenase activity. For this purpose, we used a fluorescence based general collagenase assay.

Here, a special gelatin mixture was applied on non-fixated frozen sections of CsA and SUN treated HaCaT-OTCs. Active collagenases within the tissue caused a cleavage of the collagen fibers into a green fluorescent active product, which could be detected under a fluorescence microscope (**Figure 4.18C**).

From this analysis we could see that all samples displayed a high level of collagenase activity in the epidermal compartment, especially in the further differentiated layers. While signals were absent in the dermal compartment of the control samples, weak signals were seen after CsA and SUN treatment. A combination of both caused an addition of the effects resulting in a strong display of collagenase activity in the dermal compartment, as well as in the basal cell layer.
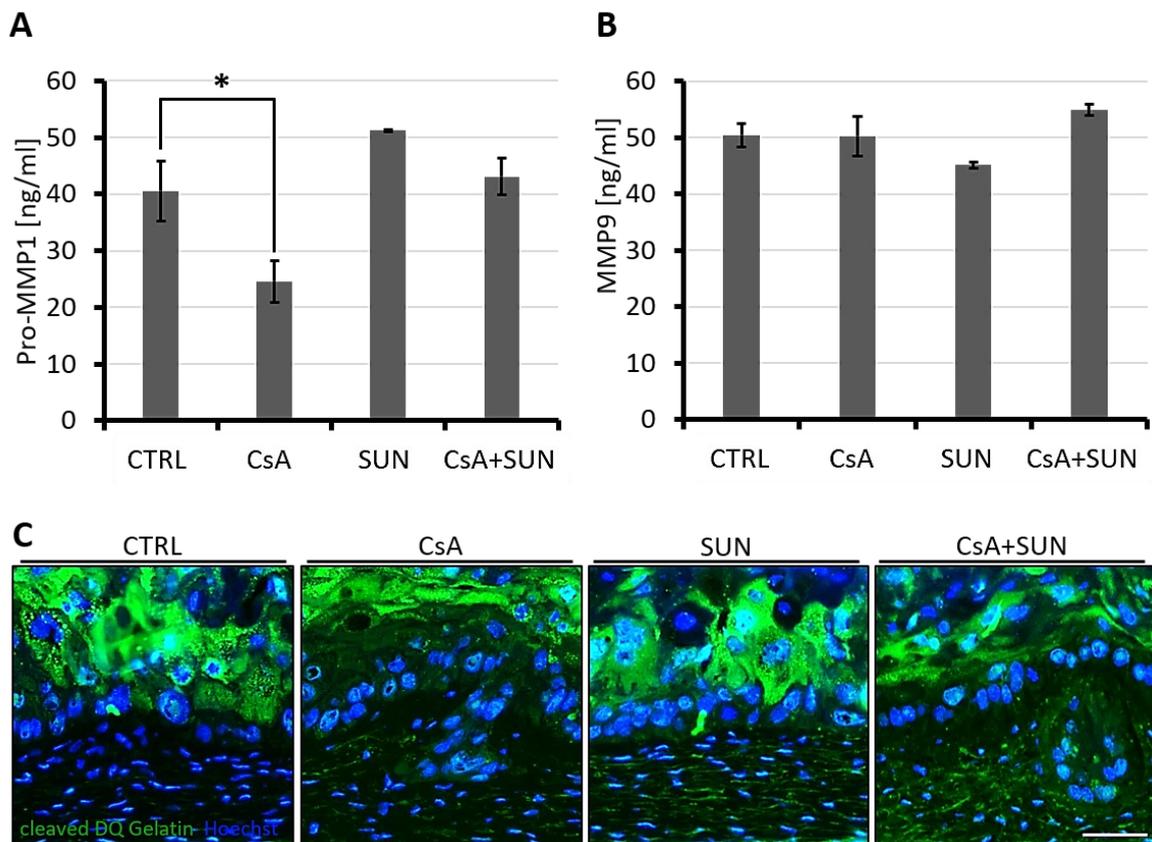


***Figure 4.18 – Induction of collagenase activity upon CsA and SUN treatment in HaCaT-OTCs:*** *Samples were treated with DMSO (CTRL) 10 µg/ml CsA or 0.65 MED SUN or a combination of both (CsA+SUN) over a period of 21 days. The conditioned media samples of the cultures were used for ELISA-based detections of Pro-MMP1 (A) and MMP9 (B). Additionally, a fluorescence-based collagenase assay was performed on non-fixated frozen sections. Displayed are representative images of control versus treated samples (C). The error bars represent the standard error mean; \* = p-value < 0.05; \*\*\* = p-value < 0.0005; n=3. The scale bar represents 50 µm.*

## 4.7. The modulation of the Akt1-mTOR pathway by CsA

The main therapeutic function of CsA is the regulation of the calcineurin signal cascade in immune cells. A regulation of the calcineurin pathway in the epithelia or dermal fibroblasts, however, could not be detected in our microarray analyses. Instead, several other pathways appeared to be modulated including p53, KRAS, mTOR and TNFα signaling. Interestingly, the p53 and the mTOR signaling cascade appeared in both the dermal and the epidermal setup.

The results presented so far revealed that a treatment with CsA led to a manipulation of several independent cellular processes in the OTCs. The most reasonable explanation for such a wide effect is the modulation of one or several signal cascades. As the mTOR pathway is involved in many cellular processes, we reasoned that deregulation of this pathway may be of particular importance for the CsA-dependent phenotype.

An association between activated mTOR signaling and enhanced cSCC malignancy, as well as CsA effects on the mTOR pathway, especially the Akt-mTOR signaling cascade, have been described before (Arumugam et al., 2012; Carr et al., 2012; Claerhout et al., 2010; Han et al., 2010b). In this specific cascade, Akt1 gets activated by phosphorylation on two different amino acids (Threonin 308 and Serine 473) upon growth factor stimulation. The activated form is inducing the mTOR pathway via activation of mTOR complex 1 (mTORC1). This then leads to the induction of cellular processes like proliferation and cell survival (Carr et al., 2012). CsA seems to promote the process of mTORC1 activation by stabilizing the phosphorylated form of Akt1 (Han et al., 2010b).

As mentioned above, the microarray analyses suggested a regulation of this particular pathway in both the epithelium and the dermal fibroblasts (a detailed list of all CsA regulated mTOR associated genes is given in **Chapter 8.3**). To investigate for a potential functional role of the mTOR signal cascade during the CsA treatment, a general blockade was required. Therefore, we decided to silence the pathway by inhibiting Akt1 activation with the Akt inhibitor V, also called Triciribine (TCN). It functions by preventing Akt to localize at the membrane and thus to bind to PDK1, the kinase that is responsible for its phosphorylation  (Berndt et al., 2010). TCN has been successfully tested in mouse skin, also in combination with CsA treatment (Arumugam et al., 2012).

### 4.7.1. Titration of the inhibitor dosage

To apply this inhibitor successfully in our OTC experiment, we first needed to determine the optimal concentration. TCN is used in mice in a dosage of 1 mg/kg bodyweight. This dosage is well

established and published in several studies. However, only few publications describe a use in *in vitro* systems, reporting concentrations in the range from 2 to 50 µM.

To determine the lowest, but still functional TCN concentration in skin cells, we conducted a titration assay for the inhibitor on HaCaT monolayer cultures. 80 % confluent HaCaT cells were supplemented with the inhibitor within a concentration range of 0.5 to 50 µM for a period of 24 h. An additional HaCaT culture was treated with 1 µm Wortmannin as a positive control. Wortmannin is an inhibitor for the epidermal growth factor receptor associated kinase Pi3K, which is responsible for the phosphorylation of Akt1 (Leslie et al., 2012). After 24 h the cultures were harvested for protein purification. The results demonstrated that a concentration of 50 µM TCN was toxic to the cultures and therefore could not be used in further studies (data not shown). The samples treated with 20 µM and less TCN were used in a Western Blot analysis to determine the levels of phosphorylated Akt1 (**Figure 4.19**).
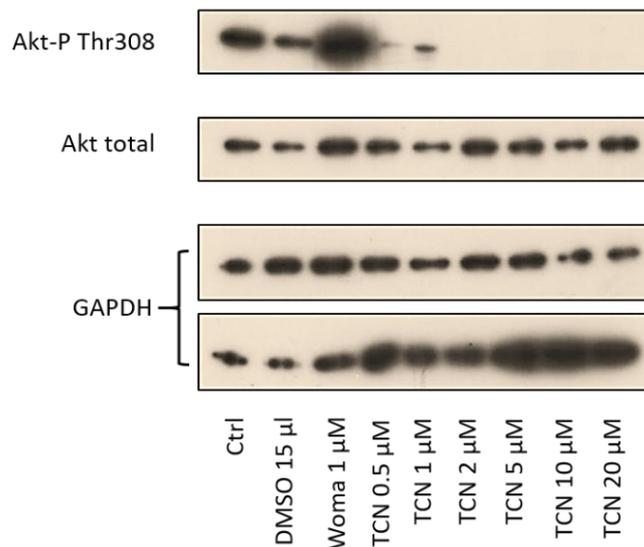


*Figure 4.19 – Titration assay of TCN effectivity:* *2D HaCaT cultures were treated with different concentrations of TCN (0.5 – 20 µM) for 24 hours. As references an untreated sample (Ctrl), a DMSO negative control and a Wortmannin positive control were included. Protein purifications were used for a Western Blot with subsequent immunodetection of total Akt, Akt phosyphorylated at Threonin 308 and GAPDH as loading control.*

The Wortmannin positive control was not functional and rather caused a boost of Akt1 phosphorylation. TCN concentration of ≥ 2 µM led to a complete loss of phosphorylation at Thr308. In comparison to the negative (untreated) control sample a concentration lower than 2 µM still showed a clear reduction of the phosphorylation level. Thus, a suitable concentration was estimated at a range between 1 to 2 µM.

As cells under different conditions, i.e. 2D versus 3D, may react differently to exogenous substances, we next performed OTC experiments using HaCaT cells and NHEK to test for their

sensitivity to the inhibitor. Here TCN was applied at a concentration of 1 µM. To determine interference of the drug with the other treatment modalities, TCN application occurred in parallel to 10 µg/ml CsA supplementation and 0.65 MED SUN irradiation over a period of 21 days for HaCaT-OTCs and 42 days for NHEK-OTCs.

While the control cultures formed an orderly stratified and differentiated epithelium, also characterized by a dry surface (no leakage of medium through the epidermis), all samples supplemented with the inhibitor, alone or in combination with the other treatments, showed a wet surface, indicative for a non-functional barrier. Cell culture medium did pass from the lower into the upper reservoir indicating a damage in the epidermal structure (**Figure 4.20A**). H&E staining on paraffin sections of these cultures revealed atrophy of the epithelia both in HaCaT- and in NHEK-OTCs. Only terminally differentiated horn sheets were maintained. (**Figure 4.20B**). Apparently, the applied concentration of TCN was toxic for the cells, both keratinocyte types as well as the fibroblasts.
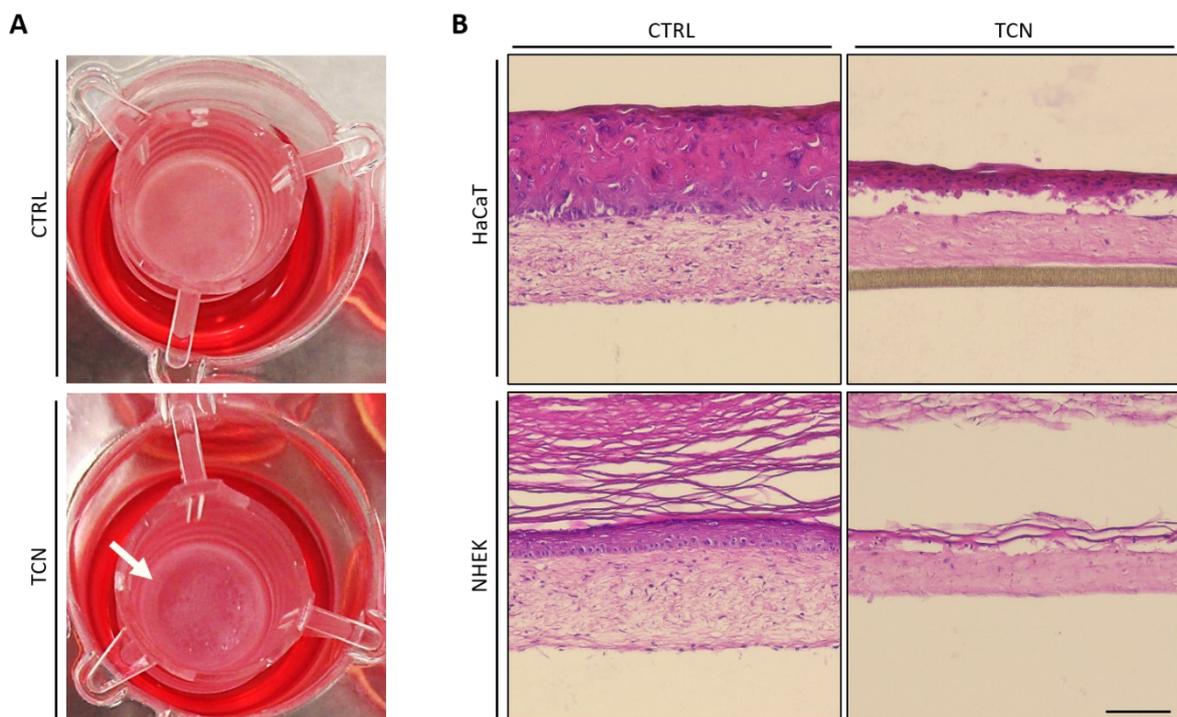


***Figure 4.20 – Effects of TCN on OTCs at 1 µM:*** *HaCaT-OTCs were treated with DMSO (CTRL) or 1 µM TCN over a period of 21 days, NHEK-OTCs were treated for 42 days. Images of the HaCaT-OTCs were taken prior to their harvest (A). The white arrow indicates cell culture medium in the upper reservoir. H&E staining was performed on paraffin sections of both culture types (B). The scale bar represents 100 µm.*

## 4.7.2. TCN effects on CsA treated HaCaT-OTCs

To minder inhibitor toxicity, the following OTC experiments were performed with a TCN concentration of 0.1 µM. Additionally, the treatment period was shortened. While the cultures were treated with CsA and SUN for 21 days, TCN was only added after 9 days of treatment, i.e. was only provided for the second half (12 days) of the culture period. This time the epithelia developed a barrier function, as indicated by dry surfaces in all OTCs (data not shown).

To investigate if the inhibitor was functional at this low concentration, parts of the OTCs were used for protein purification and subsequent Western Blot analysis to detect the levels of total Akt and Akt phosphorylated at Serine 473 (**Figure 4.21**). While CsA alone had no effect on the level of Akt phosphorylation, irradiation with SUN seem to activate the pathway showing high levels of pAKT. In contrast, the addition of TCN, despite being added only later and only for 12 days, led to a complete loss of phosphorylated Akt in all samples treated with the inhibitor.
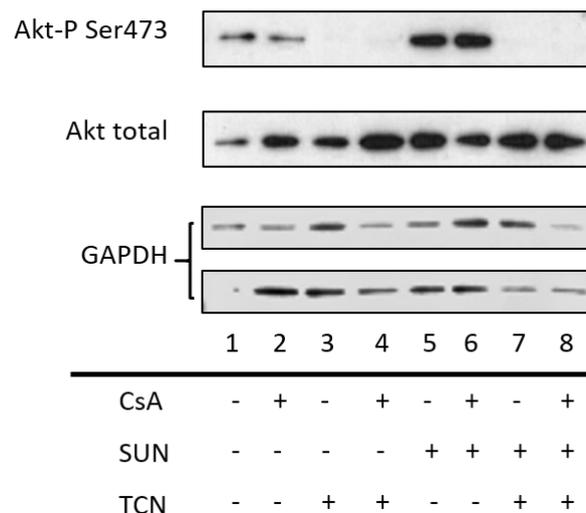


*Figure 4.21 – TCN functionality in HaCaT-OTCs: HaCaT-OTCs were treated with 10 µg/ml CsA and 0.65 MED SUN over a period of 21 days. For the last 12 days of this period 0.1 µM TCN was included. Protein purifications were used for a Western Blot with subsequent immunodetection of total Akt, Akt phosphorylated at Serine 473 and GAPDH as loading control.*

Histology on the samples showed an intact matrix and a viable epidermis (**Figure 4.22**). This indicates that the concentration of 0.1 µM TCN was no longer toxic. In addition, the concentration was sufficient to inhibit AKT phosphorylation and thus was effective in blocking the Akt mediated mTOR pathway activation. As expected, CsA alone and combined with SUN caused an invasive behavior of the HaCaT cells while the control and only SUN treated cultures remained as non-invasive surface epithelia. While TCN, on its own or in combination with SUN had no effect on

epidermal growth of the HaCaT cells, the combination with CsA caused an inhibition of the otherwise CsA-induced invasion. However, when TCN was added to the combination treatment of CsA plus SUN, invasion was not inhibited. This suggested, that the Akt/mTOR pathway is involved in the CsA-dependent invasion. However, in combination with SUN, additional regulatory pathways were activated, which by themselves were not sufficient to induce invasion, but which were able to overcome the CsA-dependent contribution through the Akt/mTOR pathway and thus allow the cells to remain invasive.
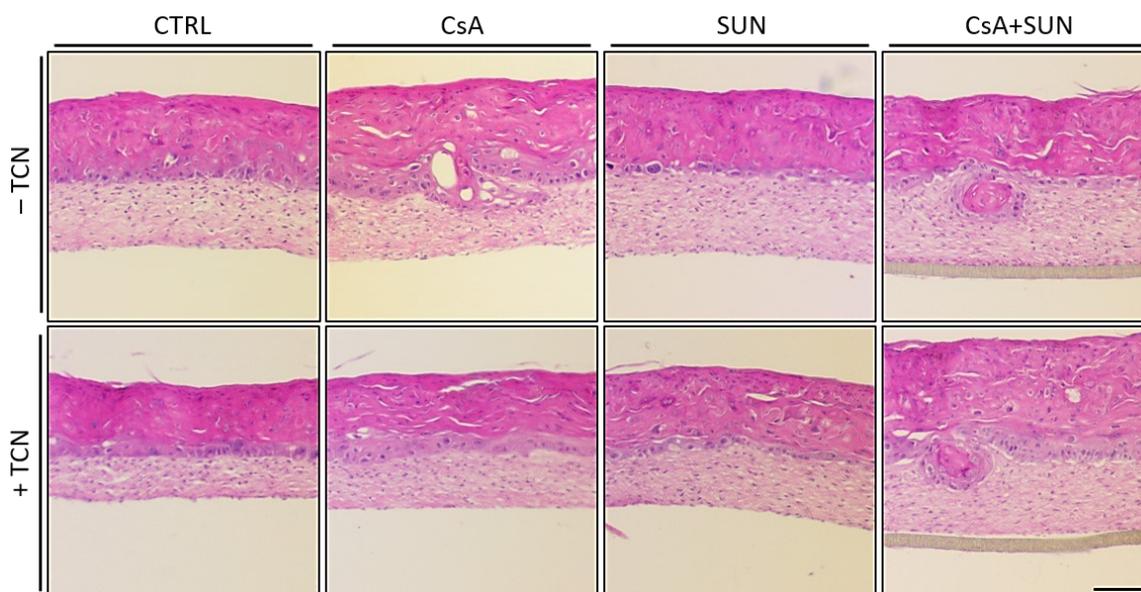


***Figure 4.22 – Effects of TCN on OTCs at 0.1 µM:*** *HaCaT-OTCs were treated with DMSO (CTRL), 10 µg/ml CsA or 0.65 MED SUN or a combination of both (CsA+SUN) over a period of 21 days. For the last 12 days of this period 0.1 µM TCN was included. H&E staining was performed on paraffin sections of the OTCs. Displayed are representative images of control versus treated cultures. The scale bar represents 100 µm.*

To test if TCN also hinders the CsA induced differentiation, frozen sections were stained for Pan-keratin (**Figure 4.23A**). As in cultures treated with CsA alone, the TCN-treated cultures showed the same switch to a more structured and organized epithelium. This was also the case for the CsA+SUN treated cultures when supplemented with TCN. An additional staining for the differentiation-specific Keratin 10 supported this observation (**Figure 4.24A**), demonstrating that the Akt inhibitor, i.e. inhibition of the Akt/mTOR pathway, was not involved in the regulation of differentiation.

A combination of the Pan-keratin detection with a Ki67-directed antibody allowed to evaluate effects of TCN on the proliferation rate (**Figure 4.23A**). As expected, the combined treatment with CsA and SUN caused an induction of proliferation while the individual treatments had no effect on the amount of Ki67 positive cells. The additional application of TCN did not change this observation, indicating that the inhibition of the Akt/mTOR pathway did not influence the proliferation rate.
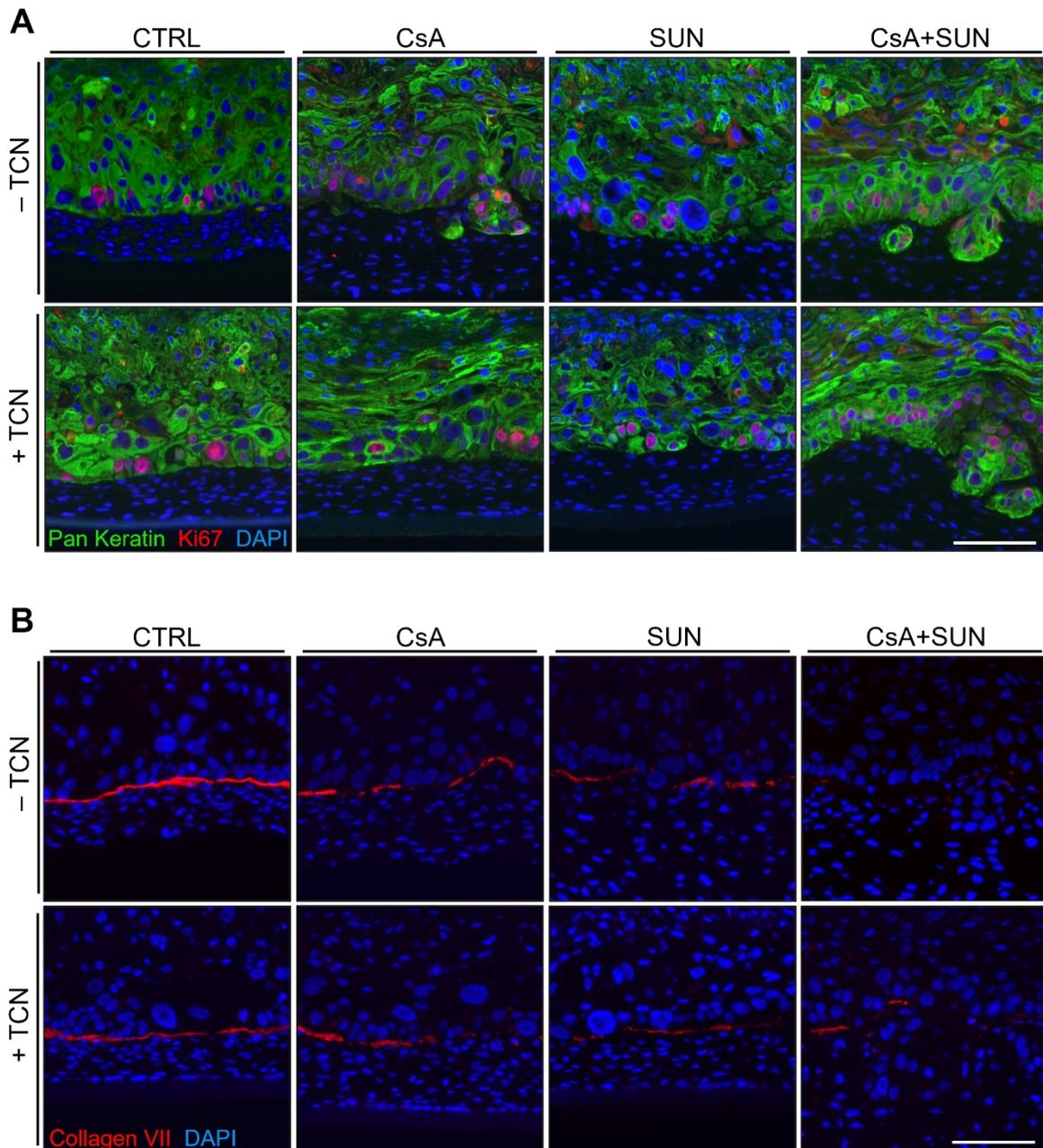
***Figure 4.23 – TCN effects on differentiation and the basement membrane structure:*** *HaCaT-OTCs were treated with 10 µg/ml CsA and 0.65 MED SUN over a period of 21 days. For the last 12 days of this period 0.1 µM TCN was included. Frozen sections were used for IIF based detection of Pan-keratin and Ki67 (A), as well as Collagen VII (B). Displayed are representative images of control versus treated cultures. The scale bars represent 100 µm.*

Like in the previous experiments, the treatment with CsA or SUN caused a degradation of Collagen VII and the combination of both treatments lead to a nearly complete loss of the protein (**Figure 4.23B**). However, inhibitor application did not have any influence on the degradation effects of CsA and SUN alone or combined. When comparing with the control sample, the application of TCN alone did not cause a change of the Collagen VII signals.
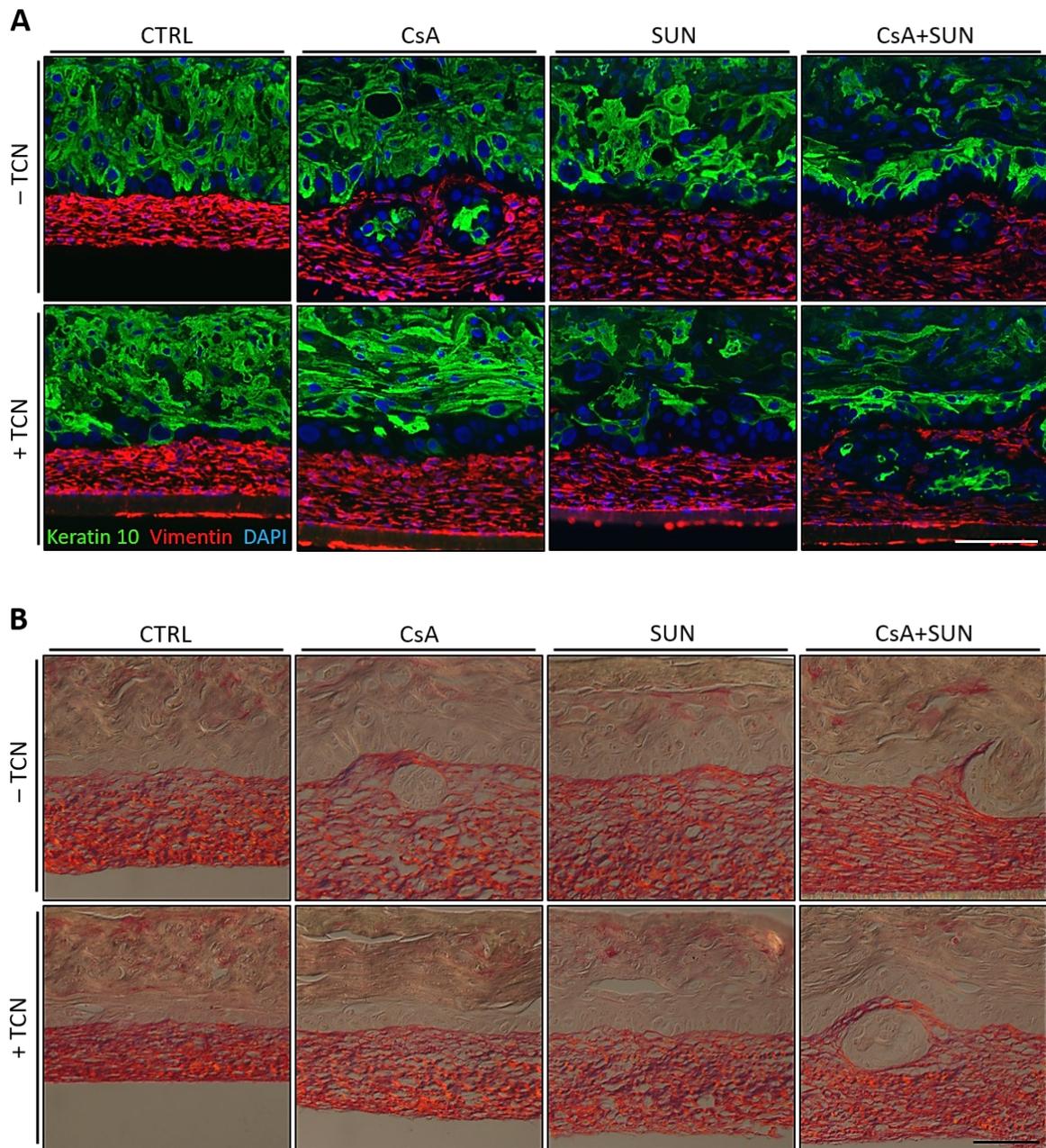
***Figure 4.24 – TCN effects on differentiation and the matrix integrity:*** *HaCaT-OTCs were treated with 10 µg/ml CsA and 0.65 MED SUN over a period of 21 days. For the last 12 days of this period 0.1 µM TCN was included. Frozen sections were used for IIF based detection of Keratin-10 and Vimentin (A). Paraffin sections were treated with picro sirius red to visualize Collagen I and III (B). Displayed are representative images of control versus treated cultures. The scale bars represent 100 µm.*

Upon staining for Vimentin, no TCN induced changes in signal intensity were seen (**Figure 4.24A**). Similar to the previous observations, fibroblast in the proximity of invasion bulges started to round up. However, this effect was more prominent in the CsA treated OTCs than in those undergoing a combined CsA+SUN treatment. Likewise, the pirco sirius red staining revealed CsA and SUN induced matrix rearrangements close to the basement membrane. Especially in the proximity of the CsA induced invasion sites, a weakened collagen structure was visible. The application of TCN seemed

to reduce these matrix effects, suggesting that regulation of genes responsible for this process (e.g. MMP expression) in the keratinocytes and/or fibroblasts may be controlled by the Akt/mTOR pathway.

In summary, by applying TCN only temporarily (9 days after start of CsA treatment) and at a low dose (0.1 µM), cytotoxicity was prevented, allowing for the development of a normal epithelium by the HaCaT cells. This TCN concentration was sufficient to hinder Akt phosphorylation, causing a successfully block of the Akt/mTOR pathway in the OTCs. Blocking Akt phosphorylation did neither interfere with the CsA-induced differentiation, nor did it alter proliferation. However, it counteracted the CsA-induced invasion of the HaCaT cells. Furthermore, TCN inhibited the CsA-dependent and invasion accompanying modulation of the collagen meshwork. These observations are suggesting that CsA-dependent invasion and matrix modulation is regulated via the Akt/mTOR pathway. Invasion induced by CsA+SUN, however, was not prevented, suggesting that by SUN exposure additional regulatory pathways are activated, which by themselves cannot induce invasion, but in addition with CsA-dependent signals (other than Akt/mTOR signaling) are able to overcome the Akt-induced deficit and allowe the HaCaT cells to stay invasive.

Though an attractive modulator, Col VII does not seem to be regulated by the Akt/mTOR pathway. TCN application to CsA+SUN treated OTCs did limit the Collagen VII degradation, but the partial degradation seen by CsA or SUN alone was not prevented upon inhibitor treatment.

# 5. Discussion

The origin of cutaneous squamous cell carcinoma (cSCC) in immunosuppressed patients is still highly debated. However, there is strong epidemiological evidence that the exposure to sunlight or artificial UV light is forming the highest risk factor for developing cSCC in immunocompetent patients (Fortina et al., 2009; Linos et al., 2016; Ponticelli et al., 2014). The reason for this is their potential to induce mutations and other genetic aberrations, changing the cell's characteristics and allow them to form tumors. Accordingly, the cancer cells in cSCCs carry a high number of gene mutations, more than cells of e.g. melanomas. Many of these genetic aberrations are indicative for UV radiation as being C to T transitions or even CC to TT double base changes (Chalmers et al., 2017; Pickering et al., 2014). In addition to this, the rate of cSCC development in immunosuppressed patients, like organ transplant recipients (OTRs), is highly elevated as compared to the healthy population and the patients are much younger, especially in cases when immunosuppression is induced by Cyclosporin A (CsA) (Grulich et al., 2007; Jensen et al., 1999; Kwa et al., 1992; Lindelof et al., 2000; Ong et al., 1999). These observations are suggesting that immunosuppression promotes UV-dependent skin carcinogenesis.

## 5.1. CsA induced tumorigenesis requires genetic predispositions

In the project presented above we first addressed the question of how genetic predispositions cooperate with CsA-induced tumorigenic conversion. This was performed by establishing three-dimensional human skin organotypic cultures (OTCs). These OTCs were loaded with keratinocytes carrying different genetic aberrations, and accordingly representing different stages of tumorigenicity, and treated with CsA over several weeks. One of our main findings was the induction of invasive behavior in OTCs carrying HaCaT cells. However, CsA failed to induce invasion in OTCs carrying normal human epidermal keratinocytes (NHEK). This supports the already published hypothesis that CsA alone is not capable of inducing cSCC in the skin of OTRs. Instead, the cSCC formation seems to be dependent on both the presence of an immunosuppressive drug like CsA and an exposure of the skin to a mutagenic component like sunlight (Bavinck et al., 1993; Burke et al., 2015; Espana et al., 2000).

As our *in vitro* model did not incorporate a functional immune system, it allowed the conduction of studies under immunosuppressive conditions. Thus, we concluded that the by us observed CsA induced invasion was not coupled to any immunosuppressive effect of the drug. Our microarray

analysis strengthened this conclusion as it did not reveal any indication for a CsA dependent regulation of immune response modulating compounds, like interleukins or cytokines.

However, since the main function of CsA is the suppression of the immune response, compounds like interleukins or cytokines are still main targets for the ongoing investigations on cSCC development in OTRs. For example, recent studies published by Abikhair and Santana claimed that CsA enhances the cSCC development by inducing the expression of IL-22 in T-cells, which promotes the migratory potential of SCC cells (Abikhair et al., 2016; Santana et al., 2017). However, both studies described that the presence of IL-22 is rather promoting the malignancy of the existing tumors than their formation, leaving the question of the cSCC induction mechanism open. Thus, the CsA caused modulation of the immune response might be an explanation for the malignant outcome of the cSCCs but it fails to explain the high skin lesion incidence rate.

Another observation during CsA induced cSCC formation in immunosuppressed patients is the enhanced expansion of beta type human papillomaviruses (HPV). In a recent multicentered study on OTRs it was described that approximately every second patient carried DNA of 5 or more different beta HPV types after immunosuppression and transplantation (Bouwes Bavinck et al., 2018). Thus, it is believed that the lack of an immune response results in a less restricted virus expansion, leading to the development of virus associated skin warts (Larsen et al., 2019). These can transform into cSCCs by stabilizing sunlight induced mutations and inhibiting p53 controlled apoptosis (Howley and Pfister, 2015; McLaughlin-Drubin, 2015; Wieland et al., 2014). However, to the best of our knowledge, neither the used HaCaT cells, nor the primary fibroblast incorporated in the 3D skin models carry any HPV strains, speaking against an enhanced virus expansion as possible explanation for our findings. Also, as described above, our *in vitro* models are not immunocompetent. Thus, the treatment with CsA did not cause a restriction of the immune response.

Taken together, our results indicate that CsA has an additional immune system independent and HPV unrelated effect on human skin cells, which is promoting cSCC development.

## 5.2. CsA affects differentiation in HaCaT cells but not in NHEK

The first signs of invasion in the HaCaT-OTCs could be seen after 21 days of treatment. The keratinocytes transited in smaller and bigger groups through a damaged basement membrane (BM) into the matrix, forming invasive buds. The cells mostly showed only weak signals of differentiation markers like Keratin-10, and ongoing keratinization could be seen in the center of larger invading bulks. This is comparable to tumors from cSCC patients, which usually show a moderate grade of

differentiation with variable degrees of keratinization in the tumor center (Leboit et al., 2005). Even though the cSCCs in immunosuppressed patients show an elevated occurrence rate and malignancy, the pathology of the tumors seems to be comparable to that from immunocompetent cSCC patients (Harwood et al., 2003). This implicates that the invasion behavior seen in our HaCaT model represents the basic characteristics of the infiltrating cSCC tumors in OTRs.

When comparing the distribution of the differentiation markers between the control and the CsA treated OTCs, also differences in the organization of the HaCaT cells could be detected. The cultures showed an improved epithelial organization upon CsA treatment which allowed the identification of individual epidermal strata. Such an organization is usually only seen in OTC carrying NHEKs. This means that the drug causes an induction of keratinization in HaCaT-OTCs and confirms the findings made by L. Schardt. Here, CsA treatment caused an induction of epidermal differentiation and an enhanced expression of differentiation related genes (Schardt, 2017). However, In OTCs with normal human epidermal keratinocytes, a treatment with CsA did not cause any changes in the epidermal organization or signs of invasion induction.

Potential effects of CsA on differentiation are already discussed for several decades. Kanikatis et al. for example described a normalization of differentiation by CsA in human keratinocyte xenografts transplanted on nude mice. Here, the expression of suprabasal keratins, usually expressed throughout the entire xenograft, became limited in the basal keratinocytes upon CsA application (Kanitakis et al., 1990). This confirms our own observations on Keratin-10 expression, where the treatment with CsA caused a restriction of the protein to the suprabasal HaCaT cells. Furthermore, in patients suffering from atopic dermatitis a treatment with CsA has been shown to reverse the signs of disease associated regenerative hyperplasia and restore the epidermal stratification (Khattri et al., 2014). Interestingly, this differentiation effect is not restricted to epidermal tissue. Also, in P19 embryonic stem cells, a common model for cardiomyogenic differentiation, a treatment with the drug was shown to promote cardiac lineage specification by enhancing cardiac differentiation (Choi et al., 2015; Yan et al., 2009).

Taken together, a treatment with CsA appears to cause a morphological rearrangement leading to a normalization of the epidermal tissue. In immunosuppressed patients this might lead to an improved protection of the tumor precursor cells against immune surveillance.

## 5.3.  CsA promotes sunlight induced proliferation in HaCaT-OTCs

During the investigation of the invasion phenotype, one of the most prominent findings was the high number of Ki67 positive HaCaT cells within the invasion bulks. This suggested for an induction of proliferation upon CsA treatment. The enhanced epidermal thickness which we observed in CsA treated HaCaT-OTCs, indicating an induction of hyperplasia, supported this assumption. However, the quantification of all Ki67 positive epidermal cells revealed that the epidermal proliferation rate remained unchanged after CsA treatment.

Monolayer studies with HaCaT cells, conducted by L. Schardt (DKFZ Heidelberg), even revealed a proliferation inhibitory effect of CsA upon concentrations of 2.5 µg/ml or higher, while lower concentrations had no effect (Schardt, 2017). Also, most published studies on that topic report a repressive effect of the drug on proliferation in keratinocytes. Accordingly, Karashima et al. described an inhibition of primary keratinocyte proliferation by CsA ($10^{-8}$ - $10^{-5}$ M $\triangleq$ 0.012 - 12 µg/ml) due to a cell cycle arrest (Karashima et al., 1996). Similar results were observed by Nickoloff et al. for primary keratinocyte cultures upon CsA application of 1 – 10 µg/ml (Nickoloff et al., 1988). Also, for immune cells, i.e. monocytes, a proliferation inhibitory effect at higher concentrations of CsA (> 6 µM $\triangleq$ 7.22 µg/ml) has been published (Roy et al., 2006; Umland et al., 1999). In contrast to these findings, Abikhair et al. described an induction of proliferation by CsA (0.05 µg/ml) on skin derived A431 SCC cells (Abikhair Burgo et al., 2018), suggesting that the effect of CsA is dependent on the genetic background of the cells.

In contrast to a treatment with CsA alone, the combination with SUN irradiation, a spectrum consisting of ultraviolet, visual, and near infrared red light, caused a boost of HaCaT proliferation in our OTC-studies. Although the irradiation alone also caused an increase of Ki67 positive cells, only the combination of both treatments led to a significant induction.

Here it is important to highlight that Ki67 is not a marker specific for proliferation, but is expressed throughout all cell cycle phases, thus marking all cycling cells (Scholzen and Gerdes, 2000). As already mentioned above, current literature suggests a repressive effect of the drug on proliferation in keratinocytes. In contrast, UVB is known to promote proliferation and cell cycle progression in human epidermal skin cells (Carr et al., 2012; Lee et al., 2002). Furthermore, near infrared light (IRA) has also been shown to promote proliferation in skin cells (Vinck et al., 2003). Thus, arguably, the enhanced cell cycle continuation is driven by the effects of chronic irradiation, while the additional CsA treatment is enhancing this effect, resulting in an even stronger cell cycle induction. CsA is known to inhibit UVB induced apoptosis and DNA repair in human keratinocytes by blocking the mitochondrial permeability transition pore and suppressing nuclear translocation

of NFAT (Ji et al., 2012; Waldmeier et al., 2002; Yarosh et al., 2005). This is most likely leading to a stabilization and cell cycle continuation of UV-damaged cells, which usually would either undergo DNA repair or apoptosis, resulting in a boost of proliferation. The absence of functional p53 in HaCaT (Lehman et al., 1993) makes the cells probably even more prone to cell cycle progression. Unfortunately, the proliferation rate of the NHEK cells was lower than needed in order to detect quantitative changes after CsA application or SUN exposure. Thus, it was not possible to analyze if a similar boost is occurring in the presence of functional of p53.

## 5.4. Several BM components get disrupted by CsA

For the basement membrane (BM) CsA specific effects could be detected, especially in HaCaT-OTCs. At sites of ongoing invasion, the presence of all three investigated BM components was reduced, indicating an active degradation process. The invasion of tumor cells into the dermis is usually accompanied by an enhanced activity of proteases, either provided by the tumor cells themselves or the stromal fibroblasts, and a disruption of the BM components (Nissinen et al., 2016). Interestingly, the regulation of Collagen VII (ColVII) was distinguishing from the other two investigated BM components. The amount of protein became restricted with time and the degradation was not only limited to the sites of ongoing invasion. Also, Col VII is the only BM marker which got reduced by CsA in the NHEK-OTCs. Especially the combination of CsA and SUN led to an almost complete loss of the protein after 42 days. This indicates that the protein is actively downregulated by CsA, alone as well as in combination with SUN. The comparable results from the HaCaT and the NHEK-OTCs demonstrate that CsA has similar effects on the two keratinocyte cell types despite their different genetic background. However, the microarray studies on the HaCaT-OTCs revealed no regulation of Col VII on the RNA level, suggesting for a destabilization of the protein upon CsA supplementation.

Collagen VII is the main component of the anchoring fibrils, which are responsible for a proper attachment of the BM to the dermis (Sakai et al., 1986). Thus, a loss of the protein may suggest the disruption of the BM from the dermis. Importantly, loss of Col VII upon mutation is linked to patients suffering from dystrophic forms of Epidermolysis Bullosa (Hovnanian et al., 1997), a disease characterized by the formation of tense blisters and erosions on the skin and an increased risk for skin cancer, especially cSCC (Anton-Lamprecht and Gedde-Dahl, 2002; Fine et al., 2009; Montaudie et al., 2016).

However, to the best of our knowledge, no study has yet described a link between Collagen VII loss and CsA or sunlight exposure as we could see it in our experiments. But our Col VII findings are supported by other studies, which have associated its knockdown with enhanced migration of SCC cells. Furthermore, they have been able to see that a restoration of this protein retards cSCC invasion (Martins et al., 2009; Ng et al., 2012). Therefore, restoration of Col VII would be a potential therapy for cSCC lesions upon immunosuppressive treatments. For Epidermolysis Bullosa patients, treatments with isotretinoin or neotigason already have been used to reduce cSCC development (Venugopal and Murrell, 2010). Hence similar therapies should be explored for the prevention of skin cancer formation in OTRs.

Collagen IV (Col IV) is a major component of the basal lamina in the basement membrane (Laurie et al., 1982). In contrast to Collagen VII, its function is to act as the preferred binding site for epidermal keratinocytes (Murray et al., 1979; Wilke and Furcht, 1990). Col IV has been related to several muscle associated disorders like the Ullrich congenital muscular dystrophy (Lampe et al., 1993). At the same time, a dislocation of the protein in the skin is known as a reliable marker to distinguish between different forms of autoimmune subepidermal bullous diseases (Yeol Lee et al., 2018). However, a link between the BM component and skin cancer lesions has, to the best of our knowledge, not yet been described.

In case of Laminin-5 the degradation did not only lead to a loss of the protein at the invasion sites, but signals were detected around the invading HaCaT cells, indicating an expression of the protein by the invading cells. This is supported by the microarray analysis, which described an upregulation of all three Laminin-5 components (α3 β3 γ2) in the epidermal compartment. Laminin-5 is an adhesion ligand for keratinocytes in the epithelial basement membrane (Carter et al., 1991). Here it serves as binding site to the hemi-desmosome subunit integrin α6β4 (Niessen et al., 1994). Additionally to its anchoring function, it can interact with integrin α3β1, leading to an induction of cell survival, proliferation and migration in both non-tumorigenic epithelial cells and cSCC cells (Kariya and Miyazaki, 2004; Marinkovich, 2007; Nikolopoulos et al., 2005). Especially its γ2 subunit is strongly expressed at the invasive sites of several different tumor forms, including SCCs (Huang et al., 2017; Pyke et al., 1995; Wang et al., 2019). Thus, Laminin-5 might be of relevance for the tumor progression in OTRs and should be taken into consideration for future studies.

## 5.5. CsA and SUN are causing matrix rearrangements

Not only the BM got affected by CsA treatment, but also in the matrix changes were detectable for the HaCaT and the NHEK-OTCs. In both culture systems a treatment with CsA alone and in combination with SUN led to a loss of collagen fibers and a condensation of the matrix. Especially in the double treated cultures the remaining collagen fibers got rearranged in thicker bundles, causing the formation of bigger gaps between the bundles. This is arguably a sign of enhanced photoaging, caused by the SUN irradiation (Yasui et al., 2013).

In HaCaT-OTCs the effect was most prominent in the proximity of the invasion sites. This suggests for an invasion associated activation of matrix remodeling enzymes, like matrix metalloproteinases (MMP), as it usually occurs during invasive cancer formation (Liotta et al., 1980). Therefore, we decided to look at protease activity in the HaCaT-OTC. We conducted a gelatinase / collagenase assay, which revealed a clear induction of collagenase activity in the dermal compartment and in the basal layer of the epithelium, as well as in the invasive buds by CsA, SUN and the combination of both. A feasible explanation for the reduction in collagen fibers in the matrix is the induction of Collagen specific MMPs such as 1, 2, 9 and 13 by CsA. This is supported by the findings of L. Schardt, which revealed an induction of MMP1, 3 and 10 in HaCaT-OTCs upon CsA treatment (Schardt, 2017). However, our own gene expression analysis only indicated an induction of MMP1 in the epidermis and a reduced expression of MMP9 in the dermal compartment. The conditioned media-based ELISA assays showed no changes on the total protein level for MMP9 (active and inactive form). Only the level of Pro-MMP1 became significantly reduced. To explain the discrepancy between these findings, further studies are required.

Enhanced MMP expression in cSCCs has been described multiple times (Ahmed Haji Omar et al., 2015; Farshchian et al., 2015). However, studies on the interplay between Cyclosporin A and MMPs are limited. Gawronska-Kozak and Kirk-Ballard reported a reducing effect of the drug on MMP gene expression in MMP overexpressing dermal fibroblasts of nude mice (Gawronska-Kozak and Kirk-Ballard, 2013). In kidney associated fibroblasts CsA has been shown to induce the production of MMP9 (Francis and Bai, 2018). In fibroblasts, derived from the conjunctiva of the eye, the protein levels of MMP3 and MMP13 became reduced upon CsA application (Kim et al., 2015). This highlights, that the effects of the immunosuppressive drug on the matrix remodeling enzymes are highly context dependent and further studies are required to elucidate their connection in cSCC formation in OTRs.

Beside the Collagen meshwork, we also investigated the effects of CsA and SUN on the hyaluronic acid (HA) structure. In HaCaT-OTCs none of the treatment parameters caused changes in the HA

distribution. However, in NHEK-OTCs the combined treatment with CsA and SUN led to a clear reduction of HA expression. This observation aligns with the finding of Tzellos et al. who reported an increased hyaluronidase expression, associated with an enhanced hyaluronic acid degradation in UV-exposed human skin, compared to unexposed skin (Tzellos et al., 2009). However, a link between CsA and hyaluronidase induction has, to the best of our knowledge, not been reported. In contrast, one publication even describes a boost of HA expression upon CsA treatment in rat kidney fibroblasts (Han et al., 2010a). Thus, the next step would be to investigate if regulation of hyaluronidases is occurring in the NHEK-OTCs upon CsA and SUN treatment. In the microarray of the HaCaT cultures no changes in hyaluronidase expression were detected. But this is not of surprise as there was also no HA phenotype present. However, from this observation we can conclude that the reduction of HA is not associated with the invasion inducing effect of CsA.

In general, the reference data on combined effects of irradiation and CsA application on dermal components is limited, as most studies focusing on the interplay between CsA and sunlight were carried out using UVB as radiation source, which fails to penetrate the dermis.

## 5.6. CsA induces a myofibroblast-like phenotype in the dermal fibroblasts

The dermal fibroblasts showed a clear change in size and shape in both HaCaT and NHEK cultures treated with CsA. The cells became bigger and rounder, while expressing more Vimentin, indicating an ongoing differentiation process, e.g. into myofibroblasts. This fibroblast differentiation state takes its name from sharing morphological characteristics with smooth muscle cells. Myofibroblast differentiation is shown to play an important role during wound healing, but has also been associated with excessive scaring and fibrosis (Darby et al., 2014). A major marker for this differentiation process is an increased expression of alpha smooth muscle actin (αSMA), which is usually induced by TGFβ via Integrin αvβ1 (Lygoe et al., 2004).
Myofibroblasts are also often found in the tumor stroma and are known to promote the migration of tumor cells (Otranto et al., 2012). Also in our HaCaT-OTC studies we observed an association of the morphologically modified fibroblasts with the sites of ongoing invasion. Furthermore, the microarray gene expression analysis of our studies revealed an upregulation of αSMA as well as Integrin αvβ1, supporting the hypothesis of a CsA induced myofibroblast transformation. A correlation between CsA exposition and enhanced expression of both Vimentin and αSMA has been already described in human epidermoid A431 xenograft tumors (Walsh et al., 2011). However,

immune staining for αSMA on OTC-sections failed to visualize a presence of the protein in the fibroblasts of the CsA treated HaCaT and NHEK cultures, speaking against a transition into myofibroblast as the result of the differentiation process.

Our studies also revealed an increased density of the fibroblasts around the invasion sites. Such a rearrangement, along with a change of differentiation, is often a sign of an ongoing fibrosis. The formation of fibrosis surrounding invading tumor fronts has already been described for non-melanoma skin cancer patients (Hassanein et al., 2005). Furthermore, CsA has been linked to tubulointerstitial fibrosis and fibroblast accumulation in the kidneys of organ transplant recipients (Francis and Bai, 2018). However, a link between CsA and dermal fibrosis has, to the best of our knowledge, not yet been described. In our microarray analysis we detected an upregulation of several fibrosis related genes, namely Periostin, Lumican and Collagen XIII, supporting the hypothesis of an induction of fibrosis.

However, the subsequent qPCR analysis could only validate an upregulation of Periostin, while for Lumican and Collagen XIII no significant regulation was detected, speaking against an induction of fibrosis. Furthermore, for fibrosis an increased deposition of ECM components, such as hyaluronic acid, fibronectin and Collagen I, are described (Wynn, 2007). In contrast to that, our studies on the HaCaT-OTCs demonstrated no changes in the expression of hyaluronic acid after treatment and the presence of Collagen I and III even was significantly reduced.

In conclusion, CsA caused a remodulation of the dermal compartment in both OTC systems, especially in the direct periphery of the HaCaT invasion sites, indicating that this new matrix organization is associated with or may even support the migration of the epidermal cells. Although this organization shows many parallels to myofibroblast- and/or cancer- associated fibrosis, a definite proof could not be established.

## 5.7. CsA promotes invasion in HaCaT-OTCs by inducing Akt1

The microarray associated pathway analysis highlighted the regulation of several signaling pathways, including the mTOR, the TGFβ and the TNFα-NFκB signaling mechanisms. All of them have also been described as CsA regulated (Du et al., 2009; Han et al., 2010b; Walsh et al., 2011). The mTOR pathway, and especially mTOR complex 1 (mTORC1) activation, has been associated with an increased malignancy of cutaneous squamous cell carcinomas several times earlier (Arumugam et al., 2012; Carr et al., 2012; Claerhout et al., 2010). Thus, we decided to further focus our studies on this particular signaling mechanism.

The mTOR pathway plays a key role in skin morphogenesis and epidermal barrier formation (Ding et al., 2016). There are several mechanisms with which mTORC1 can be induced. In case of CsA, the most important proves to be the induction via activation of Akt1, also referred to as Akt-mTOR pathway. Here, the binding of a ligand to the epidermal growth factor (EGF) receptor causes the recruitment of Akt1 to the plasma membrane, leading to its phosphorylation and activation. The activated form of Akt1 then binds to mTORC1. CsA arguably promotes this mechanism by inducing the translocation of Akt1 to the plasma membrane and suppressing the natural Akt1 inhibitor PTEN (Han et al., 2010b). In our HaCaT-OTC studies, inhibition of Akt1 with the specific inhibitor Triciribine (TCN) led to a loss of phosphorylated Akt1 and a significant reduction of CsA-induced invasion, suggesting a role of this pathway for skin tumor formation in CsA immunosuppressed patients. This assumption also aligns with the observation of a reduced NMSC development in organ transplant recipients who were treated with immunosuppressive drugs targeting the mTOR pathway (Feldmeyer et al., 2012; Guba et al., 2002). It is assumed that the mTOR inhibitors reduce keratinocyte proliferation and alter cytokine secretion, making the cells less prone to an invasive behavior (DeTemple et al., 2016).

Yet, two questions remain open: First, how does the Akt/mTOR pathway promote specifically the formation of skin lesions? Second, is CsA not only suppressing the endogenous Akt1 inhibitor but also actively inducing the Akt/mTOR pathway?

One of the most frequent aberrations in skin lesions is a mutation of the p53 gene. Both, p53 and Akt-mTOR, are known to be activated by UV light, but the activation has been shown to lead to opposing consequences (Strozyk and Kulms, 2013). The UV-dependent activation of p53 usually leads to the induction of cell cycle arrest and DNA repair, in order to prevent mitosis with damaged DNA, or even to the induction of apoptosis, in case the DNA damage is irreparable. In contrast, the UV-induced Akt/mTOR pathway can overcome the arrest and initiate proliferation to prevent major tissue loss. In healthy keratinocytes there is a balance between both pathways. Imbalance, i.e. preference for one or the other pathway, can lead to enhanced cell death or clonal expansion, respectively. The majority of cSCCs show mutations of the p53 gene (Benjamin et al., 2008; Boukamp, 2005a; Brash et al., 1991). The additional inhibition of the endogenous Akt/mTOR pathway suppression system by CsA would then lead to a strong preference towards cell preservation and clonal expansion. Furthermore, the immunosuppressive drug has been shown to inhibit apoptosis by blocking the mitochondrial permeability transition pore, leading to a stabilization of the damaged cells and further supporting the imbalance (Tang et al., 2007; Yarosh et al., 2005). As HaCaT cells also carry a non-functional form of p53, such an imbalance might explain why they are driven into invasion upon CsA application.

The answer to a CsA specific induction of the mTOR pathway might lay in the CsA response of the basement membrane components. The performed gene expression analysis indicated an upregulation of the Laminin-5 chains α3, β3 and γ2. Also, as described above, our Laminin-5 staining revealed a localized degradation of the protein structure and a parallel expression of the protein within the invasion zone. Interestingly, Schenk et al. have shown that MMP dependent degradation of Laminin-5 causes the release of the γ2 subunit, which then functions as an EGF receptor ligand and induces cell migration as well as EMT (Pei et al., 2019; Schenk et al., 2003). Since the EGF receptor is also the entry point to the Akt-mTOR pathway, there might be a link between CsA driven basement membrane degradation and mTOR induction.

Although an inhibition of the Akt-mTOR pathway caused a reduction of CsA driven invasion in our studies, it failed to do so when the OTCs were treated with a combination of CsA and SUN. It is known, that exposure of keratinocytes to UV light is leading to the activation of the EGF receptor, most likely due to an enhanced formation of reactive oxygen species, and to the subsequent phosphorylation of Akt1 (Iordanov et al., 2002; Zhang et al., 2001). We confirmed these findings by demonstrating an enhanced phosphorylation of Akt1 upon SUN irradiation. However, as in the other inhibitor treated samples, also here the application of TCN inhibited phosphorylation of Akt1. Thus, a SUN-driven activation of the Akt-mTOR pathway can largely be excluded as a reason for the maintained invasion upon double treatment of CsA and SUN. Also, the inhibitor failed to suppress other CsA effects. The enhanced epidermal differentiation and the change in fibroblast morphology were still visible after a combined CsA and TCN treatment. Taken together, this suggests that these processes are controlled via an alternative mechanism.

As mentioned above, CsA effects on the TGFβ pathway and the TNFα-NFκB signaling mechanism have been previously reported (Bai et al., 2019; Du et al., 2009; Walsh et al., 2011). In our gene expression analysis, members of both systems appeared regulated. The induction of TNFα-NFκB signaling by CsA seems to be dependent on the activation of Akt (Baud and Karin, 2001; Chen and Goeddel, 2002). In contrast, no such link between Akt-mTOR and TGFβ has been described, indicating that these pathways become affected by CsA independently from each other. TGFβ is the main inducer of myofibroblast differentiation. Thus, the change in fibroblast morphology observed here might be connected to a CsA induced activation of TGFβ signaling. Also, mice studies suggest that a CsA dependent activation of TGFβ enhances the pathogenesis of cSCCs by promoting epithelial-mesenchymal transition (Walsh et al., 2011). Thus, it might be that CsA promotes sunlight induced cSCC development by inducing both the mTOR and the TGFβ pathway. While the activation of the mTOR pathway would lead to an enhanced clonal expansion and migration of the epidermal

cells, the induction of TGFβ might contribute to changes in the dermis and the formation of a tumor supportive environment.

## 5.8.  Conclusion

Our studies could to demonstrate that CsA is having one or even several immune system independent off-target effects on the human skin. The CsA treatment leads to an enhanced epidermal differentiation and an increase of the epithelial thickness in HaCaT-OTCs. Furthermore, it causes a widening and reduction of stability in the matrix in both HaCaT and NHEK cultures. This process is associated with, most presumably, fibroblast differentiation, especially in proximity to the basement membrane. CsA alone induced an invasive behavior in the otherwise non-tumorigenic HaCaT cells. As this does not happen with normal keratinocytes, the HaCaT specific genetic make-up, including their UV-indicative p53 mutations, is therefore considered to prime the cells for the CsA-induced change of behavior.

Since invasion can be suppressed by the inhibition of Akt1, the Akt-mTOR pathway in CsA-dependent invasion is arguably playing a role. Unfortunately, a therapeutic use of an Akt / mTOR inhibitor as a replacement for Calcineurin inhibitors in OTRs is not recommended, as this inhibition is itself associated with severe side effects. However, a combinational usage of mTOR and Calcineurin inhibitors in reduced concentrations, as to achieve immunosuppression with minimized side effects, should be reevaluated.

In addition to the induction of invasion, the combination of CsA with sunlight leads to an increase in epidermal proliferation of the HaCaT cells. Interestingly, and different from CsA alone, inhibition of Akt1 here is not suppressing the invasion. There is some evidence that CsA might promote SUN driven tumorigenesis in a TGFβ dependent manner. Therefore, it would be interesting to explore, if an additional inhibition of TGFβ signaling would lead to a total suppression of CsA and sunlight induced invasion.

# 6. Acknowledgement

First, I would like to thank Prof. Dr. Petra Boukamp who gave me the great opportunity to become a part of her wonderful group as well as the possibility to conduct this project for the last four years and for introducing me into the versatile field of skin research. With her as a highly inspiring teacher on the one hand and an incredibly motivating boss on the other I could not have wished for a better doctoral advisor. Second, I want to thank Prof. Dr. Jens Fischer who kindly accepted to become the co-supervisor for my PhD studies and who became an important collaboration partner for all questions related to the fascinating field of matrix biology. Third, I am grateful to PD Dr. Joachim Altschmied who agreed to assist me during my studies as my official mentor.

A special expression of gratitude goes to my third supervisor Dr. Elizabeth Pavez Loriè. I want to thank her for taking me under her wing and accompanying me during this journey as a superior, friend and yoda. Without her guidance this dissertation would not have been possible. I also saw it as a great sign of trust by her when sharing the responsibility for the laboratory and the supervision of students and guest researchers with me. I am highly thankful for this experience and I wish her all the best for her further career.

Furthermore, I would like to express my gratitude to my collaboration partners. I want to thank Dr. Rüdiger Greinert, Dr. Beate Volkmer and Dr. Alexander Rapp, of course including their teams, for their invaluable help in all irradiation related aspects and especially during the establishment of the KAUVIR lamp in our laboratory. Also, I would like to show my greatest appreciation to Dr. Maria Herberg and Dr. Jörg Galle for their great support in the analysis of my gene expression data and in the identification of my closer research focus. I want to express my gratefulness towards Dr. Damir Krunic for assisting me with his full competence in fluorescence microscopy and in the quantitative analysis of microscopy data. And I want to thank Dr. Daniel Gorski for his support in the detection and analysis of the hyaluronic acid distribution. Last, I would like to thank Dr. Hans-Jürgen Stark and Iris Martin for their advice in all questions dealing with *in vitro* modelling and immune staining.

I want to thank Dr. Lisa Schardt for introducing me into the field of Cyclosporin research and for assisting me with the planning of my own studies on this topic. I am very proud that I got the occasion to continue such a well well-established project and her support has been a great help to establish my own research.

Special thanks go to my dear colleagues Katharina Janke and Jessica Nagel who I experienced as office mates, cell lab buddies and great friends. Sharing the struggles of a PhD life with them made

this journey a lot easier and by far more amusing. Enduring the endless sessions in the cell culture or at the microscope probably would not have been possible without their company.

I also would like to express my gratitude to Anke Hüls, Katharina Rolfes, Mana Kaveh and Marius Pollet as I could always rely on their support in scientific as well as in personal aspects. No matter if over a cup of coffee at the lab late in the day or over a glass of Altbier in the old town early in the morning, all of them always had advice for me at any time and on any topic.

It was simply great to have such reliable and helpful colleagues and I am convinced that all six of them have what it takes to become a great scientist.

There are many more colleagues who contributed to my PhD journey and deserve a mentioning in this chapter. I just want to thank everyone at the IUF for accompanying me during the last years, for supporting me in technical and scientific aspects and for being so much more than just colleagues. It is rare to find a place with such extraordinary scientists, engineers and technicians and such a warm, friendly and harmonic atmosphere among coworkers. At this institute I could experience an impressive level of cooperation and solidarity between the staff members and I can say that I greatly benefited from it. I am very thankful to have had the opportunity to be a part of this group.

My deepest gratitude I owe to my girlfriend Eva who has been at my side for the last two years and who has been sharing with my all the moments of both success and frustration. During this time, she has become my most wonderful companion and probably also my greatest fan. I am so happy to have her in my life. Обичам те мила моя за всичко на света. Заедно можем да направим всичко.

Finally, I would like to thank my brothers Thomas and Markus and my sister Barbara as well as my parents for their endless support. Throughout my entire studies they went along with me, assisting me whenever they could. It is a wonderful experience to have such supportive family on which you can rely at any circumstances.

# 7. References

Abikhair Burgo, M., Roudiani, N., Chen, J., Santana, A.L., Doudican, N., Proby, C., Felsen, D., and Carucci, J.A. (2018). Ruxolitinib inhibits cyclosporine-induced proliferation of cutaneous squamous cell carcinoma. JCI Insight *3*.

Abikhair, M., Mitsui, H., Yanofsky, V., Roudiani, N., Ovits, C., Bryan, T., Oberyszyn, T.M., Tober, K.L., Gonzalez, J., Krueger, J.G*., et al.* (2016). Cyclosporine A immunosuppression drives catastrophic squamous cell carcinoma through IL-22. JCI Insight *1*, e86434.

Ahmed Haji Omar, A., Haglund, C., Virolainen, S., Hayry, V., Atula, T., Kontio, R., Salo, T., Sorsa, T., and Hagstrom, J. (2015). MMP-7, MMP-8, and MMP-9 in oral and cutaneous squamous cell carcinomas. Oral Surg Oral Med Oral Pathol Oral Radiol *119*, 459-467.

Anton-Lamprecht, I., and Gedde-Dahl, T. (2002). Epidermolysis bullosa. In Rimoin DL, Connor JM, Pyeritz RE, Korf BR, eds Principles and practice of medical genetics (London: Churchill Livingstone), pp. 3810-3897.

Arumugam, A., Walsh, S.B., Xu, J., Afaq, F., Elmets, C.A., and Athar, M. (2012). Combined inhibition of p38 and Akt signaling pathways abrogates cyclosporine A-mediated pathogenesis of aggressive skin SCCs. Biochemical and biophysical research communications *425*, 177-181.

Athas, W.F., Hunt, W.C., and Key, C.R. (2003). Changes in nonmelanoma skin cancer incidence between 1977-1978 and 1998-1999 in Northcentral New Mexico. Cancer Epidemiol Biomarkers Prev *12*, 1105-1108.

Babu, M., and Wells, A. (2001). Dermal-Epidermal Communication in Wound Healing. Wounds: a compendium of clinical research and practice *13(5)*, 183-189.

Bahner, J.D., and Bordeaux, J.S. (2013). Non-melanoma skin cancers: photodynamic therapy, cryotherapy, 5-fluorouracil, imiquimod, diclofenac, or what? Facts and controversies. Clin Dermatol *31*, 792-798.

Bai, Z., Lu, J., and Yang, Y. (2019). [Role of TGF-beta1/ILK/FSP1 signaling pathway in cyclosporin A-induced epithelialmesenchymal transition in cultured renal tubular epithelial cells]. Nan Fang Yi Ke Da Xue Xue Bao *39*, 804-809.

Bansal, R., Nakagawa, S., Yazdani, S., van Baarlen, J., Venkatesh, A., Koh, A.P., Song, W.M., Goossens, N., Watanabe, H., Beasley, M.B*., et al.* (2017). Integrin alpha 11 in the regulation of the myofibroblast phenotype: implications for fibrotic diseases. Exp Mol Med *49*, e396.

Barker, C.F., and Markmann, J.F. (2013). Historical overview of transplantation. Cold Spring Harb Perspect Med *3*, a014977.

Baud, V., and Karin, M. (2001). Signal transduction by tumor necrosis factor and its relatives. Trends Cell Biol *11*, 372-377.

Bavinck, J.N., De Boer, A., Vermeer, B.J., Hartevelt, M.M., van der Woude, F.J., Claas, F.H., Wolterbeek, R., and Vandenbroucke, J.P. (1993). Sunlight, keratotic skin lesions and skin cancer in renal transplant recipients. The British journal of dermatology *129*, 242-249.

Benjamin, C.L., Melnikova, V.O., and Ananthaswamy, H.N. (2008). P53 protein and pathogenesis of melanoma and nonmelanoma skin cancer. Adv Exp Med Biol *624*, 265-282.

Bentata, Y. (2019). Tacrolimus: 20 years of use in adult kidney transplantation. What we should know about its nephrotoxicity. Artif Organs.

Berg, D., and Otley, C.C. (2002). Skin cancer in organ transplant recipients: Epidemiology, pathogenesis, and management. J Am Acad Dermatol *47*, 1-17; quiz 18-20.

Berndt, N., Yang, H., Trinczek, B., Betzi, S., Zhang, Z., Wu, B., Lawrence, N.J., Pellecchia, M., Schonbrunn, E., Cheng, J.Q.*, et al.* (2010). The Akt activation inhibitor TCN-P inhibits Akt phosphorylation by binding to the PH domain of Akt and blocking its recruitment to the plasma membrane. Cell Death Differ *17*, 1795-1804.

Berneburg, M., Grether-Beck, S., Kurten, V., Ruzicka, T., Briviba, K., Sies, H., and Krutmann, J. (1999). Singlet oxygen mediates the UVA-induced generation of the photoaging-associated mitochondrial common deletion. The Journal of biological chemistry *274*, 15345-15349.

Berning, M., Prätzel-Wunder, S., Bickenbach, J.R., and Boukamp, P. (2015). 3D in vitro skin and skin cancer models based upon human fibroblast-derived matrix.

Borel, J.F., Feurer, C., Gubler, H.U., and Stahelin, H. (1976). Biological effects of cyclosporin A: a new antilymphocytic agent. Agents Actions *6*, 468-475.

Boukamp, P. (2005a). Non-melanoma skin cancer: what drives tumor development and progression? Carcinogenesis *26*, 1657-1667.

Boukamp, P. (2005b). UV-induced skin cancer: similarities--variations. Journal der Deutschen Dermatologischen Gesellschaft = Journal of the German Society of Dermatology : JDDG *3*, 493-503.

Boukamp, P., Petrussevska, R.T., Breitkreutz, D., Hornung, J., Markham, A., and Fusenig, N.E. (1988). Normal keratinization in a spontaneously immortalized aneuploid human keratinocyte cell line. The Journal of cell biology *106*, 761-771.

Bouwes Bavinck, J.N., Feltkamp, M.C.W., Green, A.C., Fiocco, M., Euvrard, S., Harwood, C.A., Nasir, S., Thomson, J., Proby, C.M., Naldi, L.*, et al.* (2018). Human papillomavirus and posttransplantation cutaneous squamous cell carcinoma: A multicenter, prospective cohort study. American journal of transplantation : official journal of the American Society of Transplantation and the American Society of Transplant Surgeons *18*, 1220-1230.

Bouwes Bavinck, J.N., Hardie, D.R., Green, A., Cutmore, S., MacNaught, A., O'Sullivan, B., Siskind, V., Van Der Woude, F.J., and Hardie, I.R. (1996). The risk of skin cancer in renal transplant recipients in Queensland, Australia. A follow-up study. Transplantation *61*, 715-721.

Bragulla, H.H., and Homberger, D.G. (2009). Structure and functions of keratin proteins in simple, stratified, keratinized and cornified epithelia. J Anat *214*, 516-559.

Brash, D.E., Rudolph, J.A., Simon, J.A., Lin, A., McKenna, G.J., Baden, H.P., Halperin, A.J., and Ponten, J. (1991). A role for sunlight in skin cancer: UV-induced p53 mutations in squamous cell carcinoma. Proceedings of the National Academy of Sciences of the United States of America *88*, 10124-10128.

Breitkreutz, D., Mirancea, N., and Nischt, R. (2009). Basement membranes in skin: unique matrix structures with diverse functions? Histochem Cell Biol *132*, 1-10.

Burke, M.T., Isbel, N., Barraclough, K.A., Jung, J.W., Wells, J.W., and Staatz, C.E. (2015). Genetics and nonmelanoma skin cancer in kidney transplant recipients. Pharmacogenomics *16*, 161-172.

Burnworth, B., Arendt, S., Muffler, S., Steinkraus, V., Brocker, E.B., Birek, C., Hartschuh, W., Jauch, A., and Boukamp, P. (2007). The multi-step process of human skin carcinogenesis: a role for p53, cyclin D1, hTERT, p16, and TSP-1. European journal of cell biology *86*, 763-780.

Busch, S., Acar, A., Magnusson, Y., Gregersson, P., Ryden, L., and Landberg, G. (2015). TGF-beta receptor type-2 expression in cancer-associated fibroblasts regulates breast cancer cell growth and survival and is a prognostic marker in pre-menopausal breast cancer. Oncogene *34*, 27-38.

Calles, C., Schneider, M., Macaluso, F., Benesova, T., Krutmann, J., and Schroeder, P. (2010). Infrared A radiation influences the skin fibroblast transcriptome: mechanisms and consequences. The Journal of investigative dermatology *130*, 1524-1536.

Canning, M.T., Nay, S.L., Pena, A.V., and Yarosh, D.B. (2006). Calcineurin inhibitors reduce nuclear localization of transcription factor NFAT in UV-irradiated keratinocytes and reduce DNA repair. Journal of molecular histology *37*, 285-291.

Caroti, L., Zanazzi, M., Paudice, N., Tsalouchos, A., Carta, P., Larti, A., Pimpinelli, N., Moscarelli, L., Salvadori, M., and Bertoni, E. (2012). Conversion from calcineurin inhibitors to everolimus with low-dose cyclosporine in renal transplant recipients with squamous cell carcinoma of the skin. Transplant Proc *44*, 1926-1927.

Carr, T.D., DiGiovanni, J., Lynch, C.J., and Shantz, L.M. (2012). Inhibition of mTOR suppresses UVB-induced keratinocyte proliferation and survival. Cancer prevention research *5*, 1394-1404.

Carter, W.G., Ryan, M.C., and Gahr, P.J. (1991). Epiligrin, a new cell adhesion ligand for integrin alpha 3 beta 1 in epithelial basement membranes. Cell *65*, 599-610.

Carucci, J.A. (2004). Cutaneous oncology in organ transplant recipients: meeting the challenge of squamous cell carcinoma. The Journal of investigative dermatology *123*, 809-816.

Chalmers, Z.R., Connelly, C.F., Fabrizio, D., Gay, L., Ali, S.M., Ennis, R., Schrock, A., Campbell, B., Shlien, A., Chmielecki, J.*, et al.* (2017). Analysis of 100,000 human cancer genomes reveals the landscape of tumor mutational burden. Genome Med *9*, 34.

Chen, G., and Goeddel, D.V. (2002). TNF-R1 signaling: a beautiful pathway. Science *296*, 1634-1635.

Choi, S.C., Lee, H., Choi, J.H., Kim, J.H., Park, C.Y., Joo, H.J., Park, J.H., Hong, S.J., Yu, C.W., and Lim, D.S. (2015). Cyclosporin A induces cardiac differentiation but inhibits hemato-endothelial differentiation of P19 cells. PloS one *10*, e0117410.

Claerhout, S., Verschooten, L., Van Kelst, S., De Vos, R., Proby, C., Agostinis, P., and Garmyn, M. (2010). Concomitant inhibition of AKT and autophagy is required for efficient cisplatin-induced apoptosis of metastatic skin carcinoma. International journal of cancer Journal international du cancer *127*, 2790-2803.

Collins, C.A., Kretzschmar, K., and Watt, F.M. (2011). Reprogramming adult dermis to a neonatal state through epidermal activation of beta-catenin. Development *138*, 5189-5199.

Cowan, M.K. (2012). Microbiology : a systems approach, 3rd edn (New York, NY: McGraw-Hill).

Crabtree, G.R., and Schreiber, S.L. (2009). SnapShot: Ca2+-calcineurin-NFAT signaling. Cell *138*, 210, 210 e211.

D'Orazio, J., Jarrett, S., Amaro-Ortiz, A., and Scott, T. (2013). UV radiation and the skin. Int J Mol Sci *14*, 12222-12248.

Darby, I.A., Laverdet, B., Bonte, F., and Desmouliere, A. (2014). Fibroblasts and myofibroblasts in wound healing. Clin Cosmet Investig Dermatol *7*, 301-311.

Darr, D., and Fridovich, I. (1994). Free radicals in cutaneous biology. The Journal of investigative dermatology *102*, 671-675.

De Simone, P., Carrai, P., Coletti, L., Ghinolfi, D., Petruccelli, S., Precisi, A., Campani, D., Marchetti, P., and Filipponi, F. (2018). Everolimus vs Mycophenolate Mofetil in Combination With Tacrolimus: A Propensity Score-matched Analysis in Liver Transplantation. Transplant Proc *50*, 3615-3620.

DeTemple, V., Satzger, I., Walter, A., Schaper, K., and Gutzmer, R. (2016). Effects of mammalian target of rapamycin inhibitors on cytokine production and differentiation in keratinocytes. Experimental dermatology *25*, 775-782.

Ding, X., Bloch, W., Iden, S., Ruegg, M.A., Hall, M.N., Leptin, M., Partridge, L., and Eming, S.A. (2016). mTORC1 and mTORC2 regulate skin morphogenesis and epidermal barrier formation. Nat Commun *7*, 13226.

Donehower, L.A., Harvey, M., Slagle, B.L., McArthur, M.J., Montgomery, C.A., Jr., Butel, J.S., and Bradley, A. (1992). Mice deficient for p53 are developmentally normal but susceptible to spontaneous tumours. Nature *356*, 215-221.

Douki, T., and Cadet, J. (2001). Individual determination of the yield of the main UV-induced dimeric pyrimidine photoproducts in DNA suggests a high mutagenicity of CC photolesions. Biochemistry *40*, 2495-2501.

Douki, T., Court, M., Sauvaigo, S., Odin, F., and Cadet, J. (2000). Formation of the main UV-induced thymine dimeric lesions within isolated and cellular DNA as measured by high performance liquid chromatography-tandem mass spectrometry. The Journal of biological chemistry *275*, 11678-11685.

Du, S., Hiramatsu, N., Hayakawa, K., Kasai, A., Okamura, M., Huang, T., Yao, J., Takeda, M., Araki, I., Sawada, N.*, et al.* (2009). Suppression of NF-kappaB by cyclosporin a and tacrolimus (FK506) via induction of the C/EBP family: implication for unfolded protein response. Journal of immunology *182*, 7201-7211.

Duncan, F.J., Wulff, B.C., Tober, K.L., Ferketich, A.K., Martin, J., Thomas-Ahner, J.M., Allen, S.D., Kusewitt, D.F., Oberyszyn, T.M., and Vanbuskirk, A.M. (2007). Clinically relevant immunosuppressants influence UVB-induced tumor size through effects on inflammation and angiogenesis. American journal of transplantation : official journal of the American Society of Transplantation and the American Society of Transplant Surgeons *7*, 2693-2703.

Dziunycz, P., and Hofbauer, G.F. (2010). Immune phenotype of peripheral blood cells and skin squamous cell carcinoma in organ transplant recipients. Expert Rev Clin Immunol *6*, 359-362.

Eigentler, T.K., Leiter, U., Hafner, H.M., Garbe, C., Rocken, M., and Breuninger, H. (2017). Survival of Patients with Cutaneous Squamous Cell Carcinoma: Results of a Prospective Cohort Study. The Journal of investigative dermatology *137*, 2309-2315.

Elliott, B.M., Douglass, B.R., McConnell, D., Johnson, B., and Harmston, C. (2018). Incidence, demographics and surgical outcomes of cutaneous squamous cell carcinoma diagnosed in Northland, New Zealand. N Z Med J *131*, 61-68.

Errasti, P., Izquierdo, D., Martin, P., Errasti, M., Slon, F., Romero, A., and Lavilla, F.J. (2010). Pneumonitis associated with mammalian target of rapamycin inhibitors in renal transplant recipients: a single-center experience. Transplant Proc *42*, 3053-3054.

Espana, A., Martinez-Gonzalez, M.A., Garcia-Granero, M., Sanchez-Carpintero, I., Rabago, G., and Herreros, J. (2000). A prospective study of incident nonmelanoma skin cancer in heart transplant recipients. The Journal of investigative dermatology *115*, 1158-1160.

Euvrard, S., Kanitakis, J., and Claudy, A. (2003). Skin cancers after organ transplantation. The New England journal of medicine *348*, 1681-1691.

Euvrard, S., Morelon, E., Rostaing, L., Goffin, E., Brocard, A., Tromme, I., Broeders, N., del Marmol, V., Chatelet, V., Dompmartin, A.*, et al.* (2012). Sirolimus and secondary skin-cancer prevention in kidney transplantation. The New England journal of medicine *367*, 329-339.

Farshchian, M., Nissinen, L., Siljamaki, E., Riihila, P., Toriseva, M., Kivisaari, A., Ala-Aho, R., Kallajoki, M., Verajankorva, E., Honkanen, H.K.*, et al.* (2015). EphB2 Promotes Progression of Cutaneous Squamous Cell Carcinoma. The Journal of investigative dermatology *135*, 1882-1892.

Feldmeyer, L., Hofbauer, G.F., Boni, T., French, L.E., and Hafner, J. (2012). Mammalian target of rapamycin (mTOR) inhibitors slow skin carcinogenesis, but impair wound healing. The British journal of dermatology *166*, 422-424.

Feske, S., Okamura, H., Hogan, P.G., and Rao, A. (2003). Ca2+/calcineurin signalling in cells of the immune system. Biochemical and biophysical research communications *311*, 1117-1132.

Fine, J.D., Johnson, L.B., Weiner, M., Li, K.P., and Suchindran, C. (2009). Epidermolysis bullosa and the risk of life-threatening cancers: the National EB Registry experience, 1986-2006. J Am Acad Dermatol *60*, 203-211.

Fisher, G.J., Duell, E.A., Nickoloff, B.J., Annesley, T.M., Kowalke, J.K., Ellis, C.N., and Voorhees, J.J. (1988). Levels of cyclosporin in epidermis of treated psoriasis patients differentially inhibit growth of keratinocytes cultured in serum free versus serum containing media. The Journal of investigative dermatology *91*, 142-146.

Fogel, A.L., Hill, S., and Teng, J.M. (2015). Advances in the therapeutic use of mammalian target of rapamycin (mTOR) inhibitors in dermatology. J Am Acad Dermatol *72*, 879-889.

Fortina, A.B., Piaserico, S., Alaibac, M., and Peserico, A. (2009). Squamous cell carcinoma. Cancer Treat Res *146*, 241-261.

Francis, C.E., and Bai, Y. (2018). Differential expression of cyclosporine A-Induced calcineurin isoform-specific matrix metalloproteinase 9 (MMP-9) in renal fibroblasts. Biochemical and biophysical research communications *503*, 2549-2554.

Garrett, G.L., Lowenstein, S.E., Singer, J.P., He, S.Y., and Arron, S.T. (2016). Trends of skin cancer mortality after transplantation in the United States: 1987 to 2013. J Am Acad Dermatol *75*, 106-112.

Gawronska-Kozak, B., and Kirk-Ballard, H. (2013). Cyclosporin A reduces matrix metalloproteinases and collagen expression in dermal fibroblasts from regenerative FOXN1 deficient (nude) mice. Fibrogenesis Tissue Repair *6*, 7.

Geissler, E.K. (2009). In Skin cancer after organ transplantation (New York: Springer,), pp. 23-43.

Greinert, R., Volkmer, B., Henning, S., Breitbart, E.W., Greulich, K.O., Cardoso, M.C., and Rapp, A. (2012). UVA-induced DNA double-strand breaks result from the repair of clustered oxidative DNA damages. Nucleic acids research *40*, 10263-10273.

Grether-Beck, S., Krutmann, J., Wilkens, K., and D'Amato, K. (2017). Effect of a Blueberry-Derived Antioxidant Matrix on Infrared-A Induced Gene Expression in Human Dermal Fibroblasts. J Drugs Dermatol *16*, s125-s128.

Grulich, A.E., van Leeuwen, M.T., Falster, M.O., and Vajdic, C.M. (2007). Incidence of cancers in people with HIV/AIDS compared with immunosuppressed transplant recipients: a meta-analysis. Lancet *370*, 59-67.

Guba, M., Graeb, C., Jauch, K.W., and Geissler, E.K. (2004). Pro- and anti-cancer effects of immunosuppressive agents used in organ transplantation. Transplantation *77*, 1777-1782.

Guba, M., von Breitenbuch, P., Steinbauer, M., Koehl, G., Flegel, S., Hornung, M., Bruns, C.J., Zuelke, C., Farkas, S., Anthuber, M.*, et al.* (2002). Rapamycin inhibits primary and metastatic tumor growth by antiangiogenesis: involvement of vascular endothelial growth factor. Nat Med *8*, 128-135.

Han, D.H., Song, H.K., Lee, S.Y., Song, J.H., Piao, S.G., Yoon, H.E., Ghee, J.Y., Yoon, H.J., Kim, J., and Yang, C.W. (2010a). Upregulation of hyaluronan and its binding receptors in an experimental model of chronic cyclosporine nephropathy. Nephrology (Carlton) *15*, 216-224.

Han, W., Ming, M., He, T.C., and He, Y.Y. (2010b). Immunosuppressive cyclosporin A activates AKT in keratinocytes through PTEN suppression: implications in skin carcinogenesis. The Journal of biological chemistry *285*, 11369-11377.

Han, W., Soltani, K., Ming, M., and He, Y.Y. (2012). Deregulation of XPC and CypA by cyclosporin A: an immunosuppression-independent mechanism of skin carcinogenesis. Cancer prevention research *5*, 1155-1162.

Hanaway, M.J., Woodle, E.S., Mulgaonkar, S., Peddi, V.R., Kaufman, D.B., First, M.R., Croy, R., Holman, J., and Group, I.S. (2011). Alemtuzumab induction in renal transplantation. The New England journal of medicine *364*, 1909-1919.

Harrison, J.H., Merrill, J.P., and Murray, J.E. (1956). Renal homotransplantation in identical twins. Surg Forum *6*, 432-436.

Harwood, C.A., McGregor, J.M., Proby, C.M., and Breuer, J. (1999). Human papillomavirus and the development of non-melanoma skin cancer. J Clin Pathol *52*, 249-253.

Harwood, C.A., McGregor, J.M., Swale, V.J., Proby, C.M., Leigh, I.M., Newton, R., Khorshid, S.M., and Cerio, R. (2003). High frequency and diversity of cutaneous appendageal tumors in organ transplant recipients. J Am Acad Dermatol *48*, 401-408.

Harwood, C.A., Proby, C.M., Inman, G.J., and Leigh, I.M. (2016). The Promise of Genomics and the Development of Targeted Therapies for Cutaneous Squamous Cell Carcinoma. Acta dermato-venereologica *96*, 3-16.

Hassanein, A.M., Proper, S.A., Depcik-Smith, N.D., and Flowers, F.P. (2005). Peritumoral fibrosis in basal cell and squamous cell carcinoma mimicking perineural invasion: potential pitfall in Mohs micrographic surgery. Dermatol Surg *31*, 1101-1106.

Herman, M., Weinstein, T., Korzets, A., Chagnac, A., Ori, Y., Zevin, D., Malachi, T., and Gafter, U. (2001). Effect of cyclosporin A on DNA repair and cancer incidence in kidney transplant recipients. J Lab Clin Med *137*, 14-20.

Hiesse, C., Kriaa, F., Rieu, P., Larue, J.R., Benoit, G., Bellamy, J., Blanchet, P., and Charpentier, B. (1995). Incidence and type of malignancies occurring after renal transplantation in conventionally and cyclosporine-treated recipients: analysis of a 20-year period in 1600 patients. Transplant Proc *27*, 972-974.

Hojo, M., Morimoto, T., Maluccio, M., Asano, T., Morimoto, K., Lagman, M., Shimbo, T., and Suthanthiran, M. (1999). Cyclosporine induces cancer progression by a cell-autonomous mechanism. Nature *397*, 530-534.

Hovnanian, A., Rochat, A., Bodemer, C., Petit, E., Rivers, C.A., Prost, C., Fraitag, S., Christiano, A.M., Uitto, J., Lathrop, M.*, et al.* (1997). Characterization of 18 new mutations in COL7A1 in

recessive dystrophic epidermolysis bullosa provides evidence for distinct molecular mechanisms underlying defective anchoring fibril formation. Am J Hum Genet *61*, 599-610.

Howley, P.M., and Pfister, H.J. (2015). Beta genus papillomaviruses and skin cancer. Virology *479-480*, 290-296.

Huang, D., Du, C., Ji, D., Xi, J., and Gu, J. (2017). Overexpression of LAMC2 predicts poor prognosis in colorectal cancer patients and promotes cancer cell proliferation, migration, and invasion. Tumour Biol *39*, 1010428317705849.

Iordanov, M.S., Choi, R.J., Ryabinina, O.P., Dinh, T.H., Bright, R.K., and Magun, B.E. (2002). The UV (Ribotoxic) stress response of human keratinocytes involves the unexpected uncoupling of the Ras-extracellular signal-regulated kinase signaling cascade from the activated epidermal growth factor receptor. Molecular and cellular biology *22*, 5380-5394.

Jablonska-Trypuc, A., Matejczyk, M., and Rosochacki, S. (2016). Matrix metalloproteinases (MMPs), the main extracellular matrix (ECM) enzymes in collagen degradation, as a target for anticancer drugs. J Enzyme Inhib Med Chem *31*, 177-183.

Jensen, P., Hansen, S., Moller, B., Leivestad, T., Pfeffer, P., Geiran, O., Fauchald, P., and Simonsen, S. (1999). Skin cancer in kidney and heart transplant recipients and different long-term immunosuppressive therapy regimens. Journal of the American Academy of Dermatology *40*, 177-186.

Ji, C., Yang, B., Yang, Z., Tu, Y., Yang, Y.L., He, L., and Bi, Z.G. (2012). Ultra-violet B (UVB)-induced skin cell death occurs through a cyclophilin D intrinsic signaling pathway. Biochemical and biophysical research communications *425*, 825-829.

Ju, R.J., Stehbens, S.J., and Haass, N.K. (2018). The Role of Melanoma Cell-Stroma Interaction in Cell Motility, Invasion, and Metastasis. Front Med (Lausanne) *5*, 307.

Kanitakis, J., Urabe, A., Haftek, M., and Thivolet, J. (1990). The effect of cyclosporin A on proliferation and differentiation-associated antigens of normal human skin xenografted onto nude mice. Journal of dermatological science *1*, 103-109.

Karam, S., and Wali, R.K. (2015). Current State of Immunosuppression: Past, Present, and Future. Crit Rev Eukaryot Gene Expr *25*, 113-134.

Karashima, T., Hachisuka, H., and Sasai, Y. (1996). FK506 and cyclosporin A inhibit growth factor-stimulated human keratinocyte proliferation by blocking cells in the G0/G1 phases of the cell cycle. Journal of dermatological science *12*, 246-254.

Karia, P.S., Han, J., and Schmults, C.D. (2013). Cutaneous squamous cell carcinoma: estimated incidence of disease, nodal metastasis, and deaths from disease in the United States, 2012. J Am Acad Dermatol *68*, 957-966.

Kariya, Y., and Miyazaki, K. (2004). The basement membrane protein laminin-5 acts as a soluble cell motility factor. Experimental cell research *297*, 508-520.

Katalinic, A., Kunze, U., and Schafer, T. (2003). Epidemiology of cutaneous melanoma and non-melanoma skin cancer in Schleswig-Holstein, Germany: incidence, clinical subtypes, tumour stages and localization (epidemiology of skin cancer). The British journal of dermatology *149*, 1200-1206.

Khattri, S., Shemer, A., Rozenblit, M., Dhingra, N., Czarnowicki, T., Finney, R., Gilleaudeau, P., Sullivan-Whalen, M., Zheng, X., Xu, H.*, et al.* (2014). Cyclosporine in patients with atopic dermatitis modulates activated inflammatory pathways and reverses epidermal pathology. The Journal of allergy and clinical immunology *133*, 1626-1634.

Khorshid, S.M., Glover, M.T., Churchill, L., McGregor, J.M., and Proby, C.M. (1996). p53 immunoreactivity in non-melanoma skin cancer from immunosuppressed and immunocompetent individuals: a comparative study of 246 tumours. Journal of cutaneous pathology *23*, 229-233.

Kim, Y.H., Jung, J.C., Jung, S.Y., Kim, Y.I., Lee, K.W., and Park, Y.J. (2015). Cyclosporine A Downregulates MMP-3 and MMP-13 Expression in Cultured Pterygium Fibroblasts. Cornea *34*, 1137-1143.

Krynitz, B., Edgren, G., Lindelof, B., Baecklund, E., Brattstrom, C., Wilczek, H., and Smedby, K.E. (2013). Risk of skin cancer and other malignancies in kidney, liver, heart and lung transplant recipients 1970 to 2008--a Swedish population-based study. International journal of cancer Journal international du cancer *132*, 1429-1438.

Kwa, R.E., Campana, K., and Moy, R.L. (1992). Biology of cutaneous squamous cell carcinoma. J Am Acad Dermatol *26*, 1-26.

Lacouture, M., and Sibaud, V. (2018). Toxic Side Effects of Targeted Therapies and Immunotherapies Affecting the Skin, Oral Mucosa, Hair, and Nails. Am J Clin Dermatol *19*, 31-39.

Lampe, A.K., Flanigan, K.M., Bushby, K.M., and Hicks, D. (1993). Collagen Type VI-Related Disorders. In GeneReviews((R)), M.P. Adam, H.H. Ardinger, R.A. Pagon, S.E. Wallace, L.J.H. Bean, K. Stephens, and A. Amemiya, eds. (Seattle (WA)).

Larsen, H.K., Thomsen, L.T., Haedersdal, M., Dehlendorff, C., Schwartz Sorensen, S., and Kjaer, S.K. (2019). Risk of genital warts in renal transplant recipients-A registry-based, prospective cohort study. American journal of transplantation : official journal of the American Society of Transplantation and the American Society of Transplant Surgeons *19*, 156-165.

Laurie, G.W., Leblond, C.P., and Martin, G.R. (1982). Localization of type IV collagen, laminin, heparan sulfate proteoglycan, and fibronectin to the basal lamina of basement membranes. The Journal of cell biology *95*, 340-344.

LeBoeuf, N.R., and Schmults, C.D. (2011). Update on the management of high-risk squamous cell carcinoma. Semin Cutan Med Surg *30*, 26-34.

Leboit, P.E., Burg, G., Weedon, D., and Sarasin, A. (2005). Squamous cell carcinoma. In Pathology & Genetics: Skin Tumors, D. Weedon, M.B. Morgan, C. Gross, E. Nagore, and L.L. Yu, eds. (WHO Classification of Tumours), pp. 20-25.

Lee, J.H., An, H.T., Chung, J.H., Kim, K.H., Eun, H.C., and Cho, K.H. (2002). Acute effects of UVB radiation on the proliferation and differentiation of keratinocytes. Photodermatology, photoimmunology & photomedicine *18*, 253-261.

Lehman, T.A., Modali, R., Boukamp, P., Stanek, J., Bennett, W.P., Welsh, J.A., Metcalf, R.A., Stampfer, M.R., Fusenig, N., Rogan, E.M.*, et al.* (1993). p53 mutations in human immortalized epithelial cell lines. Carcinogenesis *14*, 833-839.

Leiter, U., Keim, U., Eigentler, T., Katalinic, A., Holleczek, B., Martus, P., and Garbe, C. (2017). Incidence, Mortality, and Trends of Nonmelanoma Skin Cancer in Germany. The Journal of investigative dermatology *137*, 1860-1867.

Leslie, N.R., Dixon, M.J., Schenning, M., Gray, A., and Batty, I.H. (2012). Distinct inactivation of PI3K signalling by PTEN and 5-phosphatases. Adv Biol Regul *52*, 205-213.

Liebel, F., Kaur, S., Ruvolo, E., Kollias, N., and Southall, M.D. (2012). Irradiation of skin with visible light induces reactive oxygen species and matrix-degrading enzymes. The Journal of investigative dermatology *132*, 1901-1907.

Lindelof, B., Granath, F., Dal, H., Brandberg, Y., Adami, J., and Ullen, H. (2003). Sun habits in kidney transplant recipients with skin cancer: a case-control study of possible causative factors. Acta dermato-venereologica *83*, 189-193.

Lindelof, B., Sigurgeirsson, B., Gabel, H., and Stern, R.S. (2000). Incidence of skin cancer in 5356 patients following organ transplantation. The British journal of dermatology *143*, 513-519.

Linos, E., Katz, K.A., and Colditz, G.A. (2016). Skin Cancer-The Importance of Prevention. JAMA Intern Med *176*, 1435-1436.

Liotta, L.A., Tryggvason, K., Garbisa, S., Hart, I., Foltz, C.M., and Shafie, S. (1980). Metastatic potential correlates with enzymatic degradation of basement membrane collagen. Nature *284*, 67-68.

Liu, J., Farmer, J.D., Jr., Lane, W.S., Friedman, J., Weissman, I., and Schreiber, S.L. (1991). Calcineurin is a common target of cyclophilin-cyclosporin A and FKBP-FK506 complexes. Cell *66*, 807-815.

Liu, J., St Clair, D.K., Gu, X., and Zhao, Y. (2008). Blocking mitochondrial permeability transition prevents p53 mitochondrial translocation during skin tumor promotion. FEBS letters *582*, 1319-1324.

Lygoe, K.A., Norman, J.T., Marshall, J.F., and Lewis, M.P. (2004). AlphaV integrins play an important role in myofibroblast differentiation. Wound Repair Regen *12*, 461-470.

Mackenzie, K.A., Wells, J.E., Lynn, K.L., Simcock, J.W., Robinson, B.A., Roake, J.A., and Currie, M.J. (2010). First and subsequent nonmelanoma skin cancers: incidence and predictors in a population of New Zealand renal transplant recipients. Nephrology, dialysis, transplantation : official publication of the European Dialysis and Transplant Association - European Renal Association *25*, 300-306.

Marcil, I., and Stern, R.S. (2000). Risk of developing a subsequent nonmelanoma skin cancer in patients with a history of nonmelanoma skin cancer: a critical review of the literature and meta-analysis. Arch Dermatol *136*, 1524-1530.

Marinkovich, M.P. (2007). Tumour microenvironment: laminin 332 in squamous-cell carcinoma. Nat Rev Cancer *7*, 370-380.

Martelli-Marzagao, F., Santos Junior, G.F., Ogawa, M.M., Enokihara, M.M., Porro, A.M., and Tomimori, J. (2016). Human papillomavirus detected in viral warts of renal transplant recipients. Transpl Infect Dis *18*, 37-43.

Martincorena, I., Roshan, A., Gerstung, M., Ellis, P., Van Loo, P., McLaren, S., Wedge, D.C., Fullam, A., Alexandrov, L.B., Tubio, J.M.*, et al.* (2015). Tumor evolution. High burden and pervasive positive selection of somatic mutations in normal human skin. Science *348*, 880-886.

Martins, V.L., Vyas, J.J., Chen, M., Purdie, K., Mein, C.A., South, A.P., Storey, A., McGrath, J.A., and O'Toole, E.A. (2009). Increased invasive behaviour in cutaneous squamous cell carcinoma with loss of basement-membrane type VII collagen. Journal of cell science *122*, 1788-1799.

McKenzie, R., Blumthaler, M., Diaz, S., Fioletov, V., Herman, J., Seckmeyer, G., Smedley, A., and Webb, A. (2014). Rationalizing Nomenclature for UV Doses and Effects on Humans (WMO/GAW Report No. 211).

McLaughlin-Drubin, M.E. (2015). Human papillomaviruses and non-melanoma skin cancer. Semin Oncol *42*, 284-290.

McMorrow, T., Gaffney, M.M., Slattery, C., Campbell, E., and Ryan, M.P. (2005). Cyclosporine A induced epithelial-mesenchymal transition in human renal proximal tubular epithelial cells.

Nephrology, dialysis, transplantation : official publication of the European Dialysis and Transplant Association - European Renal Association *20*, 2215-2225.

Merrill, J.P., Murray, J.E., Harrison, J.H., Friedman, E.A., Dealy, J.B.J., and Dammin, G.J. (1960). Successful homotransplantation of the kidney between nonidentical twins. . The New England journal of medicine *262*, 1251–1260.

Mittal, A., and Colegio, O.R. (2017). Skin Cancers in Organ Transplant Recipients. American journal of transplantation : official journal of the American Society of Transplantation and the American Society of Transplant Surgeons *17*, 2509-2530.

Montaudie, H., Chiaverini, C., Sbidian, E., Charlesworth, A., and Lacour, J.P. (2016). Inherited epidermolysis bullosa and squamous cell carcinoma: a systematic review of 117 cases. Orphanet J Rare Dis *11*, 117.

Murray, J.C., Stingl, G., Kleinman, H.K., Martin, G.R., and Katz, S.I. (1979). Epidermal cells adhere preferentially to type IV (basement membrane) collagen. The Journal of cell biology *80*, 197-202.

Nakashima, Y., Ohta, S., and Wolf, A.M. (2017). Blue light-induced oxidative stress in live skin. Free Radic Biol Med *108*, 300-310.

Ng, Y.Z., Pourreyron, C., Salas-Alanis, J.C., Dayal, J.H., Cepeda-Valdes, R., Yan, W., Wright, S., Chen, M., Fine, J.D., Hogg, F.J.*, et al.* (2012). Fibroblast-derived dermal matrix drives development of aggressive cutaneous squamous cell carcinoma in patients with recessive dystrophic epidermolysis bullosa. Cancer research *72*, 3522-3534.

Nickoloff, B.J., Fisher, G.J., Mitra, R.S., and Voorhees, J.J. (1988). Additive and synergistic antiproliferative effects of cyclosporin A and gamma interferon on cultured human keratinocytes. The American journal of pathology *131*, 12-18.

Niessen, C.M., Hogervorst, F., Jaspars, L.H., de Melker, A.A., Delwel, G.O., Hulsman, E.H., Kuikman, I., and Sonnenberg, A. (1994). The alpha 6 beta 4 integrin is a receptor for both laminin and kalinin. Experimental cell research *211*, 360-367.

Nikolopoulos, S.N., Blaikie, P., Yoshioka, T., Guo, W., Puri, C., Tacchetti, C., and Giancotti, F.G. (2005). Targeted deletion of the integrin beta4 signaling domain suppresses laminin-5-dependent nuclear entry of mitogen-activated protein kinases and NF-kappaB, causing defects in epidermal growth and migration. Molecular and cellular biology *25*, 6090-6102.

Nissinen, L., Farshchian, M., Riihila, P., and Kahari, V.M. (2016). New perspectives on role of tumor microenvironment in progression of cutaneous squamous cell carcinoma. Cell Tissue Res *365*, 691-702.

Ong, C.S., Keogh, A.M., Kossard, S., Macdonald, P.S., and Spratt, P.M. (1999). Skin cancer in Australian heart transplant recipients. J Am Acad Dermatol *40*, 27-34.

Orimo, A., Gupta, P.B., Sgroi, D.C., Arenzana-Seisdedos, F., Delaunay, T., Naeem, R., Carey, V.J., Richardson, A.L., and Weinberg, R.A. (2005). Stromal fibroblasts present in invasive human breast carcinomas promote tumor growth and angiogenesis through elevated SDF-1/CXCL12 secretion. Cell *121*, 335-348.

Otranto, M., Sarrazy, V., Bonte, F., Hinz, B., Gabbiani, G., and Desmouliere, A. (2012). The role of the myofibroblast in tumor stroma remodeling. Cell Adh Migr *6*, 203-219.

Page, A., Navarro, M., Suarez-Cabrera, C., Alameda, J.P., Casanova, M.L., Paramio, J.M., Bravo, A., and Ramirez, A. (2016). Protective role of p53 in skin cancer: Carcinogenesis studies in mice lacking epidermal p53. Oncotarget *7*, 20902-20918.

Pei, Y.F., Liu, J., Cheng, J., Wu, W.D., and Liu, X.Q. (2019). Silencing of LAMC2 Reverses Epithelial-Mesenchymal Transition and Inhibits Angiogenesis in Cholangiocarcinoma via Inactivation of the Epidermal Growth Factor Receptor Signaling Pathway. The American journal of pathology *189*, 1637-1653.

Pickering, C.R., Zhou, J.H., Lee, J.J., Drummond, J.A., Peng, S.A., Saade, R.E., Tsai, K.Y., Curry, J.L., Tetzlaff, M.T., Lai, S.Y.*, et al.* (2014). Mutational landscape of aggressive cutaneous squamous cell carcinoma. Clin Cancer Res *20*, 6582-6592.

Ponticelli, C., Cucchiari, D., and Bencini, P. (2014). Skin cancer in kidney transplant recipients. J Nephrol *27*, 385-394.

Potenza, C., Bernardini, N., Balduzzi, V., Losco, L., Mambrin, A., Marchesiello, A., Tolino, E., Zuber, S., Skroza, N., and Proietti, I. (2018). A Review of the Literature of Surgical and Nonsurgical Treatments of Invasive Squamous Cells Carcinoma. Biomed Res Int *2018*, 9489163.

Pyke, C., Salo, S., Ralfkiaer, E., Romer, J., Dano, K., and Tryggvason, K. (1995). Laminin-5 is a marker of invading cancer cells in some human carcinomas and is coexpressed with the receptor for urokinase plasminogen activator in budding cancer cells in colon adenocarcinomas. Cancer research *55*, 4132-4139.

Rogers, H.W., Weinstock, M.A., Feldman, S.R., and Coldiron, B.M. (2015). Incidence Estimate of Nonmelanoma Skin Cancer (Keratinocyte Carcinomas) in the U.S. Population, 2012. JAMA Dermatol *151*, 1081-1086.

Rognoni, E., and Watt, F.M. (2018). Skin Cell Heterogeneity in Development, Wound Healing, and Cancer. Trends Cell Biol *28*, 709-722.

Rose, C.L., Chakravarti, N., Curry, J.L., Torres-Cabala, C.A., Bassett, R., Prieto, V.G., and Tetzlaff, M.T. (2012). The utility of ATF3 in distinguishing cutaneous squamous cell carcinoma among other cutaneous epithelial neoplasms. Journal of cutaneous pathology *39*, 762-768.

Roy, M.K., Takenaka, M., Kobori, M., Nakahara, K., Isobe, S., and Tsushida, T. (2006). Apoptosis, necrosis and cell proliferation-inhibition by cyclosporine A in U937 cells (a human monocytic cell line). Pharmacol Res *53*, 293-302.

Saigal, S., Norris, S., Muiesan, P., Rela, M., Heaton, N., and O'Grady, J. (2002). Evidence of differential risk for posttransplantation malignancy based on pretransplantation cause in patients undergoing liver transplantation. Liver transplantation : official publication of the American Association for the Study of Liver Diseases and the International Liver Transplantation Society *8*, 482-487.

Sakai, L.Y., Keene, D.R., Morris, N.P., and Burgeson, R.E. (1986). Type VII collagen is a major structural component of anchoring fibrils. The Journal of cell biology *103*, 1577-1586.

Santana, A.L., Felsen, D., and Carucci, J.A. (2017). Interleukin-22 and Cyclosporine in Aggressive Cutaneous Squamous Cell Carcinoma. Dermatol Clin *35*, 73-84.

Sapijaszko, M., Zloty, D., Bourcier, M., Poulin, Y., Janiszewski, P., Ashkenas, J., and Canadian Non-melanoma Skin Cancer Guidelines, C. (2015). Non-melanoma Skin Cancer in Canada Chapter 5: Management of Squamous Cell Carcinoma. J Cutan Med Surg *19*, 249-259.

Sarasin, A. (1999). The molecular pathways of ultraviolet-induced carcinogenesis. Mutation research *428*, 5-10.

Schaper-Gerhardt, K., Walter, A., Schmitz-Rode, C., Satzger, I., and Gutzmer, R. (2018). The mTOR-inhibitor Sirolimus decreases the cyclosporine-induced expression of the oncogene ATF3 in human keratinocytes. Journal of dermatological science *92*, 172-180.

Schardt, L. (2017). The impact of Cyclosporin A on human epidermal keratinozytes. In Faculty of Biosciences (Heidelberg: Ruperto-Carola University of Heidelberg).

Schenk, S., Hintermann, E., Bilban, M., Koshikawa, N., Hojilla, C., Khokha, R., and Quaranta, V. (2003). Binding to EGF receptor of a laminin-5 EGF-like fragment liberated during MMP-dependent mammary gland involution. The Journal of cell biology *161*, 197-209.

Schieke, S.M., Ruwiedel, K., Gers-Barlag, H., Grether-Beck, S., and Krutmann, J. (2005). Molecular crosstalk of the ultraviolet a and ultraviolet B signaling responses at the level of mitogen-activated protein kinases. The Journal of investigative dermatology *124*, 857-859.

Schmults, C.D., Karia, P.S., Carter, J.B., Han, J., and Qureshi, A.A. (2013). Factors predictive of recurrence and death from cutaneous squamous cell carcinoma: a 10-year, single-institution cohort study. JAMA Dermatol *149*, 541-547.

Scholzen, T., and Gerdes, J. (2000). The Ki-67 protein: from the known and the unknown. Journal of cellular physiology *182*, 311-322.

Sennet, R., and Rendl, M. (2012). Mesenchymal–epithelial interactions during hair follicle morphogenesis and cycling. Elsevier Seminars in Cell & Developmental Biology *23(8)*, 917-927.

Siegel, R.L., Miller, K.D., and Jemal, A. (2019). Cancer statistics, 2019. CA Cancer J Clin *69*, 7-34.

Smith, J.M., and Dharnidharka, V.R. (2014). Progress in Pediatric Kidney Transplantation The Open Urology & Nephrology Journal *7*, 115-122.

Smith, K.J., Hamza, S., and Skelton, H. (2004). Histologic features in primary cutaneous squamous cell carcinomas in immunocompromised patients focusing on organ transplant patients. Dermatol Surg *30*, 634-641.

Sollinger, H.W. (1995). Mycophenolate mofetil for the prevention of acute rejection in primary cadaveric renal allograft recipients. U.S. Renal Transplant Mycophenolate Mofetil Study Group. Transplantation *60*, 225-232.

Sommerer, C., Schnitzler, P., Meuer, S., Zeier, M., and Giese, T. (2011). Pharmacodynamic monitoring of cyclosporin A reveals risk of opportunistic infections and malignancies in renal transplant recipients 65 years and older. Ther Drug Monit *33*, 694-698.

Staples, M.P., Elwood, M., Burton, R.C., Williams, J.L., Marks, R., and Giles, G.G. (2006). Non-melanoma skin cancer in Australia: the 2002 national survey and trends since 1985. Med J Aust *184*, 6-10.

Stark, L.A., Arends, M.J., McLaren, K.M., Benton, E.C., Shahidullah, H., Hunter, J.A.A., and Bird, C.C. (1994). Accumulation of p53 is associated with tumour progression in cutaneous lesions of renal allograft recipients. British journal of cancer *70*, 662.

Starzl, T.E., Marchioro, T.L., and Waddell, W.R. (1963). The Reversal of Rejection in Human Renal Homografts with Subsequent Development of Homograft Tolerance. Surg Gynecol Obstet *117*, 385-395.

Starzl, T.E., Todo, S., Fung, J., Demetris, A.J., Venkataramman, R., and Jain, A. (1989). FK 506 for liver, kidney, and pancreas transplantation. Lancet *2*, 1000-1004.

Stepkowski, S.M. (2000). Molecular targets for existing and novel immunosuppressive drugs. Expert Reviews in Molecular Medicine, Cambridge University Press *Volume 2, Issue 4*, 1-23.

Strickland, P.T. (1986). Photocarcinogenesis by near-ultraviolet (UVA) radiation in Sencar mice. The Journal of investigative dermatology *87*, 272-275.

Strozyk, E., and Kulms, D. (2013). The role of AKT/mTOR pathway in stress response to UV-irradiation: implication in skin carcinogenesis by regulation of apoptosis, autophagy and senescence. Int J Mol Sci *14*, 15260-15285.

Tang, X., Zhu, Y., Han, L., Kim, A.L., Kopelovich, L., Bickers, D.R., and Athar, M. (2007). CP-31398 restores mutant p53 tumor suppressor function and inhibits UVB-induced skin carcinogenesis in mice. J Clin Invest *117*, 3753-3764.

Thulabandu, V., Chen, D., and Atit, R.P. (2018). Dermal fibroblast in cutaneous development and healing. Wiley Interdiscip Rev Dev Biol *7*.

Tremblay, F., Fernandes, M., Habbab, F., de, B.E.M.D., Loertscher, R., and Meterissian, S. (2002). Malignancy after renal transplantation: incidence and role of type of immunosuppression. Ann Surg Oncol *9*, 785-788.

Tzellos, T.G., Klagas, I., Vahtsevanos, K., Triaridis, S., Printza, A., Kyrgidis, A., Karakiulakis, G., Zouboulis, C.C., and Papakonstantinou, E. (2009). Extrinsic ageing in the human skin is associated with alterations in the expression of hyaluronic acid and its metabolizing enzymes. Experimental dermatology *18*, 1028-1035.

Uitto, J., Olsen, D.R., and Fazio, M.J. (1989). Extracellular matrix of the skin: 50 years of progress. The Journal of investigative dermatology *92*, 61S-77S.

Umland, S.P., Shah, H., Jakway, J.P., Shortall, J., Razac, S., Garlisi, C.G., Falcone, A., Kung, T.T., Stelts, D., Hegde, V.*, et al.* (1999). Effects of cyclosporin A and dinactin on T-cell proliferation, interleukin-5 production, and murine pulmonary inflammation. Am J Respir Cell Mol Biol *20*, 481-492.

Venugopal, S.S., and Murrell, D.F. (2010). Treatment of skin cancers in epidermolysis bullosa. Dermatol Clin *28*, 283-287, ix-x.

Vinck, E.M., Cagnie, B.J., Cornelissen, M.J., Declercq, H.A., and Cambier, D.C. (2003). Increased fibroblast proliferation induced by light emitting diode and low power laser irradiation. Lasers Med Sci *18*, 95-99.

Waldmeier, P.C., Feldtrauer, J.J., Qian, T., and Lemasters, J.J. (2002). Inhibition of the mitochondrial permeability transition by the nonimmunosuppressive cyclosporin derivative NIM811. Molecular pharmacology *62*, 22-29.

Walsh, S.B., Xu, J., Xu, H., Kurundkar, A.R., Maheshwari, A., Grizzle, W.E., Timares, L., Huang, C.C., Kopelovich, L., Elmets, C.A.*, et al.* (2011). Cyclosporine a mediates pathogenesis of aggressive cutaneous squamous cell carcinoma by augmenting epithelial-mesenchymal transition: role of TGFbeta signaling pathway. Molecular carcinogenesis *50*, 516-527.

Walter, A., Barysch, M.J., Behnke, S., Dziunycz, P., Schmid, B., Ritter, E., Gnjatic, S., Kristiansen, G., Moch, H., Knuth, A.*, et al.* (2010). Cancer-testis antigens and immunosurveillance in human cutaneous squamous cell and basal cell carcinomas. Clin Cancer Res *16*, 3562-3570.

Wang, N.J., Sanborn, Z., Arnett, K.L., Bayston, L.J., Liao, W., Proby, C.M., Leigh, I.M., Collisson, E.A., Gordon, P.B., Jakkula, L.*, et al.* (2011). Loss-of-function mutations in Notch receptors in cutaneous and lung squamous cell carcinoma. Proceedings of the National Academy of Sciences of the United States of America *108*, 17761-17766.

Wang, S.H., Liou, G.G., Liu, S.H., Chang, J.S., Hsiao, J.R., Yen, Y.C., Chen, Y.L., Wu, W.L., Chang, J.Y., and Chen, Y.W. (2019). Laminin gamma2-enriched extracellular vesicles of oral squamous cell carcinoma cells enhance in vitro lymphangiogenesis via integrin alpha3-dependent uptake by lymphatic endothelial cells. International journal of cancer Journal international du cancer *144*, 2795-2810.

Watson, C.J., and Dark, J.H. (2012). Organ transplantation: historical perspective and current practice. British journal of anaesthesia *108 Suppl 1*, i29-42.

WHO (2019). How common is skin cancer? https://www.who.int/uv/faq/skincancer/en/index1.html.

Wickett, R.R., and Visscher, M.O. (2006). Structure and function of the epidermal barrier. American Journal of Infection Control *34*, S98-S110.

Wieland, U., Kreuter, A., and Pfister, H. (2014). Human papillomavirus and immunosuppression. Curr Probl Dermatol *45*, 154-165.

Wilke, M.S., and Furcht, L.T. (1990). Human keratinocytes adhere to a unique heparin-binding peptide sequence within the triple helical region of type IV collagen. The Journal of investigative dermatology *95*, 264-270.

Wu, X., Nguyen, B.C., Dziunycz, P., Chang, S., Brooks, Y., Lefort, K., Hofbauer, G.F., and Dotto, G.P. (2010). Opposing roles for calcineurin and ATF3 in squamous skin cancer. Nature *465*, 368-372.

Wynn, T.A. (2007). Common and unique mechanisms regulate fibrosis in various fibroproliferative diseases. J Clin Invest *117*, 524-529.

Xiang, F., Lucas, R., Hales, S., and Neale, R. (2014). Incidence of nonmelanoma skin cancer in relation to ambient UV radiation in white populations, 1978-2012: empirical relationships. JAMA Dermatol *150*, 1063-1071.

Yan, P., Nagasawa, A., Uosaki, H., Sugimoto, A., Yamamizu, K., Teranishi, M., Matsuda, H., Matsuoka, S., Ikeda, T., Komeda, M.*, et al.* (2009). Cyclosporin-A potently induces highly cardiogenic progenitors from embryonic stem cells. Biochemical and biophysical research communications *379*, 115-120.

Yarosh, D.B., Pena, A.V., Nay, S.L., Canning, M.T., and Brown, D.A. (2005). Calcineurin inhibitors decrease DNA repair and apoptosis in human keratinocytes following ultraviolet B irradiation. The Journal of investigative dermatology *125*, 1020-1025.

Yasui, T., Yonetsu, M., Tanaka, R., Tanaka, Y., Fukushima, S., Yamashita, T., Ogura, Y., Hirao, T., Murota, H., and Araki, T. (2013). In vivo observation of age-related structural changes of dermal collagen in human facial skin using collagen-sensitive second harmonic generation microscope equipped with 1250-nm mode-locked Cr:Forsterite laser. J Biomed Opt *18*, 31108.

Yeol Lee, H., Ham, S.P., Choi, Y.W., and Park, H.J. (2018). The Value of Type IV Collagen Immunohistochemical Staining in the Differential Diagnosis of Autoimmune Subepidermal Bullous Diseases. Acta Dermatovenerol Croat *26*, 133-138.

Zhang, Q.S., Maddock, D.A., Chen, J.P., Heo, S., Chiu, C., Lai, D., Souza, K., Mehta, S., and Wan, Y.S. (2001). Cytokine-induced p38 activation feedback regulates the prolonged activation of AKT cell survival pathway initiated by reactive oxygen species in response to UV irradiation in human keratinocytes. Int J Oncol *19*, 1057-1061.

# 8. Appendix

## 8.1. Proliferation analysis macro

**Table 8-1 – Fiji macro to determine the total epidermal proliferation rate**

```
//prepare
setTool("freehand");
setSlice(3);
roiManager("Deselect");
run("Select None");
roiManager("Reset");
title=getTitle();

//select Epidermis
run("Duplicate...", " ");
run("Grays");
run("Gaussian Blur...", "sigma=10");
run("Threshold...");
setAutoThreshold("Default dark");
waitForUser("Adjust the threshold for epidermis.");
run("Analyze Particles...", "size=10000-Infinity pixel include add");
close();
roiManager("Show All");
waitForUser("Check the selection for epidermis. If it is not good select it again and add to
ROImanager");
setSlice(3);
roiManager("Deselect");
run("Select None");


//analyze DAPI
setSlice(2);
run("Duplicate...", " ");
run("Grays");
run("Gaussian Blur...", "sigma=4");//change sigma to get more or less cells (smaller sigma -
more cells)
run("Threshold...");
setAutoThreshold("Default dark");
waitForUser("Adjust the Threshold for DAPI");
run("Find Maxima...", "noise=2 output=[Segmented Particles] above");//change noise to get
more or less cells (smaller noise - more cells)
roiManager("Select", 0);
setAutoThreshold("Default dark");
rename(title+ " DAPI count");
run("Analyze Particles...", "size=20-Infinity pixel exclude summarize add");
close();
close();
```

```
selectWindow(title);
run("Duplicate...", " ");
run("Grays");
roiManager("Show All");
waitForUser("Check the selection of DAPI");
close();

//combine dapi to count Ki67 only within DAPI which is within Epi
        roiManager("Select", 0);
        roiManager("Delete");
        print("please wait");
roiManager("Combine");
roiManager("Reset");
roiManager("Add");
roiManager("Deselect");
run("Select None");

//analyze Ki67
setSlice(1);
run("Duplicate...", " ");
run("Subtract Background...", "rolling=50 slice");
run("Grays");
run("Median...", "radius=2");
run("Threshold...");
setAutoThreshold("Default dark");
getThreshold(min, max);
setThreshold(773, max);
titleTemp=getTitle();
waitForUser("Adjust the Threshold for Ki67 ");
selectWindow(titleTemp);
roiManager("Select", 0);
setBackgroundColor(0, 0, 0);
run("Clear Outside");
rename(title+ " Ki67 count");
run("Analyze Particles...", "size=20-Infinity pixel summarize add");//change min size to get
more or less cells
close();

//display
run("Grays");
roiManager("Show All");
roiManager("Select", 0);
```

## 8.2. Calculation of MED based exposure time

In 1987 the CIE (Commission Internationale de l'Eclairage) agreed that the ability of UV radiation (200-400 nm) to elicit erythema in human skin depends strongly on wavelength and that different wavelengths contribute to a different extent to the formation of an erythema (McKenzie et al., 2014). Based on this agreement, we defined wavelength specific CIE factors to reevaluate the power
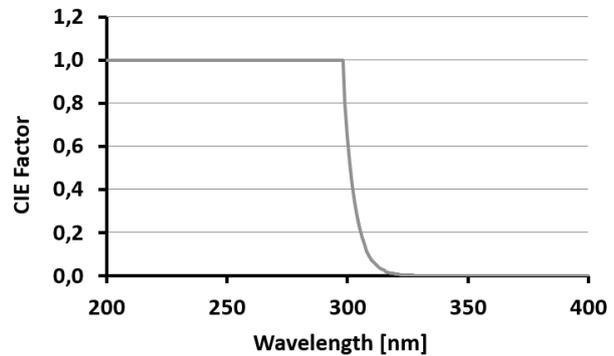


**Figure 8.1 – Representation of CIE factors for the spectral area from 200 to 400 nm**

of the KAUVIR lamp with regard to its erythema induction capability. This is defined here as the CIE scaled power of our lamp. A graph with the CIE factors is given in **Figure 8.1.**

MED describes the CIE scaled radiation intensity and time, that is required to reach a minimal erythema dosage on a person with skin type II. One MED is defined as 250 J/m$^2$ CIE scaled UVA+B light. To determine the physical intensity required for the representation of one MED, it was necessary to compare the technical / physical power of the KAUVIR lamp to the CIE scaled power.

To determine this ratio, we first looked at the intensity of our lamp in the 280-400 nm wavelength area, as this is representing the UVB and the UVA light. Initially, 40 individual measurements of that area were made with the spectrometer with all light sources running and the sensor open (*Brt.Count*).

$$Brt.Count.\lambda(280) = [Brt.Count.\lambda(280_1) + Brt.Count.\lambda(280_2) + ... + Brt.Count.\lambda(280_{40})]/40$$
$$Brt.Count.\lambda(286) = [Brt.Count.\lambda(281_1) + Brt.Count.\lambda(281_2) + ... + Brt.Count.\lambda(281_{40})]/40$$
$$Brt.Count.\lambda(287) = [Brt.Count.\lambda(282_1) + Brt.Count.\lambda(282_2) + ... + Brt.Count.\lambda(282_{40})]/40$$
$$\vdots$$
$$Brt.Count.\lambda(400) = [Brt.Count.\lambda(400_1) + Brt.Count.\lambda(400_2) + ... + Brt.Count.\lambda(400_{40})]/40$$

Then, another 40 measurements were made, but this time with a covered sensor (*Drk.Count*; exposure time = 60 ms).

$$Drk.Count.\lambda(280) = [Drk.Count.\lambda(280_1) + Drk.Count.\lambda(280_2) + ... + Drk.Count.\lambda(280_{40})]/40$$
$$Drk.Count.\lambda(281) = [Drk.Count.\lambda(281_1) + Drk.Count.\lambda(281_2) + ... + Drk.Count.\lambda(281_{40})]/40$$
$$Drk.Count.\lambda(282) = [Drk.Count.\lambda(282_1) + Drk.Count.\lambda(282_2) + ... + Drk.Count.\lambda(282_{40})]/40$$
$$\vdots$$
$$Drk.Count.\lambda(400) = [Drk.Count.\lambda(400_1) + Drk.Count.\lambda(400_2) + ... + Drk.Count.\lambda(400_{40})]/40$$

Of those 40 measurements the average was calculated and the mean value of the *Drk.Count* was subtracted from the mean value of the *Brt.Count*, in order to determine the net intensity (*Net.Count*) of the KAUVIR at an exposure time (*Exp.Time*) of 60 ms in the spectral area between 280 and 400 nm.

$$Net.Count.\lambda(280) = Brt.Count.\lambda(280) - Drk.Count.\lambda(280)$$
$$Net.Count.\lambda(281) = Brt.Count.\lambda(281) - Drk.Count.\lambda(281)$$
$$Net.Count.\lambda(282) = Brt.Count.\lambda(282) - Drk.Count.\lambda(282)$$
$$\vdots \qquad\qquad \vdots \qquad\qquad \vdots$$
$$Net.Count.\lambda(400) = Brt.Count.\lambda(400) - Drk.Count.\lambda(400)$$

For the next step the actual physical power (*Power.Tech*) had to be identified. Therefore, the *Net.Count* was multiplied with a spectrometer and wavelength specific calibration factor (*Cal.Fac.*) to exclude technical measurement mistakes and divided by the *Exp.Time*.

$$Power._{Tech}\lambda(280) = (Net.Count.\lambda(280)\, x\, Cal.Fac.)\, /\, Exp.Time$$
$$Power._{Tech}\lambda(281) = (Net.Count.\lambda(281)\, x\, Cal.Fac.)\, /\, Exp.Time$$
$$Power._{Tech}\lambda(282) = (Net.Count.\lambda(282)\, x\, Cal.Fac.)\, /\, Exp.Time$$
$$\vdots \qquad\qquad \vdots \qquad\qquad \vdots$$
$$Power._{Tech}\lambda(400) = (Net.Count.\lambda(400)\, x\, Cal.Fac.)\, /\, Exp.Time$$

However, this way the power could only be determined for the individual wavelengths at which the spectrometer monitored the light intensity. To be able to evaluate the physical power of the entire UV spectrum (*UV.Power.Tech*), it was necessary to calculate the integral over those individual wavelength specific power values. For this purpose, averaging the two values approximated the integrals between two adjacent measurements.

$$\int_{280}^{281} Spec.Power._{Tech} = \frac{Power._{Tech}\lambda(280) + Power._{Tech}\lambda(281)}{2}$$

$$\int_{281}^{282} Spec.Power._{Tech} = \frac{Power._{Tech}\lambda(281) + Power._{Tech}\lambda(282)}{2}$$

$$\int_{282}^{283} Spec.Power._{Tech} = \frac{Power._{Tech}\lambda(282) + Power._{Tech}\lambda(283)}{2}$$

$$\vdots \qquad\qquad \vdots$$

$$\int_{399}^{400} Spec.Power._{Tech} = \frac{Power._{Tech}\lambda(399) + Power._{Tech}\lambda(400)}{2}$$

Next, those small integrals were added up to the integral of the entire spectral area of interest.

$$UV.Power._{Tech} = \int\limits_{280}^{281} Spec.Power._{Tech} + \int\limits_{281}^{282} Spec.Power._{Tech} + \cdots + \int\limits_{399}^{400} Spec.Power._{Tech}$$

Next to the physical UV power of the lamp, also the CIE scaled power had to be determined. For this the wavelength specific *Power.$_{Tech}\lambda$* was multiplied with the corresponding CIE-Factor $F_\lambda$.

$$Power._{CIE}\lambda(280) = Power._{Tech}\lambda(280)\,x\,F_{280}$$
$$Power._{CIE}\lambda(281) = Power._{Tech}\lambda(281)\,x\,F_{281}$$
$$Power._{CIE}\lambda(282) = Power._{Tech}\lambda(282)\,x\,F_{282}$$
$$\vdots \qquad\qquad\qquad \vdots$$
$$Power._{CIE}\lambda(400) = Power._{Tech}\lambda(400)\,x\,F_{400}$$

As for physical UV power, the *UV.Power.$_{CIE}$* was determined by first approximating the integrals between two adjacent measurements.

$$\int\limits_{280}^{281} Spec.Power._{CIE} = \frac{Power._{CIE}\lambda(280) + Power._{CIE}\lambda(281)}{2}$$

$$\int\limits_{281}^{282} Spec.Power._{CIE} = \frac{Power._{CIE}\lambda(281) + Power._{CIE}\lambda(282)}{2}$$

$$\int\limits_{282}^{283} Spec.Power._{CIE} = \frac{Power._{CIE}\lambda(282) + Inten._{CIE}\lambda(283)}{2}$$

$$\vdots \qquad\qquad\qquad \vdots$$

$$\int\limits_{399}^{400} Spec.Power._{CIE} = \frac{Power._{CIE}\lambda(399) + Power._{CIE}\lambda(400)}{2}$$

Second, those small integrals were added up to the integral of the entire UVA+B spectra.

$$UV.Power._{CIE} = \int\limits_{280}^{281} Spec.Power._{CIE} + \int\limits_{281}^{282} Spec.Power._{CIE} + \cdots + \int\limits_{399}^{400} Spec.Power._{CIE}$$

Then the ratio between the technical and the CIE scaled power ($R_{Tech:CIE}$) was calculated and in the next step multiplied with 250 J/m2 to define technical UV intensity, required for the production of 1 MED (*UV.Inten.$_{MED}$*).

$$R_{Tech:CIE} = \frac{UV.Power._{Tech}}{UV.Power._{CIE}}$$

$$UV.Inten._{MED} = 250\,J/m^2\,x\,R_{Tech:CIE}$$

Finally, to determine the exposure time ($T_{Exp.}$) the intensity was divided by the physical UV power.

$$T_{Exp.} = \frac{UV.Inten._{MED}}{UV.Power._{Tech}}$$

## 8.3. CsA regulated mTORC1 signaling

**Table 8-2 – Members of the mTORC1-signaling pathway regulated by CsA in the epidermal and dermal equivalent of HaCaT-OTCs**

| Symbol | Gene Name | Rel. Regul. Epidermis | Rel. Regul. Dermis |
|---|---|---|---|
| ACACA | acetyl-CoA carboxylase alpha | UP | - |
| ACLY | ATP citrate lyase | - | DOWN |
| ACSL3 | acyl-CoA synthetase long chain family member 3 | UP | - |
| ACTR3 | ARP3 actin related protein 3 homolog | - | UP |
| AK4 | adenylate kinase 4 | UP | DOWN |
| ALDOA | aldolase, fructose-bisphosphate A | UP | - |
| ATP2A2 | ATPase sarcoplasmic/endoplasmic reticulum Ca2+ transporting 2 | - | UP |
| ATP6V1D | ATPase H+ transporting V1 subunit D | - | DOWN |
| CDKN1A | cyclin dependent kinase inhibitor 1A | - | UP |
| DDIT4 | DNA damage inducible transcript 4 | - | UP |
| ELOVL5 | ELOVL fatty acid elongase 5 | UP | - |
| ENO1 | enolase 1 | - | UP |
| ERO1A | endoplasmic reticulum oxidoreductase 1 alpha | - | DOWN |
| FADS1 | fatty acid desaturase 1 | UP | - |
| GAPDH | glyceraldehyde-3-phosphate dehydrogenase | DOWN | - |
| GLRX | glutaredoxin | DOWN | - |
| GOT1 | glutamic-oxaloacetic transaminase 1 | - | DOWN |
| GTF2H1 | general transcription factor IIH subunit 1 | DOWN | - |
| HK2 | hexokinase 2 | - | DOWN |
| HMGCS1 | 3-hydroxy-3-methylglutaryl-CoA synthase 1 | - | DOWN |
| HPRT1 | hypoxanthine phosphoribosyltransferase 1 | UP | - |
| IDI1 | isopentenyl-diphosphate delta isomerase 1 | UP | - |
| IFRD1 | interferon related developmental regulator 1 | DOWN | - |
| INSIG1 | insulin induced gene 1 | UP | - |
| LDLR | low density lipoprotein receptor | UP | - |
| MAP2K3 | mitogen-activated protein kinase kinase 3 | DOWN | UP |
| MLLT11 | MLLT11, transcription factor 7 cofactor | - | UP |
| MTHFD2 | methylenetetrahydrofolate dehydrogenase (NADP+ dependent) 2, methenyltetrahydrofolate cyclohydrolase | UP | UP |
| P4HA1 | prolyl 4-hydroxylase subunit alpha 1 | UP | UP |
| PNO1 | partner of NOB1 homolog | - | UP |
| PNP | purine nucleoside phosphorylase | - | DOWN |
| PRDX1 | peroxiredoxin 1 | DOWN | DOWN |
| PSMD12 | proteasome 26S subunit, non-ATPase 12 | - | UP |

| | | | |
|---|---|---|---|
| **PSMD13** | proteasome 26S subunit, non-ATPase 13 | DOWN | - |
| **PSMD14** | proteasome 26S subunit, non-ATPase 14 | DOWN | - |
| **RAB1A** | RAB1A, member RAS oncogene family | UP | - |
| **RDH11** | retinol dehydrogenase 11 (all-trans/9-cis/11-cis) | UP | DOWN |
| **SCD** | stearoyl-CoA desaturase | - | UP |
| **SDF2L1** | stromal cell derived factor 2 like 1 | UP | - |
| **SERPINH1** | serpin family H member 1 | UP | - |
| **SKAP2** | src kinase associated phosphoprotein 2 | - | UP |
| **SLC1A5** | solute carrier family 1 member 5 | UP | DOWN |
| **SLC2A1** | solute carrier family 2 member 1 | - | DOWN |
| **STC1** | stanniocalcin 1 | DOWN | - |
| **STIP1** | stress induced phosphoprotein 1 | - | DOWN |
| **TBK1** | TANK binding kinase 1 | - | UP |
| **TCEA1** | transcription elongation factor A1 | UP | UP |
| **TMEM97** | transmembrane protein 97 | DOWN | - |
| **TUBA4A** | tubulin alpha 4a | - | DOWN |
| **TXNRD1** | thioredoxin reductase 1 | UP | - |
| **UFM1** | ubiquitin fold modifier 1 | - | UP |
| **UNG** | uracil DNA glycosylase | DOWN | - |
| **XBP1** | X-box binding protein 1 | - | UP |

# 9. Publications and Abstracts

## 9.1. Publications

**Worst PL**, Schardt L, Janke K, Herberg M, Galle J, Stark HJ, Pavez Loriè E, Boukamp P *"Skin specific off-target effects of CsA and their role during induction of tumor like invasion in a long-term human skin equivalent"*
Status: In preparation

Own Contribution:
- Preparation of manuscript-Comparison of CsA effects on epithelial models with different genetic predisposition
- Induction of invasion upon CsA in HaCaT-OTCs-Improvement of epidermal organization upon CsA
- Disruption of the basement membrane integrity upon CsA-CsA and sunlight induced boost of HaCaT proliferation
- Gene expression microarray analysis of the dermal and epidermal compartment
- Role of the mTOR signaling pathway in CsA induced invasion
  → In total approx. 60%

Pavez Loriè E, Schardt L, **Worst PL**, Stark HJ, Boukamp P *"Fetal bovine serum: an indispensable but variable ingredient for long-term skin equivalents"*
Status: In preparation

Own Contribution:
- Identification of serum related effects on the epidermal differentiation and the basement membrane integrity in long-term skin equivalents
- Determination of relative proliferation between different serum setups in long-term skin equivalents
  → In total approx. 10%

## 9.2. Abstracts

**Worst PL**, Janke K, Schardt L, Pavez Loriè E, Boukamp P (2019) *'Cyclosporin A is promoting tumor like invasion in a long-term human skin equivalent'* **20th International AEK Cancer Congress**, Heidelberg, Germany, 03/2019 – poster presentation

**Worst PL**, Schardt L, Pavez Loriè E, Boukamp P (2018) *'Cyclosporin A is promoting tumour like invasion in a long-term human skin equivalent'* **3rd EACR Conference Goodbye Flat Biology**, Berlin, Germany, 09/2018 – talk

**Worst PL**, Schardt L, Pavez Loriè E, Boukamp P (2018) '*CsA is enhancing differentiation and promoting tumor like invasion in a long-term human skin equivalent'* **KVSF Spring School**, Düsseldorf, Germany, 04/2018 – poster presentation

**Worst PL**, Schardt L, Pavez Loriè E, Boukamp P (2017) '*CsA is enhancing differentiation and promoting tumor like invasion in a long-term human skin equivalent'* **RTG2099: Hallmarks of Skin Cancer (HoSC) Conference**, Heidelberg, Germany, 11/2017 – poster presentation

**Worst PL**, Schardt L, Pavez Loriè E, Boukamp P (2017) *'The immune independent effect of CsA on human keratinozytes'* **19th International AEK Cancer Congress**, EMBL Heidelberg, Germany, 03/2017 – poster presentation

Pavez Loriè E, Stark HJ, **Worst PL**, Schardt L, Boukamp P (2015) *'The different effect of UV and IRA in human skin equivalents'* **Jahrestagung der Gesellschaft für Biologische Strahlenforschung e.V. (GBS)**, Dresden, Germany, 10/2015 – talk

## 10.  Affidavit

I declare under oath that I have produced my thesis independently and without any undue assistance by third parties under consideration of the 'Principles for the Safeguarding of Good Scientific Practice at Heinrich Heine University Düsseldorf'.

This dissertation has neither been used in this or any other form as a thesis, nor been submitted to any other faculty as a dissertation. Nowhere else is an examination procedure requested.

Düsseldorf, 27 December 2019

_____

Philipp Worst